JOURNAL OF GEOPHYSICAL RESEARCH: ATMOSPHERES, VOL. 118, 5830–5866, doi:10.1002/jgrd.50331, 2013

The 2010 California Research at the Nexus of Air Quality and Climate Change (CalNex) field study

T. B. Ryerson,[1] A. E. Andrews,[2] W. M. Angevine,[1,3] T. S. Bates,[4] C. A. Brock,[1] B. Cairns,[5] R. C. Cohen,[6] O. R. Cooper,[1,3] J. A. de Gouw,[1,3] F. C. Fehsenfeld,[3] R. A. Ferrare,[7] M. L. Fischer,[8] R. C. Flagan,[9] A. H. Goldstein,[10] J. W. Hair,[7] R. M. Hardesty,[3] C. A. Hostetler,[7] J. L. Jimenez,[3,11] A. O. Langford,[1] E. McCauley,[12] S. A. McKeen,[1,3] L. T. Molina,[13,14] A. Nenes,[15] S. J. Oltmans,[3] D. D. Parrish,[1] J. R. Pederson,[12] R. B. Pierce,[16] K. Prather,[17] P. K. Quinn,[4] J. H. Seinfeld,[9] C. J. Senff,[1,3] A. Sorooshian,[18] J. Stutz,[19] J. D. Surratt,[20] M. Trainer,[1] R. Volkamer,[11] E. J. Williams,[1] and S. C. Wofsy[21]

Received 23 October 2012; revised 11 March 2013; accepted 12 March 2013; published 13 June 2013.

[1] The California Research at the Nexus of Air Quality and Climate Change (CalNex) field study was conducted throughout California in May, June, and July of 2010. The study was organized to address issues simultaneously relevant to atmospheric pollution and climate change, including (1) emission inventory assessment, (2) atmospheric transport and dispersion, (3) atmospheric chemical processing, and (4) cloud-aerosol interactions and aerosol radiative effects. Measurements from networks of ground sites, a research ship, tall towers, balloon-borne ozonesondes, multiple aircraft, and satellites provided *in situ* and remotely sensed data on trace pollutant and greenhouse gas concentrations, aerosol chemical composition and microphysical properties, cloud microphysics, and meteorological parameters. This overview report provides operational information for the variety of sites, platforms, and measurements, their joint deployment strategy, and summarizes findings that have resulted from the collaborative analyses of the CalNex field study. Climate-relevant findings from CalNex include that leakage from natural gas infrastructure may account for the excess of observed methane over emission estimates in Los Angeles. Air-quality relevant findings include the following: mobile fleet VOC significantly declines, and NO_x emissions continue to have an impact on ozone in the Los Angeles basin; the relative contributions of diesel and gasoline emission to secondary organic aerosol are not fully understood; and nighttime NO_3 chemistry contributes significantly to secondary organic aerosol mass in the San Joaquin Valley. Findings simultaneously relevant to climate and air quality include the following: marine vessel emissions changes due to fuel sulfur and speed controls result in a net warming effect but have substantial positive impacts on local air quality.

[1]Chemical Sciences Division, National Oceanic and Atmospheric Administration, Boulder, Colorado, USA.
[2]Global Monitoring Division, National Oceanic and Atmospheric Administration, Boulder, Colorado, USA.
[3]Cooperative Institute for Research in Environmental Sciences, University of Colorado, Boulder, CO, USA.
[4]Pacific Marine Environmental Laboratory, National Oceanic and Atmospheric Administration, Seattle, Washington, USA.
[5]Goddard Institute for Space Studies, National Aeronautics and Space Administration, Greenbelt, Maryland, USA.
[6]Department of Chemistry, University of California, Berkeley, California, USA.
[7]Langley Research Center, National Aeronautics and Space Administration, Hampton, Virginia, USA.
[8]Environmental Energy Technologies Division, Lawrence Berkeley National Laboratory, Berkeley, California, USA.
[9]Department of Chemical Engineering, California Institute of Technology, Pasadena, California, USA.
[10]Department of Civil and Environmental Engineering, University of California, Berkeley, California, USA.
[11]Department of Chemistry and Biochemistry, University of Colorado, Boulder, Colorado, USA.
[12]Atmospheric Processes Research Section, California Air Resources Board, Sacramento, California, USA.
[13]Department of Earth, Atmospheric, and Planetary Sciences, Massachusetts Institute of Technology, Cambridge, MA, USA.
[14]Molina Center for Energy and the Environment, La Jolla, CA, USA.
[15]School of Earth and Atmospheric Sciences, Georgia Institute of Technology, Atlanta, Georgia, USA.
[16]National Environmental Satellite, Data, and Information Service, National Oceanic and Atmospheric Administration, Madison, Wisconsin, USA.
[17]Department of Chemistry and Biochemistry, University of California, San Diego, California, USA.
[18]Chemical and Environmental Engineering, University of Arizona, Tucson, Arizona, USA.
[19]Department of Atmospheric and Oceanic Sciences, University of California, Los Angeles, California, USA.
[20]Environmental Sciences and Engineering, University of North Carolina, Chapel Hill, North Carolina, USA.
[21]Atmospheric and Environmental Chemistry, Harvard University, Boston, Massachusetts, USA.

Corresponding author: T. B. Ryerson, Chemical Sciences Division, National Oceanic and Atmospheric Administration, Boulder, CO, USA. (thomas.b.ryerson@noaa.gov)

2169-897X/13/10.1002/jgrd.50331

Citation: Ryerson, T. B., et al. (2013), The 2010 California Research at the Nexus of Air Quality and Climate Change (CalNex) field study, *J. Geophys. Res. Atmos.*, *118*, 5830–5866, doi:10.1002/jgrd.50331.

1. Introduction

[2] The California Research at the Nexus of Air Quality and Climate Change (CalNex) 2010 field project was undertaken to provide improved scientific knowledge for emissions control strategies to simultaneously address the two interrelated issues of air quality and climate change. Air quality and climate change issues are linked because in many cases, the agents of concern are the same and the sources of the agents are the same or intimately connected. Examples include tropospheric ozone (O_3), which is both an air pollutant and a greenhouse gas (GHG), and atmospheric particulate matter (PM), which has effects on the radiative budget of the atmosphere as well as human and ecosystem health, visibility degradation, and acidic deposition. Efforts to address one of these issues can be beneficial to the other, but in some cases, policies addressing one issue without additional consideration can have unintended detrimental impacts on the other. The goal of CalNex 2010 is to improve and advance the science needed to support continued and effective air quality and climate management policy for the State of California.

[3] Over the past several decades in the U.S., emissions reductions implemented for vehicles and point sources have significantly improved air quality in most metropolitan areas. In recent years, the rate of improvement in air quality in most regions of the U.S. has slowed, both in terms of regional ozone concentrations and ozone exceedance days (e.g., Figure 1 for California). At the same time, accelerating emissions of greenhouse gases have increased the net radiative forcing of the climate system. Overall, from 1990 to 2005, total emissions of carbon dioxide (CO_2) in the U.S. were estimated to have increased by 20% (from 5062 to 6090 Tg/yr) [*EPA*, 2007].

[4] California was chosen as the site for this joint study because it has well-documented air quality problems and faces the difficult task of managing them with an increasing population and demand for goods and services. The CalNex study was designed to build upon the knowledge developed through decades of previous atmospheric research field projects in California. Consistent themes across the many studies include quantifying anthropogenic emissions and their changes over time, notably in tunnel studies [e.g., *Harley et al*., 2005] and by roadside monitoring [e.g., *Bishop and Stedman*, 2008]; the role that regional transport plays in shaping pollutant concentrations, forced either by the sea breeze [e.g., *Boucouvala and Bornstein*, 2003; *Cass and Shair*, 1984; *Shair et al*., 1982], by complex terrain [e.g., *Langford et al*., 2010; *Skamarock et al*., 2002; *Wakimoto and McElroy*, 1986], or both [*Lu and Turco*, 1996; *Rosenthal et al*., 2003]; the roles of chlorine chemistry [e.g., *Finlayson-Pitts*, 2003; *Knipping and Dabdub*, 2003] and the weekend effect [e.g., *Blanchard and Tanenbaum*, 2003; *Marr and Harley*, 2002] in ozone formation; and studies of the sources and chemistry leading to atmospheric haze formation [e.g., *Hersey et al*., 2011; *Schauer et al*., 1996; *Turpin and Huntzicker*, 1995]. The literature from previous field studies in California is extensive; initial descriptions can be found in the project overview papers for the Southern California Air Quality Study (SCAQS; which took place in 1987) [*Hering and Blumenthal*, 1989], the Southern California Ozone Study (SCOS, 1997) (www.arb.ca.gov/research/scos/scos.htm), the California Regional Particulate Air Quality Study (CRPAQS, 1999–2001) [*Chow et al*., 2006; *Qin and Prather*, 2006; *Rinehart et al*., 2006], the Central California Ozone Study (CCOS, summer 2000) [*Bao et al*., 2008; *Liang et al*., 2006; *Tonse et al*., 2008], the Intercontinental Transport and Chemical Transformation of Anthropogenic Pollution (ITCT, spring 2002) study [*Parrish et al*., 2004], the Intercontinental Chemical Transport Experiment-North America (INTEX-NA, summer 2004) study, the Study of Organic Aerosols at Riverside (SOAR, 2005) [*Docherty et al*., 2011], the Arctic Research of the Composition of the Troposphere from Aircraft and Satellites-California Air Resources Board (ARCTAS-CARB, summer 2008) study [*Jacob et al*., 2010], the Pre-CalNex (summer 2009) study [*Langford et al*., 2010], and the Pasadena Aerosol Characterization Observatory study (PACO, 2009–2010) study [*Hersey et al*., 2011].

[5] In addition to its long-standing focus on air quality issues, in 2006 California led the nation's effort to address global climate change by implementing Assembly Bill 32 (AB32; arb.ca.gov/cc/ab32/ab32.htm) as the Global Warming Solutions Act of 2006, mandating controls on the emissions of greenhouse gases within, or attributable to, the state. Thus, California is particularly interested in finding the most effective way to simultaneously manage the two challenges of air quality and climate change. The CalNex study was organized to address issues simultaneously relevant to both, including (1) emission inventory assessment, (2) atmospheric transport and dispersion, (3) atmospheric chemical processing, and (4) cloud-aerosol interactions and aerosol radiative effects.

[6] The CalNex project was loosely coordinated with the U.S. Department of Energy (DOE)-sponsored Carbonaceous Aerosol and Radiative Effects Study (CARES; http://campaign.arm.gov/cares) in Sacramento and the Central Valley, and the multi-institutional CalMex study (http://mce2.org/en/activities/cal-mex-2010) based in Tijuana, Mexico. CARES took place in June of 2010 with a focus on the evolution of secondary and black carbon aerosols and their climate-relevant properties in the Sacramento urban plume. The scientific objectives, deployment approach, and a summary of initial findings from this project are described in *Zaveri et al*. [2012]. CalMex took place in May and June of 2010 with a focus on characterizing the sources and processing of emissions in the California-Mexico border regions to better understand their transport [*Bei et al*., 2012], transformation, impacts on regional air quality and climate [e.g., *Takahama et al*., 2012] and to support the design and implementation of emission control strategies at local, regional, and transboundary scales.

[7] The many science foci of the CalNex study are detailed in the science plan available online at www.esrl.

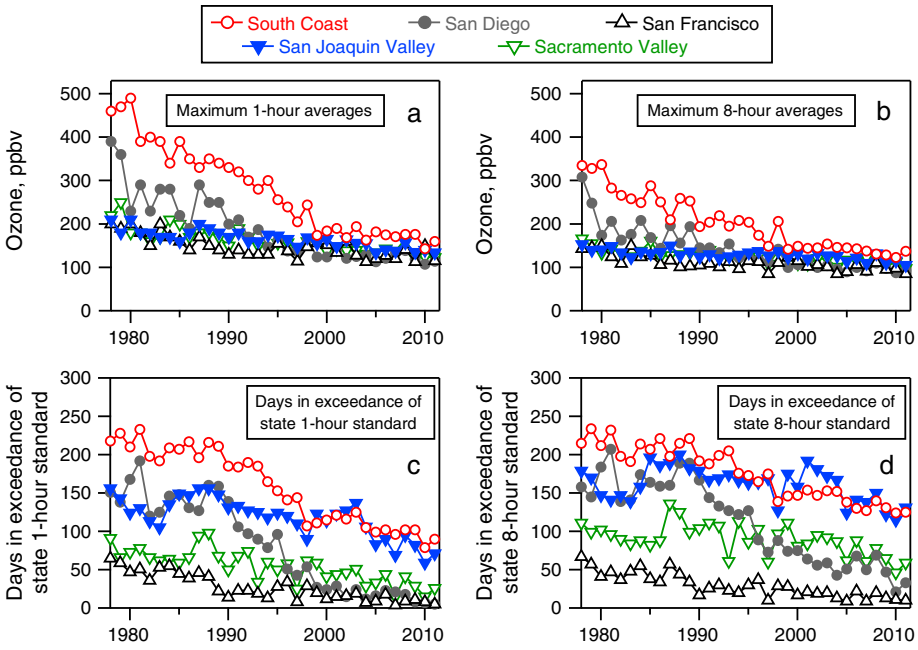

Figure 1. Maximum 1 h (a) and 8 h (b) averaged surface O_3 data, and number of days in exceedance of the state 1 h (c) and 8 h (d) O_3 standards, for selected air basins in California (www.arb.ca.gov/adam/trends/trends1.php).

noaa.gov/csd/projects/calnex/scienceplan.pdf. Examples of the major foci are mentioned briefly below.

[8] One major focus of the CalNex study was to use ambient data to quantitatively evaluate the accuracy of state and federal emissions inventories. Top-down assessments of different GHG, ozone precursor, and aerosol precursor emissions, accomplished using several different analytical methods, are described in section 4.1, Emission Inventory Assessment.

[9] The second focus of the CalNex study and its ensuing analyses was to provide a better understanding of the chemical factors shaping O_3 formation in California. Maxima in observed 8 h O_3 exceedances have been decreasing over time in both the Central Valley and LA basins but have been decreasing at different rates (Figure 1). The underlying reasons are not well known, and two general hypotheses helped to frame the CalNex study science questions. The first hypothesis invoked an increasingly large contribution of a locally irreducible background transported into California from the Pacific Ocean [*Parrish et al.*, 2010]. Daily ozonesonde launches in the IONS network in California [*Cooper et al.*, 2011] and routine vertical profiles by the NOAA P-3 aircraft during CalNex were carried out to provide additional data to quantify this hypothesis. Several reports incorporated CalNex data to better quantify upwind transport of O_3 into California; these are discussed in section 4.2, Atmospheric Transport and Dispersion.

[10] The second hypothesis suggests that the emissions differences result in mixtures of NO_x and VOC precursors in the two basins that are fundamentally different, leading to different sensitivities and limitations on O_3 photochemistry in each airshed [*Pusede and Cohen*, 2012]. The two heavily instrumented ground sites, one in Pasadena and one in Bakersfield, were established in part to provide data to quantify the extent that differences in photochemical precursor abundance have had on the responsiveness of each basin to emissions control strategies. CalNex analyses touching on this hypothesis are discussed further in section 4.3, Atmospheric Chemical Processing.

[11] The third CalNex focus was to study the effects of new California air quality regulations governing emissions from oceangoing ships, with potential for impacts with both air quality and climate implications. The resulting findings from airborne and research vessel measurements are described in section 4.1, Emission Inventory Assessment, and in section 4.4, Aerosol Optical Properties and Radiative Effects.

[12] The fourth focus of the CalNex project was to better understand the sources of secondary organic aerosol (SOA) mass in California by measuring its spatial distribution, chemical composition, radiocarbon content, and observing its association with known or suspected precursor gases in order to deduce and apportion sources. The reports detailing initial findings are described briefly in section 4.1, Emission Inventory Assessment.

2. Components of CalNex Observations

2.1. Longer-Term Sites: Existing Networks of Surface Monitors

[13] The State of California is divided into 15 air districts of somewhat distinctive geological, meteorological, and anthropogenic characteristics. The California Air Resources Board (CARB) and local air quality districts operate monitoring networks to routinely measure the atmospheric parameters necessary to

[14] 1. document air quality relative to ambient air quality standards (AAQS) established to protect public health,

[15] 2. forecast daily atmospheric conditions so that efforts can be taken to protect personal health and reduce the emission of pollutants,

Table 1a. NOAA P-3 CalNex Flights; Dates Are Based on UTC Takeoff Times

Flight Date in 2010	Description	Coordination and Overflights
Friday, 30 April	Transit from Denver to LA; San Juan and Four Corners power plants; Phoenix urban plume	–
Tuesday, 4 May	Emissions and chemistry in the LA Basin; export to desert	Pasadena
Friday, 7 May	Southern San Joaquin Valley survey; Fresno and Bakersfield urban plumes; Harris Ranch plume; PBL heights over cultivated and fallow lands near Tulare Lake; transport layers; coastal upwelling in Morro Bay	Pasadena
Saturday, 8 May	Ships in the LA Bight; emissions and chemistry in the LA Basin; transport layers; export to desert	Pasadena
Tuesday, 11 May	Emissions from Sacramento Valley rice fields prior to flooding and planting; stratospheric intrusion; urban emissions transported into Central Valley; coastal upwelling offshore Pt. Arena	WGC tower; Pasadena; Bakersfield
Wednesday, 12 May	Oakland; Salinas, Silicon, and Northern San Joaquin Valleys; agriculture and dairy farm emissions; stratospheric intrusion; cloud study and coastal upwelling offshore Monterey	WGC tower; Pasadena; Bakersfield
Friday, 14 May	Cloud study and coastal upwelling in LA Bight; emissions and chemistry in the LA Basin	Pasadena
Sunday, 16 May	Cloud study and coastal upwelling in LA Bight; emissions and chemistry in the LA Basin; export to desert	R/V *Atlantis*; MODIS; Pasadena; NASA B200
Wednesday, 19 May	Emissions and chemistry in the LA Basin; aerosol direct radiative effects experiment; export to desert	CIRPAS Twin Otter; Pasadena; NASA B200
Friday, 21 May	Maersk vessel fuel switch experiment (flight terminated early)	Pasadena; NASA B200
Monday, 24 May	Day-into-night flight (4 P.M.–11 P.M.); southern San Joaquin Valley survey; transport layers; LA Basin survey	Pasadena; NASA B200
Sunday, 30 May	Day-into-night flight (7 P.M.–1:30 A.M.); outflow to LA Bight; LA Basin survey	NOAA Twin Otter
Monday, 31 May	Night flight (10 P.M.–4 A.M.); outflow to LA Bight; LA Basin; export to desert and Salton Sea	–
Wednesday, 2 June	Sunrise flight (1 A.M.–7 A.M.); outflow to LA Bight; LA Basin; export to desert and Salton Sea	–
Thursday, 3 June	Sunrise flight (1 A.M.–8 A.M.); outflow to LA Bight; LA Basin; export to desert and Salton Sea (7–11 *June: Redeployed to Gulf of Mexico in support of the Deepwater Horizon oil spill response*)	–
Monday, 14 June	Emissions from Sacramento Valley rice fields during growing season; PBL heights over different land use; Sacramento urban plume; cloud study and coastal upwelling offshore Pt. Arena	WGC tower; Bakersfield; Pasadena
Wednesday, 16 June	Southern San Joaquin Valley survey; Fresno and Bakersfield urban plumes; Harris Ranch plume; PBL heights over cultivated and fallow lands near Tulare Lake	Bakersfield; Pasadena
Friday, 18 June	Oakland; Salinas, Silicon, and Northern San Joaquin Valleys; agriculture and dairy farm emissions; offshore Monterey cloud study; coastal upwelling	WGC tower; DOE G1; NASA B200; NOAA Twin Otter; Bakersfield; Pasadena
Sunday, 20 June	Santa Barbara Channel; emissions and chemistry in the LA Basin; export to desert	Pasadena
Tuesday, 22 June	Transit from LA to Denver; export to desert; Las Vegas urban plume; Moapa, San Juan, and Four Corners power plants; South Fork, NM and Flagstaff, AZ forest fires; Denver urban plume	BAO tower, Erie, CO

[16] 3. track progress toward attaining the federal and state AAQS goals,

[17] 4. facilitate data analyses that improve understanding of pollutant emissions and atmospheric processes so that efforts to attain AAQS are effective, and

[18] 5. provide inputs for air quality and climate models that inform scientists and decision makers about likely impacts of potential actions within a complex system of interactions and feedbacks.

[19] In general, these measurements are made with federal reference or equivalent methods (FRM/FEM) and are subjected to defined quality assurance and quality control programs (www.arb.ca.gov/aaqm/qa/qa.htm). The primary monitoring networks with relevance to CalNex are for criteria pollutants (pollutants for which ambient air quality standards have been established), climate change pollutants (pollutants that cause the atmosphere to warm or cool over the long term, i.e., affect the radiative balance of the earth), and meteorological parameters (atmospheric conditions that can concentrate, disperse, transform, or remove pollutants).

2.1.1. Criteria Pollutant Network

[20] The State and Local Air Monitoring Station (SLAMS) network for criteria pollutants in (or near) California during CalNex in 2010 was very similar to its current configuration (www.arb.ca.gov/adam/netrpt). The gaseous pollutant network monitored O_3 at 202 sites, carbon monoxide (CO) at 120 sites, nitrogen dioxide (NO_2) at 135 sites, and sulfur dioxide (SO_2) at 83 sites. The aerosol pollutant network measured PM <2.5 microns in diameter (PM2.5) at 88 sites and <10 microns in diameter (PM10) at 182 sites. Near-real-time and historical air quality data can be accessed via the CARB Air Quality and Meteorology Information System (AQMIS; www.arb.ca.gov/aqmis2/aqmis2.php). Historical air quality data and statistics can be accessed via the CARB Aerometric Data Acquisition and Management system (www.arb.ca.gov/adam).

Table 1b. NOAA P-3 Gas-Phase Measurements

Measurement	Reference	Technique	Sample Interval	Accuracy at High S/N (±1–sigma)	Precision at Low S/N (±1–sigma)
NO, NO_2, NO_y, and O_3	*Pollack et al.* [2010], *Ryerson et al.* [1998], and *Ryerson et al.* [1999]	Gas-phase chemiluminescence	1 s	3, 4, 12, and 2%	10, 30, 40, and 15 pptv
NO_3, N_2O_5, NO, NO_2, and O_3	*Wagner et al.* [2011]	Cavity ring-down spectroscopy (CRDS)	1 s	20, 10, 5, 5, and 5%	2, 2, 70, 45, and 60 pptv
CO	*Holloway et al.* [2000]	Vacuum ultraviolet resonance fluorescence spectroscopy	1 s	5%	0.5 ppbv
CO_2, CH_4, CO, and N_2O	*Kort et al.* [2011]	Quantum cascade laser absorption spectroscopy (QCLS)	1 s	0.1 ppmv, 1, 3.5, and 0.2 ppbv	0.02 ppmv, 0.5, 0.15, and 0.1 ppbv
CO_2 and CH_4	*Peischl et al.* [2012]	Wavelength-scanned cavity ring-down spectroscopy (WS-CRDS)	1 s	0.1 ppmv and 1.2 ppbv	≤0.15 ppmv and ≤2 ppbv
HNO_3	*Neuman et al.* [2002]	SiF_5^- chemical ionization mass spectrometry (CIMS)	1 s	(15% + 40 pptv)	12 pptv
NH_3	*Nowak et al.* [2007]	Protonated acetone dimer CIMS	1 s	(30% + 170 pptv)	80 pptv
SO_2	*Ryerson et al.* [1998]	Pulsed UV fluorescence	3 s	20%	250 pptv
C_2–C_{10} NMHCs	*Colman et al.* [2001]	GC-FID of whole air samples	3–8 s	5–10%	3 pptv
C_1–C_2 halocarbons	*Schauffler et al.* [2003]	GC-MS of whole air samples	3–8 s	<10%	<0.1 pptv
C_1–C_5 alkyl nitrates	*Schauffler et al.* [2003]	GC-MS of whole air samples	3–8 s	10–20%	0.2 pptv
CH_3CN, HCHO, isoprene, aromatics, and monoterpenes	*de Gouw and Warneke* [2006]	Proton-transfer-reaction mass spectrometry (PTRMS)	1 s every 17 s	20%; (30–100% for HCHO)	
Peroxyacetyl nitrate (PAN) and $ClNO_2$	*Osthoff et al.* [2008], *Zheng et al.* [2011b]	I^- CIMS	2 s	20%	5 and 50 pptv
280–640 nm actinic flux; photolysis frequencies	*Stark et al.* [2007]	Spectrally resolved radiometry	1 s	30% $jO(^1D)$ 15% jNO_2 9% jNO_3	$3 \times 10^{-7}\,s^{-1}$ $jO(^1D)$ $3 \times 10^{-7}\,s^{-1}$ jNO_2 $2 \times 10^{-5}\,s^{-1}$ jNO_3
300–1700 nm spectrally resolved irradiance; 4.5–40 μm broadband irradiance	*Pilewskie et al.* [2003]	VIS-NIR spectrometry; IR filter radiometry	1 s	5%	<0.05 W/m^2/nm
H_2O	–	Chilled mirror hygrometry	1 s	1.0°C	1.0°C

2.1.2. Climate Change Network

[21] Two sites of the nascent CARB GHG monitoring network were in operation during CalNex: Mt. Wilson in the San Gabriel Mountains and Arvin in the southern San Joaquin Valley. The continuous measurements at that time by CARB included CO_2 and CH_4 at both sites and ancillary measurements of CO at Arvin. Other sites with longer-term monitoring records are located on the Pacific coastline and include Scripps Pier in La Jolla (southern California) and Trinidad Head, a NASA Advanced Global Atmospheric Gases Experiment (AGAGE) site and a NOAA baseline observatory, near Arcata in northern California.

2.1.3. Meteorological Network

[22] The meteorological monitoring network acquires data from a variety of federal, state, regional, and local sources. During CalNex, the long-term meteorological monitoring network included wind speed and direction at 157 sites, air temperature at 139 sites, relative humidity at 62 sites, and solar radiation at 38 sites. Current and historical meteorological data can be accessed via the AQMIS site (www.arb.ca.gov/aqmis2/metselect.php).

2.2. CALGEM Tall Tower Sites

[23] Collaborative atmospheric measurements between the California Greenhouse Gas Emissions Measurement (CALGEM; calgem.lbl.gov) and the NOAA tall tower and cooperative flask sampling networks project were made from two towers, one located on Mount Sutro (STR; 37.7553°N, 122.4517°W, base at 262 m above sea level (asl)) and one near Walnut Grove, California (WGC; 38.2650°N, 121.4911°W, base at 0 m asl) (Figure 2). Daily flask samples were collected from 91 and 485 m above ground level (agl) at STR and WGC, respectively, at 1500 Pacific Standard Time for later analysis of the major greenhouse gases (e.g., CO_2, CH_4, N_2O, and halocarbons) and a suite of other gases at the NOAA Earth Science Research Laboratory in Boulder, CO. Additionally, *in situ* instruments at WGC measured CO_2, CH_4, and CO at 30, 91, and 483 m agl on a 15 min repeat cycle. Measurements from both flask and *in situ* sampling are tied to WMO calibration scales, facilitating their use in studies of regional CH_4 and N_2O emissions from Central California [*Jeong et al.*, 2012a, 2012b].

2.3. Summer 2010 Intensive Measurements

2.3.1. Mobile Platforms

[24] (I) NOAA P-3 aircraft

[25] The NOAA P-3 was instrumented to measure a wide variety of trace gases; aerosol particle composition; microphysics; cloud nucleating and optical properties; hydrometeor concentration, size, and morphology; solar actinic fluxes; and solar irradiance (Tables 1b and 1c). In addition to instrumentation carried in prior field projects [e.g., *Brock et al.*, 2011; *Parrish et al.*, 2009], the CalNex P-3 payload included new measurements of methane (CH_4) [*Kort et al.*, 2011; *Peischl et al.*, 2012], nitrous oxide (N_2O) [*Kort et al.*, 2011], nitryl chloride ($ClNO_2$) [*Osthoff et al.*, 2008], and aerosol light absorption [*Lack et al.*, 2012b]. Seventeen P-3 research flights

Table 1c. NOAA P-3 Aerosol Measurements

Measurement	Reference	Technique	Sample Interval	Accuracy at High S/N (±1–sigma)	Precision at Low S/N (±1–sigma)
Low turbulence inlet	*Wilson et al.* [2004]	Boundary layer suppression by suction	–	–	–
Size distributions 0.004–1.0 μm (fine), 1.0–8.3 μm (coarse)	*Brock et al.* [2008]	5 parallel CPCs, and white and laser light scattering	1 s	*(See note 1)*	*(See note 1)*
Single-particle refractory black carbon mass	*Schwarz et al.* [2008]	Single-particle soot photometry (SP2)	1 s	30%	Greater of 12 ng/kg or 25%
Optical extinction (dry; 532 nm) and γ(RH)	*Langridge et al.* [2011]	Cavity ring-down spectroscopy	1 s, 10 s	<2%	4 Mm^{-1} at 10 Mm^{-1} ambient
Optical absorption (dry; 404, 532, 658 nm)	*Lack et al.* [2012b]	Laser photoacoustic spectroscopy	1 s	10%	~1 Mm^{-1}
Optical absorption (467, 530, and 660 nm) on filter media	*Bond et al.* [2004]	Particle soot absorption photometry (PSAP)	1 s	<20%	~1 Mm^{-1}
Size-resolved nonrefractory NH_4^+, NO_3^-, SO_4^{2-}, Cl^- and organic composition for PM_1	*Bahreini et al.* [2009]	Aerosol mass spectrometry (AMS)	10 s	17, 17, 18, 18, and 19%	0.06, 0.01, 0.01, 0.01, and 0.06 μg/m^3
Cloud condensation nuclei (CCN) concentration (cm^{-3} at STP) and supersaturation (%)	*Moore and Nenes* [2009] and *Roberts and Nenes* [2005]	Continuous-flow streamwise thermal-gradient CCN counter with scanning flow CCN analysis (SFCA)	1 s	10% relative in CCN cm^{-3}, 0.04% absolute in supersaturation	≤10 CCN cm^{-3}, 0.04% absolute in supersaturation
Cloud particle size distribution (0.6–50 μm)	*Baumgardner et al.* [2001]	Laser light forward and back scattering	1 s		
Cloud particle size distribution (3–50 μm)	*Lance et al.* [2010]	Laser light forward scattering	1 s		
Cloud particle size distribution (50–6000 μm), morphology	*Lance et al.* [2010]	Droplet imaging probe	1 s		
Cloud liquid water content	*King et al.* [1978]	Hot wire probe	1 s	10%	0.05 g/m^3

Note 1: Uncertainty of fine mode aerosol number is ± (9% + 14/cm^3), surface area is + (17% + 0.2 μm^2/cm^3), −(8% + 0.2 μm^2/cm^3), and volume is + (26% + 0.03 μm^3/cm^3), −(12% + 0.03 μm^3/cm^3). Uncertainty of coarse mode aerosol number is ± (20% + 0.02/cm^3), surface area is + (32% + 0.14 μm^2/cm^3), −(14% + 0.14 μm^2/cm^3), and volume is + (52% + 0.12 μm^3/cm^3), −(20% + 0.12 μm^3/cm^3).

during CalNex, totaling 127 flight hours and including five flights after dark, sampled the daytime and nighttime planetary boundary layer (PBL), marine surface layer (ML), and the overlying free troposphere (FT) throughout California and offshore (Figure 3). These flights and the transit flights to and from the P-3 base in Ontario, CA, provide data on atmospheric emissions, chemistry, transport and mixing, and removal. The NOAA Air Quality and NOAA Climate Change Programs supported these flights. The P-3 data from CalNex are publicly available at www.esrl.noaa.gov/csd/tropchem/2010calnex/P3/DataDownload.

[26] (II) CIRPAS Twin Otter aircraft

[27] The CIRPAS Twin Otter was instrumented to measure a wide variety of aerosol parameters including single-particle and bulk chemical composition,

Table 2a. CIRPAS Twin Otter CalNex Flights

Flight Date in 2010	Description	Coordination and Overflights
Tuesday, 4 May	LA Basin with missed approaches at airports throughout the Basin	–
Wednesday, 5 May	LA Basin with missed approaches at airports throughout the Basin	–
Thursday, 6 May	LA Basin after morning marine layer	–
Friday, 7 May	LA Basin	–
Monday, 10 May	LA Basin source characterization: focused on western side in clean, windy conditions	Pasadena
Wednesday, 12 May	LA Basin with outflow to Salton Sea	Pasadena
Thursday, 13 May	LA Basin with outflow to Salton Sea	Pasadena
Friday, 14 May	LA Basin	Pasadena
Saturday, 15 May	LA Basin, humid/hazy morning	Pasadena
Tuesday, 18 May	San Joaquin Valley, day after passage of a front	Pasadena; Bakersfield
Wednesday, 19 May	LA Basin	NOAA P-3; NASA B200
Thursday, 20 May	San Joaquin Valley, after cloudy morning in Bakersfield	Bakersfield; NASA B200
Friday, 21 May	LA Basin with El Cajon and Banning Pass outflows	Pasadena; NASA B200
Saturday, 22 May	San Joaquin Valley, sampling north-south line between Bakersfield and Fresno	Bakersfield; NASA B200
Monday, 24 May	LA Basin with El Cajon outflow to Apple Valley and Banning Pass outflow to Palm Springs; clear and cool, no marine layer but slight aerosol haze	Pasadena; NASA B200
Tuesday, 25 May	LA Basin with El Cajon outflow to Apple Valley and Banning Pass outflow to Palm Springs	Pasadena; NASA B200
Thursday, 27 May	LA Basin after cloudy and cool morning	Pasadena
Friday, 28 May	LA Basin with mostly clear morning	Pasadena

Table 2b. CIRPAS Twin Otter Aerosol Measurements

Measurement	Reference	Technique	Sample Interval	Accuracy at High S/N (±1–sigma)	Precision at Low S/N (±1–sigma)
Diffusion inlet	*Hegg et al*. [2005]	Two-stage diffuser	–	–	–
Dry particle size distributions: 0.005–0.2 μm and 0.015–1.0 μm	*Russell et al*. [1996] and *Wang and Flagan* [1990]	2 parallel differential mobility analyzers	1.5 min	~20%	~20%
Aerosol size distributions: 0.1–3 μm	–	Laser light forward scattering (PCASP)	1 s	~10%	~10%
Total particle number concentration	–	3 parallel CPCs	1 s	~5%	5 cm^{-3}
Size-resolved nonrefractory NH_4^+, NO_3^-, SO_4^{2-}, Cl^- and organic composition for submicron particles	*Bahreini et al*. [2009]	Aerosol mass spectrometry (AMS)	1 min	17, 17, 18, 18, and 19%	0.06, 0.02, 0.01, 0.01, and 0.08 $\mu g/m^3$
Single particle composition and size	*Pratt et al*. [2009]	Aerosol time-of-flight mass spectrometer (ATOFMS)	1 min	–	–
Water-soluble organic carbon: $D_p < 2.5$ μm	*Sullivan et al*. [2006]	Particle-into-liquid sampler coupled to a total organic carbon analyzer (PILS-TOC)	4 min	10%	0.1 $\mu g/m^3$
Cloud condensation nuclei concentration (STP cm^{-3}) and supersaturation (%)	*Moore and Nenes* [2009] and *Roberts and Nenes* [2005]	Continuous-flow streamwise thermal-gradient CCN counter employing scanning flow CCN analysis (SFCA)	1 s	10% relative in CCN cm^{-3}, 0.04% absolute in supersaturation	≤10 CCN cm^{-3}, 0.04% absolute in supersaturation
Aerosol hygroscopicity (growth factors) for 150, 175, 200, and 225 nm dry particles at 74 and 92% relative humidity	*Sorooshian et al*. [2008]	Differential aerosol sizing and hygroscopicity spectrometer probe (DASH-SP)	17–45 s	4.3%	Growth factor of 0.04–0.13
Single-particle refractory black carbon mass and coating state	*Schwarz et al*. [2008]	Single-particle soot photometry (SP2)	1 s	30%	30%
Optical absorption and scattering (405, 532, and 781 nm)	*Arnott et al*. [1999]	Photoacoustic Soot Spectrometer (PASS3)	2 s	~30%	~30%
Optical absorption (467, 530, and 660 nm) on filter media	*Bond et al*. [2004]	Particle soot absorption photometry (PSAP)	1 s	20%	~1 Mm^{-1}

hygroscopicity, microphysics, cloud nucleating, and optical properties (Table 2b). Eighteen CIRPAS Twin Otter research flights during CalNex, totaling approximately 90 h, were based in Ontario, California, and sampled the daytime PBL and overlying FT within the California South Coast Air Basin (SoCAB) containing the Los Angeles (LA) urban complex (Table 2a and Figure 4). Three of the 18 flights were to the San Joaquin Valley (SJV). These flights were supported by the NOAA Climate Change Program. Its deployment and flight plans were focused on providing data to better understand the origin, composition, hygroscopicity, and cloud nucleating behavior of aerosol particulate matter in LA, its outflow regions, and in the SJV. The CIRPAS Twin Otter was also used to investigate the effect of photochemical aging on aerosol composition and oxidation state, and the radiative implications of the regional aerosol.

[28] (III) NOAA Twin Otter aircraft

[29] The NOAA Twin Otter was equipped with the TOPAZ differential absorption lidar (DIAL) to measure vertically resolved O_3 and aerosol backscatter nadir profiles [*Alvarez et al*., 2011; *Langford et al*., 2011], a scanning Doppler lidar to measure nadir wind fields [*Pearson et al*., 2009], and an airborne multi-axis differential optical absorption spectrometer (AMAX-DOAS) to measure aerosol extinction and variety of trace gas column densities, among them nitrogen dioxide (NO_2), formaldehyde (HCHO), glyoxal (CHOCHO), and nitrous acid (HONO) [*Baidar et al*., 2012; *Volkamer et al*., 2009] (Table 3b). The NOAA Twin Otter also carried an *in situ* O_3 sensor, a radiometer to measure surface temperature and upward and downward irradiance sensors to retrieve surface albedo at 360, 479, 630, and 868 nm. Fifty-one NOAA Twin Otter research flights during CalNex, totaling 207 h, took place between 19 May and 19 July 2010. Of these, 33 flights were based in Ontario, California, and 15 were based in Sacramento, California, in coordination with the DOE CARES program [*Zaveri et al*., 2012] (Table 3a and Figure 5); three were transit flights to and from California. These flights were supported by CARB and the NOAA Air Quality Program. Its deployment and flight plans were focused on providing data to better understand the emissions sources of NO_x to the atmosphere; the three-dimensional distribution of O_3, NO_2, CHOCHO, and particulate matter in different regions of California; and the key transport processes affecting spatial and temporal distributions of these pollutants. Preliminary DIAL O_3 data from the CalNex project are publicly available at http://www.esrl.noaa.gov/csd/lidar/calnex/data_archive.

[30] Typically, the NOAA Twin Otter flew one of two generic flight plans during CalNex. Morning flights were dedicated to mapping horizontal distributions of trace gases and obtaining high-resolution vertical profiles of trace gases and the aerosol backscatter coefficient from the surface to 4 km asl at selected locations in the LA basin, including a coastal site, over the high desert, and in the Central Valley. The morning observations were primarily aimed at constraining the boundary conditions of atmospheric

Table 3a. NOAA Twin Otter CalNex Flights

Flight date in 2010	Description	Coordination and Overflights
Wednesday, 19 May	Second leg of the transit flight from Colorado to California; pollution survey over LA Basin	Pasadena
Sunday, 23 May	O_3 distribution over Southern California associated with a stratospheric intrusion	
Tuesday, 25 May A	Pollution survey over LA Basin	Pasadena
Tuesday, 25 May B	Pollution survey over LA Basin	Pasadena
Saturday, 29 May	O_3 distribution over LA Basin and Mojave Desert associated with a stratospheric intrusion	Pasadena
Sunday, 30 May	Day-into-night flight (6 P.M.–9:30 P.M.); pollutant distribution over LA Basin and LA Bight	NOAA P-3; Pasadena
Monday, 31 May A	Pollution survey over LA Basin	Pasadena
Monday, 31 May B	Pollution survey over eastern LA Basin; Doppler lidar test	
Tuesday, 1 June	Outflow of pollution from LA Basin to Mojave Desert; NO_2 comparison with OMI satellite	Pasadena
Thursday, 3 June A	Dawn flight: Pollution survey over LA Basin	Fontana-Arrow
Thursday, 3 June B	Pollution survey over LA Basin	Pasadena
Friday, 4 June	Pollution survey over LA Basin; transport to Mojave Desert and Imperial Valley	Pasadena
Saturday, 5 June A	Pollution survey over LA Basin	Pasadena
Saturday, 5 June B	Pollution survey over LA Basin; transport to Mojave Desert and Imperial Valley	
Monday, 7 June A	Pollution survey over LA Basin	Pasadena
Monday, 7 June B	Pollution survey over LA Basin; transport to Mojave Desert and Imperial Valley	Pasadena
Tuesday, 15 June A	First leg of transit flight from Ontario to Sacramento; pollution survey over Bakersfield area; NO_2 comparison with OMI satellite	Bakersfield
Tuesday, 15 June B	Second leg of transit flight from Ontario to Sacramento; pollution survey over San Joaquin Valley	
Friday, 18 June A	Pollution survey over Sacramento area and northern San Joaquin Valley	WGC tower
Friday, 18 June B	Pollution survey over San Joaquin Valley	NOAA P-3; DOE G1; NASA B200; Bakersfield
Monday, 21 June A	Pollution survey over Sacramento and east of Bay Area	
Monday, 21 June B	Pollution survey over Sacramento, southern Bay Area, and northern San Joaquin Valley	
Tuesday, 22 June A	Pollution survey over Sacramento and east of Bay Area	WGC tower
Tuesday, 22 June B	Inflow of Asian pollution over Northern Coast and Sacramento Valley; OMI	
Wednesday, 23 June	Pollution survey over Sacramento, east of Bay Area, and over Sierra Nevada Foothills	
Thursday, 24 June A	Pollution survey over Sacramento and east of Bay Area	
Thursday, 24 June B	Pollution survey over Sacramento, east of Bay Area, and over Sierra Nevada Foothills	
Saturday, 26 June	Pollution survey over Sacramento and east/south of Bay Area; transport to San Joaquin Valley, inflow of Asian pollution	WGC tower
Sunday, 27 June A	Pollution survey over Sacramento and east of Bay Area	
Sunday, 27 June B	Pollution survey over Sacramento, east of Bay Area, and over Sierra Nevada Foothills	WGC tower
Monday, 28 June	Pollution survey over Sacramento and east of Bay Area	WGC tower
Tuesday, 29 June A	First leg of transit flight from Sacramento to Ontario; pollution survey near Point Reyes, north and east of Bay Area	WGC tower
Tuesday, 29 June B	Second leg of transit flight from Sacramento to Ontario; pollution survey over San Joaquin Valley and Mojave Desert; transport of pollutants between air basins	
Wednesday, 30 June A	Pollution survey over Salton Sea, along Mexican border, and over portion of northern Mexico; cross-border pollution transport	
Wednesday, 30 June B	Pollution survey over San Diego, near Mexican border, and between San Diego and LA; cross-border pollution transport	
Friday, 2 July	Pollution survey over LA Basin; transport to Mojave Desert and Imperial Valley	Pasadena
Sunday, 4 July	Pollution survey over LA Basin; transport to Mojave Desert and Imperial Valley	Pasadena
Monday, 5 July A	Pollution survey over LA Basin and transport to Mojave Desert; OMI	Pasadena
Monday, 5 July B	Pollution survey over LA Basin; transport to Mojave Desert and Imperial Valley	Pasadena
Tuesday, 6 July	Pollution survey over LA Basin; transport to Mojave Desert and Imperial Valley	Pasadena
Monday, 12 July	Pollution survey over LA Basin and transport to Mojave Desert; OMI	Pasadena
Wednesday, 14 July	Ontario to Monterey; pollution survey over San Joaquin Valley and Sierra Nevada; transport by mountain slope flows	Bakersfield
Thursday, 15 July A	Day-into-night flight (7 PM–11 PM); Monterey to Ontario: pollution survey over San Joaquin Valley and Sierra Nevada; transport by mountain slope flows and low level jet	Bakersfield
Thursday, 15 July B	Pollution survey over LA Basin and transport to Mojave Desert	Pasadena
Friday, 16 July A	Pollution survey over LA Basin; transport to Mojave Desert and Imperial Valley	Pasadena
Friday, 16 July B	Pollution survey over LA Basin; transport to Mojave Desert and Imperial Valley	Pasadena
Saturday, 17 July	Pollution survey over LA Basin; transport to Mojave Desert and Imperial Valley	Pasadena
Sunday, 18 July A	Dawn flight: Pollution survey over LA Basin	Fontana-Arrow
Sunday, 18 July B	Pollution survey over San Diego, near Mexican border, and between San Diego and LA; cross-border pollution transport	
Monday, 19 July A	First leg of the transit flight from California to Colorado; pollution transport from LA Basin to Mojave Desert and southern Nevada	
Monday, 19 July B	Second leg of the transit flight from California to Colorado; Four Corners and San Juan Power plants	

Table 3b. NOAA Twin Otter Measurements

Measurement	Reference	Technique	Sample Interval	Accuracy at High S/N (±1–sigma)	Precision at Low S/N (±1–sigma)
O_3 profiles	*Alvarez et al*. [2011] and *Langford et al*. [2011]	Differential absorption lidar	10 s	5–10 % (up to 30% for low SNR)	< 5% (up to 15% for low SNR)
Aerosol backscatter profiles	*Davis et al*. [1999] and *White et al*. [1999]	Differential absorption lidar	10 s	~ 10 %	< 30 %
BL height	*Pearson et al*. [2009]	Differential absorption lidar	10 s	~ 50 m	~ 50 m
Line-of-sight wind speed profiles (at 4 azimuth angles)	*Pearson et al*. [2009]	Doppler lidar	2–6 s	0.1 m/s	up to 0.1 m/s
Relative aerosol backscatter profiles (1.6 μm)		Doppler lidar	1 s	uncalibrated	uncalibrated
O_3	www.twobtech.com/model_202.htm	UV light absorption	10 s	1 ppbv / 2%	1 ppbv / 2%
Temperature	www.ti.com/lit/ds/symlink/lm35.pdf	Thermistor	1 s	< 0.2 K	0.2 K
Surface temperature	www.heitronics.com/fileadmin/content/Prospekte/KT15IIP_e_V510.pdf	IR pyrometer	1 s	0.06 K	0.5 K
NO_2 vertical column density (VCD)		AMAX-DOAS	2 s	~7%	1.5×10^{15} molec cm^{-2}
NO_2, HCHO, CHOCHO vertical profiles		AMAX-DOAS	Ascent/ descent	~10%	Depends on gas and average time
Aerosol extinction profiles (360, 477, 630 nm)		AMAX-DOAS	Ascent/ descent	~5%	~ 0.01–0.03 km^{-1}
Surface albedo		4-channel UV and vis irradiance	30s	~5%	~5%

models, characterizing pollutant concentrations aloft, and testing of satellite retrievals (J. Oetjen et al., Airborne MAX-DOAS measurements over California: testing the NASA OMI tropospheric NO2 product, submitted to Journal of Geophysical Research, 2012). During afternoon flights, the plane stayed at one altitude, typically about 4 km asl, to map out the ozone, wind, and aerosol structure beneath the aircraft when photochemical production of ozone was high and to observe transport of O_3, NO_2, and aerosol into and out of the various air basins of Southern California.

[31] (IV) NASA B200 aircraft

[32] The NASA B200 King Air provided an airborne remote-sensing capability and was equipped with a high-spectral-resolution lidar (HSRL) [*Hair et al*., 2008; *Rogers et al*., 2009] to provide calibrated measurements of vertically resolved aerosol backscatter, extinction, and optical thickness (Table 4b). Mixed layer heights were also derived from the HSRL profiles of aerosol backscatter [*Fast et al*., 2012] (A.J. Scarino et al., Comparison of mixed layer heights from airborne high spectral resolution lidar, ground-based measurements, and the WRF-Chem model during CalNex and CARES, submitted to Journal of Geophysical Research, 2012). The NASA B200 also carried the Research Scanning Polarimeter (RSP) to provide total and linearly polarized reflectance in nine spectral channels [*Knobelspiesse et al*., 2011] (Table 4b). Six NASA B200 research flights based in Ontario, CA, and totaling 23 h took place between 11 May and 24 May 2010 (Table 4a and Figure 6). These flights were supported by the DOE Atmospheric Systems Research Program and the NASA Radiation Sciences and Tropospheric Chemistry Programs. Its deployment and flight plans were focused on providing data to better understand the vertical and horizontal distributions of aerosols and aerosol optical properties within and above the PBL, evaluation of

Table 4a. NASA B200 CalNex Flights

Flight date in 2010	Description	Coordination and Overflights
Wednesday, 12 May	Transit from Tucson AZ	–
Thurday, 13 May	Salton Sea and LA basin	–
Sunday, 16 May	LA Basin. San Gabriel and San Bernardino Mtns.	Pasadena; NOAA P-3
Wednesday, 19 May	LA Basin, export to desert. Catalina Is. low level cloud study	Pasadena; NOAA P-3, CIRPAS Twin Otter
Thursday, 20 May	LA Basin. Southern San Joaquin Valley	Pasadena; CIRPAS Twin Otter
Friday, 21 May	LA Basin, export to desert	Pasadena; CIRPAS Twin Otter
Saturday, 22 May	San Joaquin Valley, Salton Sea, Over water near Catalina Is., LA Basin	Pasadena; CIRPAS Twin Otter
Monday, 24 May	LA Basin. Salton Sea. Catalina Is.	Pasadena; CIRPAS Twin Otter
Tuesday, 25 May (3–28 *June*)	LA Basin. Salton Sea, Southern San Joaquin Valley, Transit to Sacramento (*Redeployed to Sacramento for DOE CARES Mission; see Zaveri et al*. [2012])	Pasadena; CIRPAS Twin Otter
Monday, 14 June (Flight 2 on this day)	Sacramento urban plume, SF Bay area inflow	NOAA P-3; DOE T0, T1 sites
Friday, 18 June	Sacramento, Northern San Joaquin Valley, Intercomparison	NOAA P-3; DOE G1; DOE T0, T1 sites

Table 4b. NASA B200 Measurements

Measurement	Reference	Technique	Sample Interval	Measurement Precision	Bias/Systematic Uncertainty
Backscatter Ratio (532 nm)	*Hair et al.* [2008]	High spectral resolution lidar	10 s	5%	0.01
Backscatter coefficient (532 and 1064 nm)	*Hair et al.* [2008]	High spectral resolution lidar	10 s	5%	0.16 (Mm-sr)$^{-1}$ (532 nm)
Extinction coefficient (532 nm)	*Hair et al.* [2008]	High spectral resolution lidar	1 min	10%	10 Mm^{-1}
Depolarization Ratio (532 and 1064 nm)	*Hair et al.* [2008]	High spectral resolution lidar	10 s	3%	0.004
Aerosol Optical Thickness (532 nm)	*Hair et al.* [2008]	High spectral resolution lidar Research scanning polarimeter	1 min	10%	0.02

CALIPSO satellite instrument retrieval algorithms, providing vertical context for *in situ* measurements on other CalNex aircraft, and using those *in situ* measurements to evaluate new combined (active + passive) aerosol retrieval algorithms. B200 flights during its deployment from Ontario were highly coordinated with the NOAA P-3 to maximize the overlap between the *in situ* and remotely sensed data provided by the two aircraft.

[33] Following its deployment in collaboration with CalNex, the NASA B200 continued research flights in California from 4 June to 28 June 2010 in conjunction with the DOE CARES study based in Sacramento, CA [*Zaveri et al*., 2012].

[34] (V) WHOI R/V *Atlantis*

[35] The Woods Hole Oceanographic Institute (WHOI) R/V *Atlantis* provided both *in situ* and remote-sensing capabilities and was instrumented to measure a wide variety of trace gases; aerosol particle composition; microphysics; cloud nucleating and optical properties; hydrometeor concentration, size, and morphology; solar actinic fluxes; solar irradiance; and meteorological and cloud parameters (Table 5b and 5c). The R/V *Atlantis* research cruise took place offshore California between 15 May and 8 June 2010 (Table 5a and Figure 6). This cruise was supported by the NOAA Climate Change Program. Its deployment and cruise tracks were focused on providing data to better understand atmospheric emissions from oceangoing shipping and port facilities, the chemistry of SOA formation in the clean and polluted marine boundary layer (MBL), nighttime halogen chemistry involving chloride-containing aerosols, the radiative and cloud microphysical effects of atmospheric aerosols, and the production and flux of sea spray particles to the atmosphere. The R/V *Atlantis* gas-phase data from the CalNex project are available at http://www.esrl.noaa.gov/csd/tropchem/2010calnex/Atlantis/DataDownload, and the aerosol data are available at http://saga.pmel.noaa.gov/data.

2.3.2. Surface Sites

[36] (I) Pasadena

[37] The CalNex Los Angeles (CalNex-LA) ground site was located on the campus of the California Institute of Technology (Caltech) in Pasadena, approximately 18 km northeast of downtown Los Angeles (34.1408°N, 118.1223°W, 230 m asl) (Figure 2). Measurements were made from 15 May to 16 June 2010. Close to 40 research groups participated at the field site, providing measurements of an extensive suite of atmospheric species (Tables 6a, 6b, 6c).

[38] *in situ* gas-phase measurements, including observations of radicals, reactive nitrogen compounds, volatile organic compounds (VOCs), oxygenated VOCs, O_3, CO, CO_2, and solar actinic fluxes, were made from one of two 10 m high scaffolding towers located on an empty campus parking lot.

[39] Remote sensing of O_3, NO_2, NO_3, HONO, HCHO, and SO_2 was performed at five height intervals (covering 32–550 m agl) by long-path differential optical absorption spectroscopy (DOAS) between the roof of the Caltech Millikan library and the mountains 5–7 km northeast of the library building. The library roof also housed *in situ* NO_2 and CHOCHO measurements as well as a multi-axis DOAS system. Good agreement between *in situ* and long-path observations of O_3, NO_2, and SO_2 showed that the ground site was generally representative for the larger area around Caltech, except for a few nights when near-surface air was isolated from air masses aloft. Only sporadically were very local emissions from vehicles close to the sampling site found to impact the measurements. The main ground site also hosted an aerosol backscatter ceilometer that provided a measurement of the local boundary layer height [*Haman et al*., 2012].

[40] A large number of aerosol instruments (Tables 6b and 6c) sampled from a second 10 m high scaffolding tower or from the top of their respective laboratory trailers at the main ground site. The instruments included standard measurements of aerosol size distributions, aerosol mass spectrometers, aerosol extinction measurements, and more experimental instrumentation described elsewhere in this issue.

[41] Fourteen aerosol samplers were also operated on the roof of a three-story (12 m) building on the Caltech campus and were co-located with an extensive suite of meteorological measurements including turbulent momentum and heat fluxes (Table 6c).

[42] (II) Bakersfield

[43] The CalNex Bakersfield sampling site was located at the Kern Cooperative Extension compound in the southern part of the city (35.35°N, 118.97°W, 20 m asl) (Figure 2). Bakersfield is located in the southern portion of the SJV and is bordered on the west by the Coastal Range (~50 km), on the east by the Sierra Nevada Mountains (~25 km), and on the south by the Tehachapi Mountains (~25 km). Measurements were made from 19 May to 28 June 2010. More than 15 research groups participated at the field site, providing measurements of an extensive array of gas-phase and particle-phase species (Tables 7a and 7b).

[44] Meteorological measurements included relative humidity, wind speed and direction, and photosynthetically active radiation. *In situ* gas-phase measurements, including measurements of radicals, ozone, reactive nitrogen species,

Table 5a. WHOI R/V *Atlantis* Sampling Locations

Category	Start Time, UTC	End Time, UTC	Details
Offshore/background (clean marine) air	14 May/1800	15 May/1130	Transit San Diego to Santa Monica Bay
	16 May/1800	16 May/2300	Coordinated cloud study with P-3 aircraft
	23 May/0000	23 May/0800	Catalina Island
	23 May/1530	23 May/2000	Catalina Island
	25 May/1730	26 May/0130	Shipping lanes off Santa Monica Bay
	27 May/1930	28 May/0130	Sea lanes south of Pt. Fermin
	30 May/0600	30 May/0730	Catalina Island; P-3 flyover at 0710
	30 May/2300	31 May/0530	West of Santa Barbara
	01 June/0200	02 June/0000	Transit Santa Barbara to Monterey Bay
	02 June/0000	02 June/1700	Monterey Bay
	02 June/1700	02 June/2330	Transit Monterey Bay to Golden Gate
	06 June/1900	07 June/1900	Farallon Islands; whales
Santa Monica Bay; LAX approaches	15 May/1130	16 May/1500	Santa Monica Bay 1–5 nm offshore
	17 May/0130	17 May/0730	Santa Monica Bay 1–5 nm offshore
	21 May/1000	21 May/2000	Santa Monica Bay 1–5 nm offshore
	24 May/0600	24 May/2130	Santa Monica Bay 1–5 nm offshore
	25 May/0530	25 May/1700	Santa Monica Bay 1–5 nm offshore
	29 May/0500	29 May/1600	On station west of Palos Verdes Pt.
	29 May/1600	30 May/0400	Transit Santa Monica Bay coastline
	30 May/0800	30 May/1300	Santa Monica Bay near Palos Verdes
	30 May/1830	30 May/2130	Transit Santa Monica Bay coastline
Santa Barbara Channel area	18 May/0930	18 May/2200	Off Port Hueneme
	31 May/0800	31 May/1500	Off Ventura
	31 May/1900	01 May/0200	Off Santa Barbara; methane seeps
Los Angeles/Long Beach harbors	20 May/1600	20 May/2000	Transit LA harbor to Long Beach harbor and return
	22 May/0200	22 May/2200	LA harbor; cruise ship terminal
	26 May/1630	27 May/1600	LA harbor; west basin
	27 May/1600	27 May/1730	Transit through Long Beach harbor to San Pedro Bay
	28 May/1300	28 May/2030	San Pedro Bay; LA harbor; media event at dock
San Pablo Bay; San Francisco/Oakland harbors	03 June/0000	03 June/0300	Golden Gate to Martinez/San Pablo Bay
	06 June/0100	06 June/1530	East of Martinez at Anchorage 26
	06 June/1530	06 June/1900	Transit Anchorage 26 to Golden Gate
	06 June/1900	07 June/2330	Oakland harbor
	07 June/2330	08 June/1400	Anchored east of San Francisco
Sacramento River transits; Sacramento harbor	03 June/1530	03 June/2200	Transit Martinez to W. Sacramento/DOE G-1 at 2005
	03 June/2200	04 June/2230	West Sacramento turning basin
	04 June/2230	05 June/0400	Transit south and back to West Sacramento
	05 June/1930	06 June/0100	Transit from West Sacramento to Anchorage 26
Marine vessel emission studies	17 May/1300	18 May/0000	Santa Barbara/Port Hueneme ships and oil platforms
	18 May/0000	18 May/0400	NOAA R/V *Miller Freeman*
	19 May/0530	20 May/1600	San Pedro Bay anchorage
	23 May/1000	23 May/1500	San Pedro Bay shipping lanes
	23 May/2200	24 May/0330	San Pedro Bay shipping lanes
	24 May/2230	25 May/0230	San Pedro Bay shipping lanes
	25 May/0300	25 May/0345	Offshore; *Margrethe Maersk* experiment
	26 May/0800	26 May/1500	East of San Pedro Bay shipping lanes
	28 May/0330	28 May/1300	San Pedro Bay; Huntington Beach
	29 May/0200	29 May/0300	San Pedro Bay shipping lanes; cruise ship
	30 May/1300	30 May/1400	Offshore; *Mathilde Maersk* experiment
Ocean-derived aerosol studies	14 May/2150	15 May/0110	Off La Jolla
	15 May/2230	16 May/0155	Santa Monica Bay
	18 May/1600	18 May/2200	South of sea lanes off Port Hueneme
	23 May/0120	23 May/0550	South of Catalina Island
	23 May/1510	23 May/1930	South of Catalina Island
	24 May/1800	24 May/2100	Santa Monica Bay
	25 May/1900	26 May/0110	Sea lanes south of Pt. Dume
	27 May/1930	28 May/0115	Sea lanes south of Pt. Fermin
	30 May/2330	31 May/0510	South of sea lanes off Port Hueneme
	31 May/2325	01 June/0155	Off Santa Barbara
	06 June/2030	07 June/0200	Southeast of Farallon Islands

VOCs, CO_2, N_2O, and CH_4, were made from various heights on the 20 m high scaffolding tower located at the sampling site. A large number of aerosol instruments also sampled from the tower or from the tops of laboratory trailers that were located surrounding the tower. The instruments included an aerosol mass spectrometer, a Sunset Labs EC/OC instrument, and instruments to measure chemically speciated organics, organic nitrates, and water-soluble anions and cations. Multiple high-volume aerosol samplers were also operated at the base of the tower to provide filter samples for off-line analysis of organic compounds, organosulfates, and nitroxyorganosulfates.

[45] (III) Mt. Wilson

[46] Mt. Wilson is located in the San Gabriel Mountains 26 km northeast of downtown Los Angeles and immediately north of the LA basin (Figure 2). The Mt. Wilson Observatory

Table 5b. WHOI R/V *Atlantis* Gas-Phase Measurements

Measurement	Reference	Technique	Sample Interval	Accuracy at High S/N (±1–sigma)	Precision at Low S/N (±1–sigma)
NO, NO_2	*Lerner et al.* [2009]	Gas-phase chemiluminescence; LED photolysis	1 min	4%, 11%	0.020 ppbv, 0.030 ppbv
NO, NO_2	*Fuchs et al.* [2009]	Cavity ring-down spectroscopy (CRDS)	1 min	3%, 3%	0.10, 0.10 ppbv
N_2O_5	*Wagner et al.* [2011]	Cavity ring-down spectroscopy (CRDS)	1 min	10%	2 pptv
NO_y	*Williams et al.* [2009]	Gas-phase chemiluminescence; heated Au tube	1 min	25%	0.050 ppbv
O_3	*Williams et al.* [2006b]	UV absorption; gas-phase chemiluminescence	1 min, 1 min	2%, 2%	1 ppbv, 0.1 ppbv
O_3	*Bates et al.* [2008]	UV absorption	1 min	2%	1 ppbv
$ClNO_2$ and Cl_2	*Kercher et al.* [2009]	Chemical Ionization Mass Spectrometry (I^-)	5 min	30%	2 and 11 pptv
HCOOH and HCl	*Bertram et al.* [2011]	Chemical Ionization Mass Spectrometry (ToF-CIMS)	1 s	<30% and <50%	15 pptv
H_2O_2	*Lee et al.* [1995]	Aqueous collection, HPLC separation, fluorescence detection	30 s every 150 s	(5% + 10 pptv)	10 pptv
CH_3OOH	*Lee et al.* [1995]	Aqueous collection, HPLC separation, fluorescence detection	30 s every 2.5 m	(10% + 20 pptv)	20 pptv
CH_2O	*Heikes* [1992]	Aqueous collection, fluorescence detection	1 min	(10% + 25 pptv)	25 pptv
CO	*Lerner et al.* [2009]	Vacuum ultraviolet resonance fluorescence spectroscopy	1 min	3%	1 ppbv
CO_2	*Lerner et al.* [2009]	Nondispersive infrared absorption spectroscopy	1 min	0.08 ppmv	0.07 ppmv
SO_2	*Williams et al.* [2009]	Pulsed UV fluorescence	1 min	10%	0.13 ppbv
SO_2	*Bates et al.* [2008]	Pulsed UV fluorescence	1 min	5%	0.10 ppbv
C_2–C_7 NMHCs	*Bon et al.* [2011]	In situ GC-FID	30 min	= ~ 10%	~2 pptv
$(CH_3)_2S$, CH_3CN, isoprene, methanol, acetone, acetaldehyde, aromatics, and monoterpenes	*de Gouw and Warneke* [2006]	Proton-transfer-reaction mass spectrometry (PTRMS)	1 min	20%	(18,23,33,267,37, 99,14,31 pptv)
HCHO, OCS	*Herndon et al.* [2007]	Quantum cascade laser absorption spectroscopy (QCLS)	1 min, 1 min	7%, 15%	75 pptv, 10 pptv
Gaseous elemental mercury (GEM)	*Landis et al.* [2002]	Cold vapor atomic fluorescence spectroscopy (CVAFS)	5 min	5%	25 pg Hg m^{-3}
H_2O	–	chilled mirror hygrometry	1 s	1.0°C	1.0°C
Radon	*Whittlestone and Zahorowski* [1998]	Radon gas decay	13 min		
280–640 nm actinic flux; photolysis frequencies	*Stark et al.* [2007]	3-wavelength filter radiometry	1 min	30% $jO(^1D)$ 15% jNO_2 9% jNO_3	3 x10^{-7} s^{-1} $jO(^1D)$ 3 x10^{-7} s^{-1} jNO_2 2 x10^{-5} s^{-1} jNO_3
300–1700 nm spectrally resolved irradiance; 4.5–40 μm broadband irradiance	*Pilewskie et al.* [2003]	VIS-NIR spectrometry; IR filter radiometry	1 s	5%	<0.05 W/m^2/nm

(34.22°N, 118.06°W, 1770 m asl) provided a high-altitude site for both *in situ* and remote-sensing measurements. Samples at this site routinely show a strong diurnal trend in many trace gases [*Gorham et al.*, 2010]. Maxima in carbon monoxide (CO) and urban hydrocarbons are typically observed during the afternoon, when upslope flows transport boundary-layer air from the western LA basin to the site. Conversely, minima in these species are typically observed at this site after dark, when surface cooling inhibits upslope flow and the top of the boundary layer has subsided below the height of the Observatory. Downslope or synoptic flow then typically advects cleaner air to the site, resulting in different sampling footprints for daytime and nighttime samples. However, the variability within just daytime samples provides a measure of atmospheric emissions ratios of urban pollutants, integrated over the upwind western LA basin, for species that are conserved over the relevant atmospheric transport time scales [*Gorham et al.*, 2010; *Hsu et al.*, 2010].

[47] Whole-air samples were taken at Mt. Wilson twice per day at approximately 0200 and 1400 Pacific standard time beginning on 30 April 2010 and continued beyond the conclusion of the CalNex field project. Samples were returned to the NOAA Global Monitoring Division laboratory in Boulder, CO, and analyzed for a variety of halocarbon, hydrocarbon, greenhouse, and other gases (Table 8).

[48] Spatial distributions of carbon dioxide (CO_2), CH_4, N_2O, CO, NO_2, HCHO, and aerosol extinction in the Los Angeles basin were measured from the NASA-Jet Propulsion Laboratory (JPL) California Laboratory for Remote Sensing (CLARS) at Mt. Wilson by remote-sensing Fourier transform spectroscopy (FTS) in a joint project of the JPL and the University of California-Los Angeles (UCLA). This project was supported by NASA, NOAA, and CARB. Data were obtained

Table 5c. WHOI R/V *Atlantis* Aerosol, Cloud, Meteorological, and Seawater Measurements

Measurement	Reference	Technique	Sample Interval	Accuracy at High S/N (±1–sigma)	Precision at Low S/N (±1–sigma)
Aerosol number concentration	*Bates et al.* [2001]	CNC (TSI 3010, 3025)	1 s	10%	
Aerosol size distributions 0.02–10 μm	*Bates et al.* [2005]	Parallel Aitken DMPS, accumulation mode DMPS, and an Aerodynamic Particle Sizer	5 min	10%	
Aerosol thermal volatility 0.02–0.5 μm at 230°C	*Bates et al.* [2012] and *Russell et al.* [2009]	Parallel (heated and unheated) SMPSs	5 min	10%	
Sub-1 and sub-10 μm scattering and backscattering (450, 550, 700 nm) and γ(RH)	*Quinn and Bates* [2005]	Parallel TSI 3563 Nephelometers	1 min	14%	0.13 Mm^{-1}
Sub-1 and sub-10 μm optical extinction (405, 532, 662 nm) and γ(RH)	*Baynard et al.* [2007] and *Langridge et al.* [2011]	Cavity ring-down spectroscopy	2–5 s	<2%	0.5 Mm^{-1} at 532 nm (varies with)
Sub-1 and sub-10 μm optical absorption (dry: 406, 532 nm; thermodenuded: 406, 532 nm)	*Lack et al.* [2012b]	Laser photoacoustic spectroscopy	2 s	10%	~1 Mm^{-1}
Sub-1 and sub-10 μm optical absorption (467, 530, and 660 nm) on filter media	*Bond et al.* [1999]	Particle soot absorption photometry (PSAP)	1 s	>20%	~1 Mm^{-1}
Aerosol Optical Depth	*Quinn and Bates* [2005]	Microtops sun photometer	Intermittent	20%	0.015 at 500 nm
Single-particle refractory black carbon mass and coating state	*Schwarz et al.* [2008]	Single-particle soot photometry (SP2)	1 s	40%	greater of 12 ng/kg or 25%
Concentration of BC nonrefractory coating material	*Cappa et al.* [2012]	Soot Particle Aerosol Mass Spectrometer (SP-AMS)	1 min		0.03 $\mu g/m^3$
Volatility and hygroscopicity of aerosol particles (50, 100, and 145 nm)	*Villani et al.* [2008]	Volatility-hygroscopicity tandem differential mobility analyzer	20 min	0.05 units in growth factor	
Air ion size distribution (0.8–0.42 nm)	*Mirme et al.* [2007]	Air ion spectrometer	1.5 min	10^1 $/cm^{-3}$	
Cloud condensation nuclei concentration for sub-1 μm aerosol at five supersaturations	*Quinn et al.* [2008]	Continuous-flow thermal-gradient CCN counter	5 min	10%	5 cm^{-3}
Cloud condensation nuclei concentration for 60 nm aerosol at five supersaturations	*Quinn et al.* [2008]	Continuous-flow thermal-gradient CCN counter coupled with an SMPS	5 min	10%	5 cm^{-3}
Sub-1 and sub-10 μm composition of inorganic ions, trace elements, OC, EC and total aerosol mass	*Bates et al.* [2008]	Impactors with IC, XRF, thermal-optical, and gravimetric analysis	3–16 h	6–31%	
Sub-1 μm alkane, hydroxyl, amine, and carboxylic acid functional groups and total submicron mass	*Russell et al.* [2009]	Fourier transform infrared (FTIR) spectroscopy	3 to 16 h	20%	0.09, 0.02, 0.01, and 0.008 μmol of bond
Size-resolved chemistry of single particles	*Gard et al.* [1997]	Aerosol time-of-flight Mass Spectrometry (ATOFMS)	300 s	15–20%	N/A
Cloud liquid water path	*Turner et al.* [2007]	Microwave radiometer	15 s	N/A	N/A
Cloud-base height	*Fairall et al.* [1997]	Ceilometer	15 s		30 m
Cloud structure and precip	*Lhermitte* [1987]	W band cloud radar	1 hr		
Temperature/RH profiles	*Wolfe et al.* [2007]	Radiosondes	5 s		0.3°C and 4%
Wind profiles	*Law et al.* [2002]	915 MHz wind profiler	5 min		1.4 $m\,s^{-1}$
Wind profiles/microscale turbulence	*Frisch et al.* [1989]	C band radar	5 min		1.0 $m\,s^{-1}$
High resolution boundary layer turbulence structure		Doppler mini-Sodar			
Turbulent fluxes	*Bradley and Fairall* [2006]	Bow-mounted eddy covariance	20 s, 10 min, 1 hr		25% at 1 h
Seawater DMS	*Bates et al.* [2000]	Sulfur chemiluminescence	15 min	8%	0.2 nM

on 31 noncloudy days from 14 May to 20 June 2010 and continued beyond the conclusion of the CalNex field project.

[49] (IV) Radar wind profiler network

[50] Twenty Doppler radar wind profilers [e.g., *Carter et al.*, 1995] from the Physical Sciences Division (PSD) at NOAA and from cooperative agencies in California were available for the CalNex study (Table 10 and Figure 2). These instruments provided hourly averaged wind profile measurements from ~120 m agl up to ~4 km or higher, depending on atmospheric conditions. Radio acoustic sounding systems (RASS) [*May et al.*, 1990] were operated in conjunction with nineteen of the wind profilers to measure temperature profiles up to ~1.5 km. The vertical resolutions of both the wind and temperature measurements were 60, 100, or 200 m depending on instrument operating configurations. The wind profile observations were quality controlled after the data collection period using the continuity technique [*Weber et al.*, 1993] and by visual inspection (final wind profiler datasets are available at ftp://ftp1.esrl.noaa.gov/users/tcoleman/CalNex2010/). During CalNex, NOAA PSD provided an online tool (www.esrl.noaa.gov/psd/programs/2010/calnexqc/traj/; *White et al.*, [2006]) that used

Table 6a. Pasadena ground site gas-phase measurements

Measurement	Reference	Technique	Sample Interval	Accuracy at High S/N (±1–sigma)	Precision at Low S/N (±1–sigma)
O_3, NO_2, SO_2, NO_3, HONO, HCHO profiles	*Wang et al.* [2006]	Long-path differential optical absorption spectrometry (DOAS)	30 min	3, 4, 3, 10, 5, and 5%	0.8 ppbv and 60, 25, 1.2, 23, and 170 pptv
C_2–C_{10} NMHCs	*Kuster et al.* [2004]	GC-MS			
C_1–C_2 halocarbons	*Kuster et al.* [2004]	GC-MS			
O_3		UV absorption			
NO, NO_2, and NO_y	*Drummond et al.* [1985], *Pollack et al.* [2010], and *Williams et al.* [1988]	Gas-phase chemiluminescence	10 s		
SO_2		Pulsed UV fluorescence			
CO	*Gerbig et al.* [1999]	Vacuum ultraviolet resonance fluorescence spectroscopy		4%	0.2 ppbv
CO_2	*Peischl et al.* [2010]	NDIR absorption	1 min	0.14 ppmv	0.02 ppmv
CO_2 and $^{13}CO_2$		WS-CRDS		0.10 ppmv and 0.35 ‰	
NO_2	*Fuchs et al.* [2009]	CRDS	1 min	3%	4 pptv
HONO and CHOCHO	*Washenfelder et al.* [2008]	Incoherent broadband cavity-enhanced absorption spectrometry	10 min	15 and 30%	13 and 52 pptv
HNO_3, HONO, HNCO, and organic acids	*Veres et al.* [2008]	Negative-ion proton-transfer chemical ionization mass spectrometry	1 min	30%	40 pptv
PAN and $ClNO_2$	*Mielke et al.* [2011]	I^- CIMS			
PAN	*Flocke et al.* [2005]	GC-electron capture detection (ECD)			
HCHO		Liquid-phase fluorescence using the Hantzsch reaction			
HO, HO_2, and HO reactivity	*Dusanter et al.* [2009]	Laser-induced fluorescence			
280–420 nm actinic flux; photolysis frequencies	*Shetter and Müller* [1999]	spectrally resolved radiometry			
Volatile and semivolatile organic compounds	*Holzinger et al.* [2010]	High resolution proton transfer reaction time-of-flight mass spectrometry			
Water-soluble gas-phase organic carbon	*Hennigan et al.* [2008]	Mist chamber and online TOC measurement			
Total gas-phase volatile and semivolatile organic carbon		High-resolution electron impact time-of-flight mass spectrometry			
Gas-phase semivolatile organic carbon		Sorbent tubes and offline solvent extraction with GC-MS	3 hr	22%	10–80 pptv
Meteorology and eddy covariance					
NO_2, HCHO, HONO, CHOCHO	*Coburn et al.* [2011]	Multi-axis DOAS	5 min	5, 10, 10, and 10%	(2.5, 10, 3, and 1.5) × 10^{14} molec/cm^2 vertical column density
CH_3CN, isoprene, aromatics, and monoterpenes	*Warneke et al.* [2005]	Proton-transfer ion trap mass spectrometry	5 min	15–25%	15–120 pptv
NH_3	*Ellis et al.* [2010]	Quantum cascade tunable infrared laser differential absorption spectrometry			
NO_2 and CHOCHO	*Thalman and Volkamer* [2010]	Light-emitting-diode cavity-enhanced DOAS	1 min	5%	11 and 7 pptv
HONO		Wet chemical derivitization/HPLC	10 min	6%	10 pptv

real-time observations from the profiler network to calculate forward or backward trajectories. The trajectory tool was used during the study to assist with flight mission planning and, following the study and using the quality controlled wind profiles, to illustrate regional transport patterns and quantify pollution source apportionment.

2.3.3. IONS-2010 Ozonesonde Network

[51] The Intercontinental Chemical Transport Experiment Ozonesonde Network Study (IONS)-2010 network [*Cooper et al.*, 2011] was implemented during CalNex to better define baseline O_3 from the surface to the tropopause along the US west coast. IONS-2010 was supported by the NOAA Health of the Atmosphere Program, the NASA Tropospheric Chemistry Program, the U. S. Navy, Environment Canada, and the NOAA National Air Quality Forecast Capability. Ozonesondes were launched in the mid-afternoon Pacific time 6 days per week (Monday–Saturday) between 10 May and 19 June 2010 from the network of seven sites, one in southern British Columbia and six in California including Trinidad Head, where ozonesondes have been launched on a

Table 6b. Pasadena Ground Site Continuous and Semicontinuous Aerosol Measurements

Measurement	Reference	Technique	Sample Interval	Accuracy at High S/N (±1–sigma)	Precision at Low S/N (±1–sigma)
Size-resolved nonrefractory NH_4^+, NO_3^-, SO_4^{2-}, Cl^- and organic composition for PM_1	*DeCarlo et al.* [2006]	High-resolution time-of-flight aerosol mass spectrometry (HR-ToF-AMS)	5 min	30%	10–100 ng/m^3
Potential aerosol mass	*Kang et al.* [2007]	AMS and SMPS following exposure of ambient air to OH			
Submicron number distribution		Scanning mobility particle sizing	5 min	5% for size; 15% for concentration	
Submicron number distribution		UHSAS	1 min		
Total particle number		Condensation particle counter	1 min		
Number distribution (300 nm–10 μm)		Optical particle counter	1 min		
Submicron aerosol volatility	*Huffman et al.* [2008]	Thermal denuder with AMS and SMPS	2 h		
Organic and elemental carbon		Thermal-optical analysis	1 h		
Water-soluble organic carbon	*Weber et al.* [2001]	Particle-into-liquid sampling and TOC measurement (PiLS-TOC)	10 min		
Carboxylic acids for aerodynamic diameter < 2.5 μm		PiLS-ion chromatography			
Speciated organic composition	*Canagaratna et al.* [2007] and *Williams et al.* [2006a]	Combined thermal desorption aerosol GC-MS (TAG) and HR-ToF-AMS: TAG-AMS	1 h		
Speciated organic composition	*Worton et al.* [2012]	Two-dimensional TAG	2 h		
Speciated organic composition	*Holzinger et al.* [2010]	High-resolution PTR-TOF-MS			
Water-soluble organic- and nitrogen-containing compounds	*Bateman et al.* [2010]	PiLS followed by high-resolution electrospray ionization mass spectrometry	30 min		
Single-particle refractory black carbon mass and coating state	*Schwarz et al.* [2008]	Single-particle soot photometry (SP2)	5 min	2.5%	10%
Single-particle refractory black carbon mass and coating composition	*Onasch et al.* [2012]	SP-AMS	5 min		
Black carbon mass	*Arnott et al.* [2005]	Aethalometry	5 min	45%	50%
Optical absorption	*Arnott et al.* [2006]	Photoacoustic soot spectrometer	5 min	0.7 Mm^{-1} at 532 nm	5% at 532 nm
Optical extinction (523 and 630 nm)	*Massoli et al.* [2010]	Cavity-attenuated phase shift spectroscopy	1 s	0.8 Mm^{-1}	5%
Aerosol extinction, scattering, and albedo	*Dial et al.* [2010] and *Thompson et al.* [2012]	CRDS/integrating sphere nephelometry	1 min	1–2 Mm^{-1}	
Single-particle optical size and single-scattering albedo at 672 nm	*Sanford et al.* [2008]	Laser scattering and extinction in a high-Q cavity			
Single-particle composition and number fractions for particle classes	*Froyd et al.* [2009] and *Murphy et al.* [2006]	Particle analysis by laser mass spectrometry (PALMS)		15% for particle classificiation number fraction	
Single-nanoparticle composition	*Zordan et al.* [2008]	Nano-aerosol mass spectrometer			

Table 6b. (continued)

Measurement	Reference	Technique	Sample Interval	Accuracy at High S/N (±1–sigma)	Precision at Low S/N (±1–sigma)
Size-resolved cloud condensation nuclei	*Roberts and Nenes* [2005]	Continuous-flow streamwise cloud condensation nuclei (CCN) spectrometry			
Vertically resolved backscatter (355, 532, and 1064 nm)	*Kovalev et al.* [2009]	Scanning LIDAR			
Column aerosol optical depth	*Holben et al.* [2001]	AERONET sun photometry			
Boundary layer backscatter and mixing height	*Haman et al.* [2012]	Aerosol backscatter gradient ceilometer	5 min	20 m (stable conditions) to 100 m (unstable conditions)	2 m (stable conditions) to 20 m (unstable conditions)
Size-resolved particle number concentrations for $0.5 < D < 5\ \mu m$	Hayes et al. [2012]	White-light optical particle counter	10 s		

weekly basis since 1997 by NOAA GMD (Figure 2). This network was implemented to provide data on pathways, abundance, and latitudinal variation of O_3 transported into the continental U.S.; determine the influence of PBL processes on transport of FT O_3 to the surface [*Parrish et al.*, 2010]; and provide an extensive data set for evaluation of O_3 simulations by chemical transport models and O_3 retrievals from satellites [*Cooper et al.*, 2011; *Lin et al.*, 2012a, 2012b].

2.3.4. Satellite Observations With Relevance to CalNex

[52] An integrated, multiplatform, and multisensor approach that combined *in situ* and remotely sensed data from surface, aircraft, and satellite with numerical model simulations was essential to accomplish several of the stated science objectives of CalNex. This integrated approach was exemplified by coordinated cloud optical and microphysical measurements in persistent stratus cloud decks offshore, using simultaneous measurements from *in situ* and remote-sensing instruments onboard the R/V *Atlantis*, the P-3 aircraft, and NOAA and NASA satellites. A combination of *in situ* and remotely sensed measurements from the P-3 and the *Atlantis* was used to validate stratus cloud drop effective radius retrievals from solar spectral flux radiometers (SSFRs) carried aboard both platforms. In turn, the SSFR retrievals were used to validate cloud optical thickness and effective radius retrievals from sensors aboard the NOAA Geostationary Operational Environmental Satellite (GOES) and the Moderate Resolution Imaging Spectroradiometer (MODIS) aboard the NASA Terra satellite [*McBride et al.*, 2012]. Further, GOES cloud fractions from Pathfinder Atmospheres Extended (PATMOS-x) retrievals [*Heidinger et al.*, 2012] were used to assess the fidelity of high-resolution Weather Research and Forecasting (WRF) and Naval Research Laboratory (NRL) Coupled Ocean/Atmosphere Mesoscale Prediction System (COAMPS) model coastal cloud forecasts [*Angevine et al.*, 2012]. These regional forecast models provided key input information for deployment and optimal coordination of the research vessel and aircraft during CalNex.

[53] Satellite data also contributed to CalNex planning activities through real-time assimilation of satellite O_3 and aerosol retrievals. O_3 profiles retrieved from microwave limb sounder (MLS) measurements [*Froidevaux et al.*, 2008; *Livesey et al.*, 2008] and aerosol optical depth (AOD) retrievals from MODIS measurements [*Chu et al.*, 2002; *Remer et al.*, 2005] were assimilated within the Real-time Air Quality Modeling System (RAQMS) [*Pierce et al.*, 2010; *Pierce et al.*, 2007] which provided daily chemical and aerosol forecasts at $2^\circ \times 2^\circ$ resolution of long-range transport for CalNex planning activities. Data denial experiments during CalNex demonstrated the positive impact of MLS O_3 profile and MODIS AOD assimilation on RAQMS forecasts.

3. Meteorological Context for the CalNex Study Period

[54] Local land-sea breeze and mountain valley circulations drive much of the pollutant transport in California [*Bao et al.*, 2008; *Langford et al.*, 2010; *Lu and Turco*, 1996]; however, synoptic-scale meteorology significantly influences both transport patterns and photochemical processing. This section provides an overview of the overall climate and synoptic weather patterns during CalNex. *Fast et al.* [2012] provided

Table 6c. Pasadena Ground Site Aerosol Sampler Measurements

Measurement	Reference	Technique	Sample Interval	Accuracy at High S/N (±1–sigma)	Precision at Low S/N (±1–sigma)
Organosulfates and Nitrated Organosulfates	*Surratt et al.* [2008] and *Zhang et al.* [2011a]	Filter collection with subsequent UPLC/DAD/ESI-HR-Q-TOFMS analyses	Every 3–6 h and 23 h	10–30%	1%
Nitro-Aromatics	*Surratt et al.* [2008] and *Zhang et al.* [2011a]	Filter collection with subsequent UPLC/DAD/ESI-HR-Q-TOFMS analyses	Every 3–6 h and 23 h	10–30%	1%
WSOCs		Filter collection with subsequent H-NMR analyses	Every 3–6 h and 23 h		
Organic Acids	*Kristensen and Glasius* [2011]	Filter collection with subsequent HPLC/ESI-HR-Q-TOFMS analyses	Every 3–6 h and 23 h	25%	0.5–1.5 ng LOD
^{14}C of OC and TC	*Szidat et al.* [2006]	Filter collection with subsequent off-line accelerator mass spectrometry	Every 3–4 h	1–5%	5–15%
OC/EC	*Schauer et al.* [2003]	Filter collection with subsequent thermal-optical measurements	Every 3–4 h	OC 5–15% and EC 25%	OC LOD 0.3μgC/cm^2
Organics		Filter collection with subsequent solvent extraction, with and without prior derivatization, for GC/MS analyses	Every 3–6 h and 23 h		
Oxidized Organics		Filter collection with subsequent 2D-GC/ToFMS	Every 3–6 h and 23 h	10–30%	5%
Organics	*Goldstein et al.* [2008]	Filter collection with subsequent TAG-2D-GC/MS analyses with prior derivatization	Every 3–6 h and 23 h		
Submicron alkane, organic hydroxyl, amine, carboxylic acid, and nonacid carbonyl functional groups and total submicron organic mass	*Gilardoni et al.* [2007] and *Russell et al.* [2009]	Filter collection with subsequent Fourier transform infrared (FTIR) spectroscopy analyses	Every 3–6 h and 23 h	21% (Total organic mass)	0.09, 0.02, 0.01. 0.008, and 0.005 μmol of bond
Precursor-specific SOA tracers		Filter collection with subsequent GC/MS analyses with prior derivatization	Daily (23 h)	21% for total organic mass	0.09, 0.02, 0.01, 0.008, and 0.005 μmol of bond
Primary organic tracers and compound-specific stable isotope analysis	*Sheesley et al.* [2004]	Filter collection with subsequent GC/MS and GC-IRMS analysis	Every 3–6 h and 9–13 h	20%	5%
^{14}C and OC/EC	*Schauer et al.* [2003]	Filter collection with subsequent offline accelerator mass spectrometric analyses for ^{14}C and thermal-optical measurement for OC/EC	Daily (23 h)	1% for ^{14}C and 20% for OC/EC	1% for ^{14}C and 5% for OC/EC
Elements and Metals	*Bukowiecki et al.* [2009]	Rotating drum impactor (RDI) and subsequent synchrotron radiation-induced XRF analysis	2 h	30–40%	5%
Molecular characterization of organics in bulk samples; Microscopy and microanalysis of individual particles	*Laskin et al.* [2006], *Moffett et al.* [2010a], *Moffett et al.* [2010b], *Nizkorodov et al.* [2011], and *Roach et al.* [2010]	MOUDI impactor with different substrates for subsequent analysis by Nano-DESI-HR-Orbitrap MS[†]; Computer Controlled SEM/EDX[‡]; Scanning Transmission X-ray Microscopy[#]	6 h	N/A	N/A
Microanalysis	*Adachi and Buseck* [2008]	Microanalysis particle samplers with subsequent transmission electron microscopy (TEM) analyses	4.8 min	N/A	N/A
VOCs		Tenax tubes with subsequent thermal desorption-GC/MS analyses	3 h	10%	25%

Table 7a. Bakersfield Ground Site Gas-Phase Measurements

Measurement	Reference	Technique	Sample Interval	Accuracy at High S/N (±1–sigma)	Precision at Low S/N (±1–sigma)
HO, HO_2, OH loss rate, naphthalene, and potential aerosol mass					
NO_2, $\sum RO_2NO_2$, $\sum RONO_2$, HNO_3					
NO					
O_3	*Gearn* [1961]	UV absorption	1 min	±0.5%	±1 ppbv
CO, N_2O, CH_4, CO_2, H_2O, and stable isotopes of CO_2					
VOCs		GC-MS and GC-FID	15 min	±5–20%	
HCHO		Laser-induced fluorescence	30 s	±30%	±70 pptv
Glyoxal and α-dicarbonyls		Laser-induced phosphorescence	30 s	±20%	5 pptv
NH_3, HNO_3, HCl, HONO, SO_2					
HONO	*Ren et al.* [2010]	CRDS	1 min	±15%	1 ppbv
HNO_3, organic acids, peroxides, and oxygenates		CF_3O^- CIMS	16 s	±25%	25 pptv
PAN, PPN, MPAN, and other acyl peroxynitrates		I^- TD-CIMS	1 min	±(3 pptv + 21%) ± (3 pptv + 21%) MPAN	± 3 pptv

an overview of the meteorology and transport during CARES with an emphasis on the Sacramento Valley.

[55] Spring 2010 was cooler and wetter than normal over most of California with frequent cold fronts and upper air disturbances. Fog was frequent in the coastal areas and western Los Angeles basin and the monthly average temperature for the state during May was 2.3°C below the long-term average of 13.0°C (Figure 7; http://www.wrcc.dri.edu/monitor/cal-mon/). There were 62 new record low minimum temperatures and 5 record high maximum temperatures set in California during the month. These conditions followed the weakening El Niño, which dissipated during May as positive sea surface temperature (SST) anomalies decreased across the equatorial Pacific Ocean and negative SST anomalies emerged across the eastern half of the Pacific (http://www.cpc.ncep.noaa.gov).

[56] The synoptic meteorology in May was dominated by a series of deep upper level troughs that moved off the Pacific Ocean into California on 9, 17, 22, and 27 May. Cold fronts associated with these systems brought low temperatures, high winds, and precipitation to many parts of the state. The first system brought up to 20 cm of snow to the central Sierra Nevada between Yosemite and Sequoia National Parks. Bishop, CA, tied the all-time May low temperature of –4°C on 11 May. The second system brought cold and rain to much of the SJV, with another 8–15 cm of snow to the Sierras. The third system brought more rain to the southern SJV and led to record low temperatures at 22 locations across the state from Redding to Riverside on 23 May; Bishop tied the all-time May record low of –4°C once again on that day, and the record lows were tied in both San Francisco and Sacramento. Storms associated with the 27–29 May trough brought more snow and thunderstorms to the southern Sierra and wind gusts in excess of 50 mph to the Tehachapi Mountains. Deep stratospheric intrusions associated with all four of these troughs were detected by IONS-2010 ozonesondes [*Cooper et al.*, 2011] and the NOAA P-3 and Twin Otter aircraft [*Langford et al.*, 2012; *Lin et al.*, 2012a].

[57] Conditions became more seasonal in early June, which was slightly drier than average for most of California;

Table 7b. Bakersfield Ground Site Aerosol Measurements

Measurement	Reference	Technique	Sample Interval	Accuracy at High S/N (±1–sigma)	Precision at Low S/N (±1–sigma)
Size-resolved nonrefractory NH_4^+, NO_3^-, SO_4^{2-}, Cl^- and organic composition for PM_1		Aerosol mass spectrometry (AMS)	5 min	30%	0.03 μg/m^3
IR-active functional groups	*Russell* [2003] and *Russell et al.* [2009]	Fourier transform infrared spectroscopy on filter sample extracts	2–4 h	21% for total organic mass	0.001–0.09 μmol of analyte
Trace elements in fine aerosol	*Liu et al.* [2009]	X-ray fluorescence on filter samples	2–4 h	6–40%	0.001–0.16 μg
Water-soluble anions and cations					
Speciated organics		Thermal desorption aerosol GC-MS (TAG)			
Organic nitrates in the gas/particle phase					
Organic and elemental carbon					
MOUDI impactor		Nano-DESI with high-resolution MS			
Speciated organics					
Organosulfates and α-dicarbonyls					
Nitrooxysulfate and organosulfate		UPLC/ESI-HR-Q-TOFMS	23 h	1–30%	1%
Nitrooxysulfate and organosulfate					

Table 8. Species Measured in Whole-Air Samples by NOAA GMD at Mt. Wilson, CA During CalNex

Halocarbons	Hydrocarbons	Others
$CHBr_3$	C_6H_6	CO
CCl_4	C_2H_2	CO_2
CH_3I	C_3H_8	$^{14}CO_2$
$CHCl_3$	*n*-C_4H_{10}	CH_4
CH_2Br_2	*n*-C_5H_{12}	N_2O
CH_2Cl_2	*i*-C_5H_{12}	SF_6
CH_3Br		CS_2
CH_3Cl		OCS
C_2Cl_4		
CCl_3F (CFC-11)		
CCl_2F_2 (CFC-12)		
$CClF_3$ (CFC-13)		
$C_2Cl_3F_3$ (CFC-113)		
C_2ClF_5 (CFC-115)		
CHF_3 (HFC-23)		
C_2HF_5 (HFC-125)		
CH_2FCF_3 (HFC-134a)		
$C_2H_3F_3$ (HFC-143a)		
$C_2H_4F_2$ (HFC-152a)		
CF_2ClBr (Halon 1211)		
$CBrF_3$ (Halon 1301)		
$C_2Br_2F_4$ (Halon 2402)		
$CHClF_2$ (HCFC-22)		
$C_2H_3ClF_2$ (HCFC-142b)		

the monthly mean temperature was 19.3°C, 0.1°C higher than the long-term average. The weather patterns during the first week of June were dominated by the presence of a low-pressure system over the Gulf of Alaska and an upper level high-pressure ridge over the southern half of the state. A weak upper level trough over northern California brought record precipitation to Crescent City on both 1 and 2 June (6 cm and 5 cm of rain, respectively) and slightly cooler temperatures to Sacramento and Bakersfield. The warm temperatures and subsiding air associated with the ridge led to the first prolonged ozone episode of the year in the Los Angeles basin, and the highest 8 h ozone concentrations measured in the state during 2010, 123 parts per billion by volume (ppbv) at Crestline on 5 June. Temperatures warmed to 27°C (low 80 s in °F) in downtown Los Angeles by 5 and 6 June, exceeding 36°C (high 90 s in °F) the central and southern SJV. Warming in the southern Sierra Nevada initiated rapid melting of the snowpack and afternoon cumulus formation in the SJV. A series of upper level lows in the Pacific Northwest kept the ridge from growing northward and produced strong winds over much of the state.

[58] Temperatures fell over the southern half of the state as another upper level trough moved into California off the Pacific on 9 June. This system developed into a cutoff low and spawned another tropopause fold with possible influence on surface ozone in southern California on 12 June [*Lin et al*., 2012a]. Cooler than normal temperatures persisted through 11 June with light rain over the southern Sierra Nevada and persistent high winds in the Tehachapi Mountains and west side of the SJV. Temperatures rose as high pressure followed the trough with near normal temperatures on 12 June; the first 37.8°C (100°F) day in Fresno occurred on 14 June, 1 week later than normal. However, two more upper level troughs on 15–17 and 21–23 June moderated the surface temperatures in the Central Valley through the third week of June, disrupting the local mountain-valley circulation patterns. The final trough brought a few showers to the central SJV and Southern Sierra Nevada during the morning of 25 June. A high-pressure ridge built up into California on 26 June as the trough passed through, with 38.3°C observed in both Bakersfield and Fresno on 27 June, with Fresno tying the record high of 42.2°C (108°F) on 28 June.

[59] Most of the CalNex field operations had ceased by the end of June, but following its redeployment for a series of flights in the Sacramento and Central Valleys, the NOAA Twin Otter returned to southern California from 30 June to 18 July. Although the July monthly mean temperature for the state was slightly above average, southern California remained cooler than average with frequent coastal fog that persisted into the afternoon. Temperatures were particularly low near the coast, and Los Angeles Airport reached monthly record low maximum temperatures twice, with readings of 19°C on 6 July followed by 18°C on 8 July. The first 6 days of July 2010 were cooler than the first 6 days of January 2010 for downtown Los Angeles, Los Angeles Airport, Long Beach Airport, Santa Barbara Airport, and Oxnard. San Diego also tied its lowest maximum temperature on 8 July with a reading of 64°F. This broke the daily record low maximum temperature of 65°F set in 1902. Temperatures along the coast increased on 13 July and remained several degrees above normal through 18 July.

4. Overview of Initial Results

4.1. Emission Inventory Assessment

[60] Top-down assessment of emissions inventories is a focus of analysis of the combined CalNex data set. Measured atmospheric concentrations in source regions, for pairs of co-emitted species that are chemically conserved on time scales long compared to their atmospheric residence time between emission and sampling, provide a critical assessment of the corresponding emissions ratio in the state and federal inventories that underpin atmospheric models. These assessments provide a stringent test of the bottom-up approach used in inventory tabulations and establish a benchmark for relative emissions changes over time in response to control strategies. Further, if the total mass emission for a single species in an inventory is accurately known, the total mass emissions for other co-emitted species can be calculated based on their characteristic atmospheric enhancement ratios. For example, the California CO inventory (www.arb.ca.gov/cc/inventory/inventory.htm) is believed to be sufficiently accurate to serve as a benchmark against which other mass emissions are calculated from observed enhancement ratios [e.g., *Barletta et al*., 2011; *Hsu et al*., 2010; *Wennberg et al*., 2012; *Wunch et al*., 2009]. Finally, under favorable meteorological conditions,

Table 9. Species Measured by Remote-Sensing Techniques at Mt. Wilson, CA During CalNex

Measurement	Reference	Technique	Sample Interval
NO_2, HCHO, glyoxal, aerosol extinction (O_4)	*Pikelnaya et al*. [2007]	Multi-axis DOAS	1 min
CO_2, CH_4, N_2O, CO, O_2		Near-IR Fourier Transform Spectroscopy	1 min

Table 10. Radar Wind Profiler and Radio Acoustic Sounding System Network Operational During CalNex

Location	Designation	Latitude, deg	Longitude, deg	Elevation, m	Sponsor
Bakersfield	BKF	35.35	−118.98	120	NOAA/PSD[a]
Bodega Bay	BBY	38.32	−123.07	12	NOAA/PSD
Chico	CCO	39.69	−121.91	41	NOAA/PSD
Chowchilla	CCL	37.11	−120.24	76	NOAA/PSD
Gorman	GMN	34.72	−118.80	912	NOAA/PSD
Irvine	IRV	33.69	−117.73	122	SCAQMD[b]
Livermore	LVR	37.70	−121.90	109	BAAQMD[c]
Los Angeles	USC	34.02	−118.28	67	SCAQMD
Lost Hills	LHS	35.62	−119.69	80	NOAA/PSD
Miramar	MRM	32.90	−117.10	126	SDAPCD[d]
Moreno Valley	MRV	33.87	−117.22	452	SCAQMD
Oakhurst	OHT	37.38	−119.63	955	NOAA/PSD
Ontario	ONT	34.06	−117.58	280	SCAQMD
Pacoima	WAP	34.26	−118.41	300	SCAQMD
Sacramento	SAC	38.30	−121.42	6	SMAQMD[e]
San Nicolas Island	SNS	33.28	−119.52	15	NOAA/PSD
Simi Valley	SIM	34.30	−118.80	283	VCAPCD[f]
Tracy	TCY	37.70	−121.40	60	SJVAPCD[g]
Truckee	TRK	39.32	−120.14	1796	NOAA/PSD
Visalia	VIS	36.31	−119.39	81	SJVAPCD[g]

All locations except Truckee were equipped with a radio-acoustic sounding system (RASS).
[a]NOAA Physical Sciences Division;
[b]South Coast Air Quality Management District (AQMD);
[c]Bay Area AQMD;
[d]San Diego Air Pollution Control District (APCD);
[e]Sacramento Metropolitan AQMD;
[f]Ventura County APCD;
[g]San Joaquin Valley APCD.

atmospheric measurements can quantify mass emissions from large point and area sources [*Nowak et al*., 2012; *Peischl et al*., 2013]. Several analyses of CalNex data have used these top-down emissions assessment approaches to help quantify inventories of greenhouse gases, the ozone precursors NO_x and VOCs, and aerosol precursor compounds.

4.1.1. Greenhouse Gases

[61] Emissions of greenhouse gases from California averaged over 2002–2004 accounted for 2% of the global total [*CARB*, 2008]. The provisions in the California Global Warming Solutions Act of 2006 call for regulations to reduce emissions by 2020 to levels equivalent to those estimated for 1990; full implementation has been delayed, but this would constitute a 15% reduction from the 2002–2004 average by 2020. Implementation requires the state to establish a GHG inventory and evaluate emissions reduction progress against this inventory baseline. In favorable situations, atmospheric measurements can provide independent assessments of the state inventory and demonstrate the degree to which mandated emissions controls have resulted in the desired atmospheric concentration changes over time.

4.1.2. Carbon Dioxide

[62] Anthropogenic CO_2 is emitted primarily from combustion processes; its annually averaged emissions account for 86% of the calculated 100 year global warming potential (GWP) and thus dominate the CARB inventory of directly emitted greenhouse gases [*CARB*, 2011] (Figure 8). The ubiquity of anthropogenic CO_2 emission sources, coupled with significant diurnal variability in biosphere CO_2 sources and sinks, complicates accurate top-down assessments of CO_2 emissions based on atmospheric measurements [e.g., *Djuricin et al*., 2010; *Newman et al*., 2008]. Despite this difficulty, *Newman et al*. [2012] used ground-based and airborne measurements during CalNex to show that the midday enhancement in column CO_2 over Pasadena, CA, is nearly completely attributable to fossil fuel combustion and suggest that this variability derived from future midday passive satellite column CO_2 retrievals can be used to infer anthropogenic emissions in the Los Angeles basin.

4.1.3. Methane

[63] CH_4 emissions account for 7% of the total GWP in the 2009 California annual inventory [*CARB*, 2011] (Figure 8). This inventory suggests that 56% of the total CH_4 emissions comes from animal husbandry (primarily dairy cattle) and is split equally between enteric fermentation and manure management sources. A total of 21% of inventoried CH_4 comes from landfills; 11% from the combined emissions of wastewater treatment, oil and gas development, rice cultivation, and vehicular traffic sources; and 12% from sources listed as "other" in the tabulated statewide annual inventory. The variety of source types leads to significant spatial and temporal heterogeneity of CH_4 emissions in California.

[64] Methane measurements made during the CalNex intensive at the Bakersfield ground site and from the NOAA P-3 research aircraft complement the longer-term CH_4 data record at instrumented tall towers on Mt. Sutro and in Walnut Grove (Figure 2) [e.g., *Jeong et al*., 2012a] and the NOAA flask samples taken at Mount Wilson Observatory.

4.1.3.1. Urban CH_4

[65] Ground-based Fourier transform spectrometer (FTS) measurements of atmospheric column abundances of CH_4 above Pasadena, CA, in 2007 and 2008 [*Wunch et al*.,

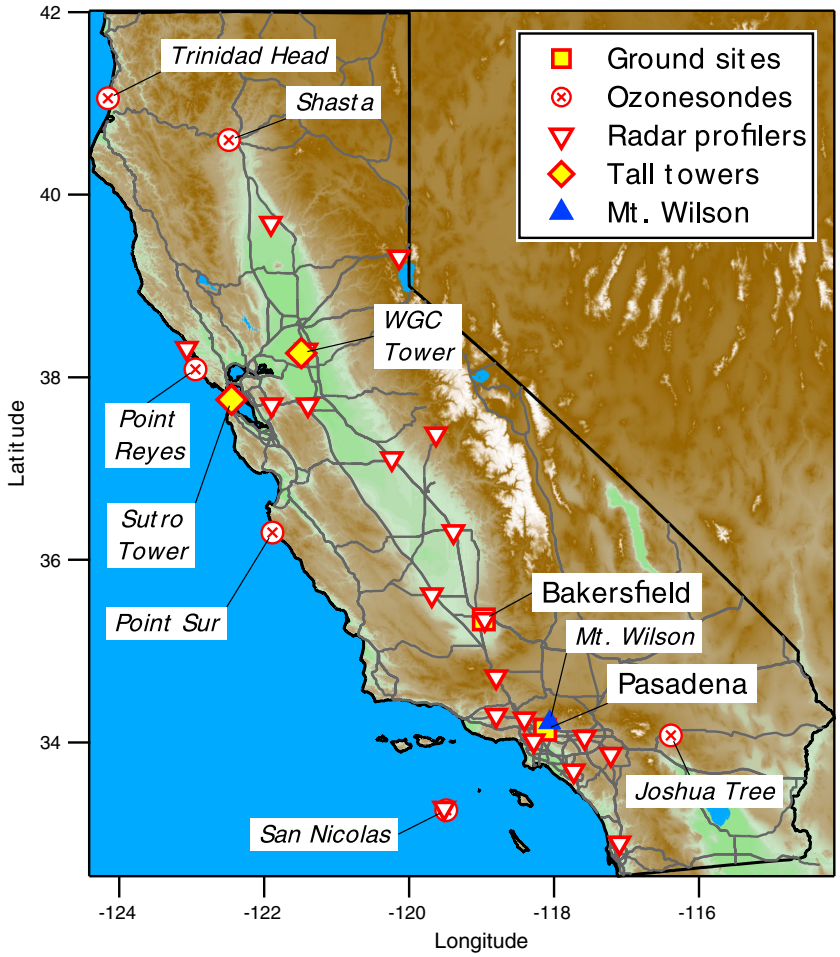

Figure 2. Map of selected ground sites relevant to the CalNex project in 2010.

2009] had suggested that a significant source of CH_4, up to one half of the derived total of 0.6 Tg/yr, was unaccounted for in the CARB emissions inventory for the urbanized South Coast Air Basin (SoCAB) that includes the Los Angeles megacity. Following these studies, *Wennberg et al*. [2012], G.W. Santoni et al. (California's methane budget derived from CalNex P-3 aircraft observations and a Lagrangian transport model, submitted to Journal of Geophysical Research, 2012), and *Peischl et al*. [2013] analyzed CalNex ground and airborne data and separately concluded that CH_4 sources continue to be significantly underestimated in the Los Angeles basin inventory. *Wennberg et al*. [2012] noted that atmospheric CH_4 enhancement ratios to ethane (C_2H_6) are similar to those in natural gas supplied to the basin in both 2008 and 2010 and concluded that leakage from the natural gas distribution infrastructure in the basin is the most likely source of excess atmospheric CH_4. Their study did not rule out natural gas seeps or industrial emissions as significant potential sources. *Peischl et al*. [2013] examined CH_4 enhancement ratios to C_2 through C_5 alkanes (ethane, propane, and the isomers of butane and pentane) and utilized the geographic distribution of airborne samples taken during CalNex to exclude traffic, dairy feedlots, landfills, and wastewater treatment plants as significant sources of the missing CH_4 in the LA basin. They attribute the missing methane to leaks from natural gas extraction, production, and distribution, based on the observed correlations with the light alkanes. Santoni et al. (submitted 2012) used an inverse model constrained by the P-3 data and calculated emissions in the LA basin of 0.30 Tg CH_4/yr, consistent with an assumed leak rate of 2.5% from the natural gas delivery infrastructure in the basin. Thus, these CalNex reports implicate larger-than-expected CH_4 emissions from the oil and gas sector in Los Angeles as the likely source missing from the inventory but differ on the root cause. Further, spatially resolved measurements in Los Angeles, possibly including CH_4 stable isotope data [*Townsend-Small et al*., 2012] both in atmospheric samples and in direct samples of potential source emissions, are needed to identify and attribute the excess CH_4 that appears to be a consistent feature of the Los Angeles urban atmosphere.

4.1.3.2. Agricultural CH_4

[66] Data from two flights of the NOAA P-3 in CalNex were used to illustrate the spatial consistency of CH_4 emissions from rice paddies during the growing season in the Sacramento Valley [*Peischl et al*., 2012]. This report demonstrated that rice emissions dominated other potential sources of CH_4 in the region, including oil and gas development, dairy farms, and wastewater treatment facilities. However, the expected daytime uptake of CO_2 from early season rice growth was difficult to quantify above background variability along the flight track due to high variability from

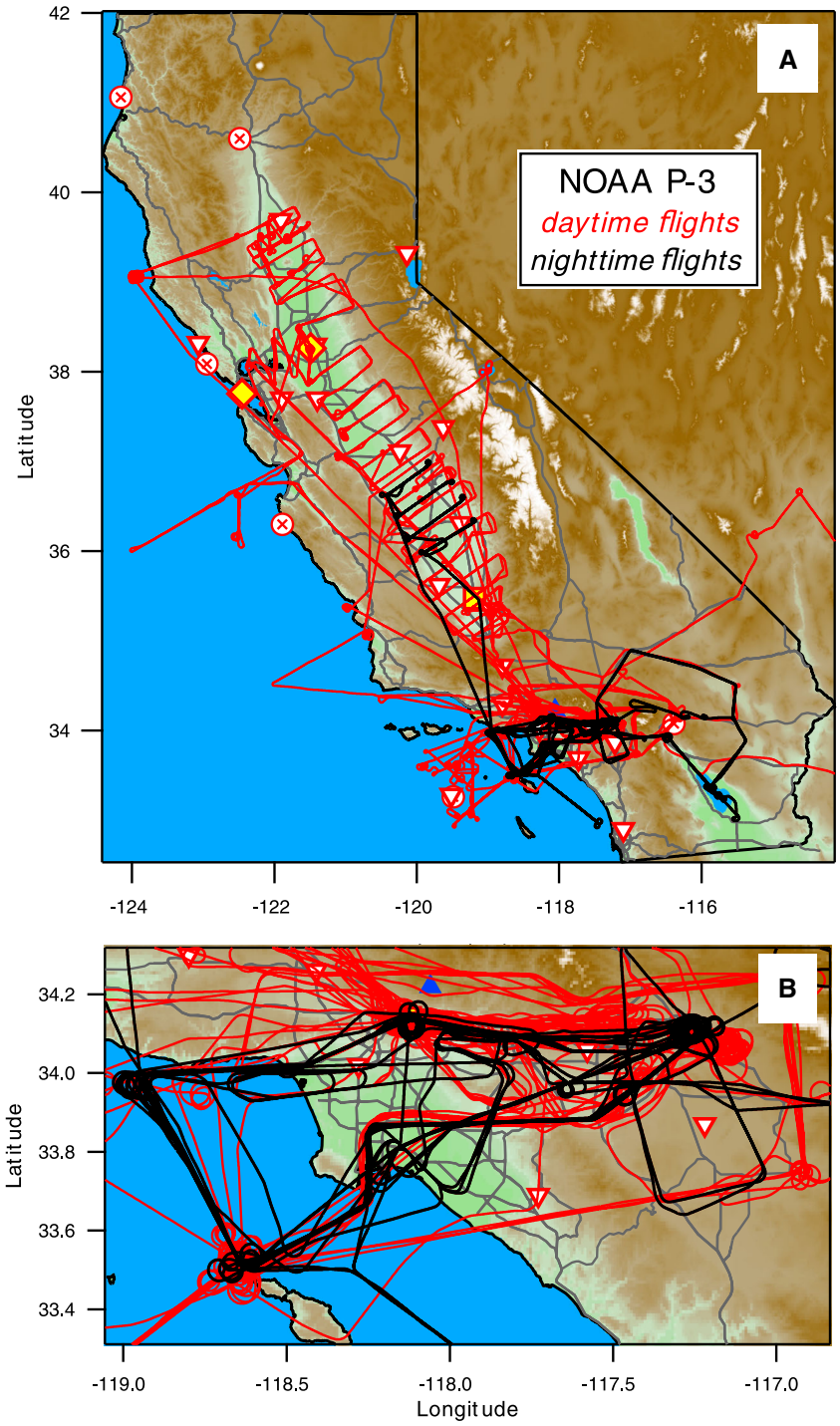

Figure 3. (a) Daytime (red lines) and nighttime (black lines) NOAA P-3 research aircraft flight tracks in California between 30 April and 22 June 2010. (b) As in Figure 3a, showing details of P-3 flight segments within the South Coast Air Basin.

transported urban emissions. Despite these difficulties, the analysis of CH_4 measurements from the P-3 aircraft by *Peischl et al*. [2012] showed that earlier long-term measurements of CH_4 and CO_2 at a single paddy [*McMillan et al*., 2007] were generally representative of emissions from rice cultivation throughout the California Sacramento Valley. *Peischl et al*. further note that the annual average CH_4 emissions from rice in *McMillan et al*. are factors of 2 to 3 greater than that in the CARB annual inventory and attributed this inventory discrepancy to the lack of accounting for changes in residual crop management following a 2001 ban on most rice straw burning in the Sacramento Valley. Inverse model results reported by Santoni et al. (submitted 2012) are also consistent with a low bias, by about a

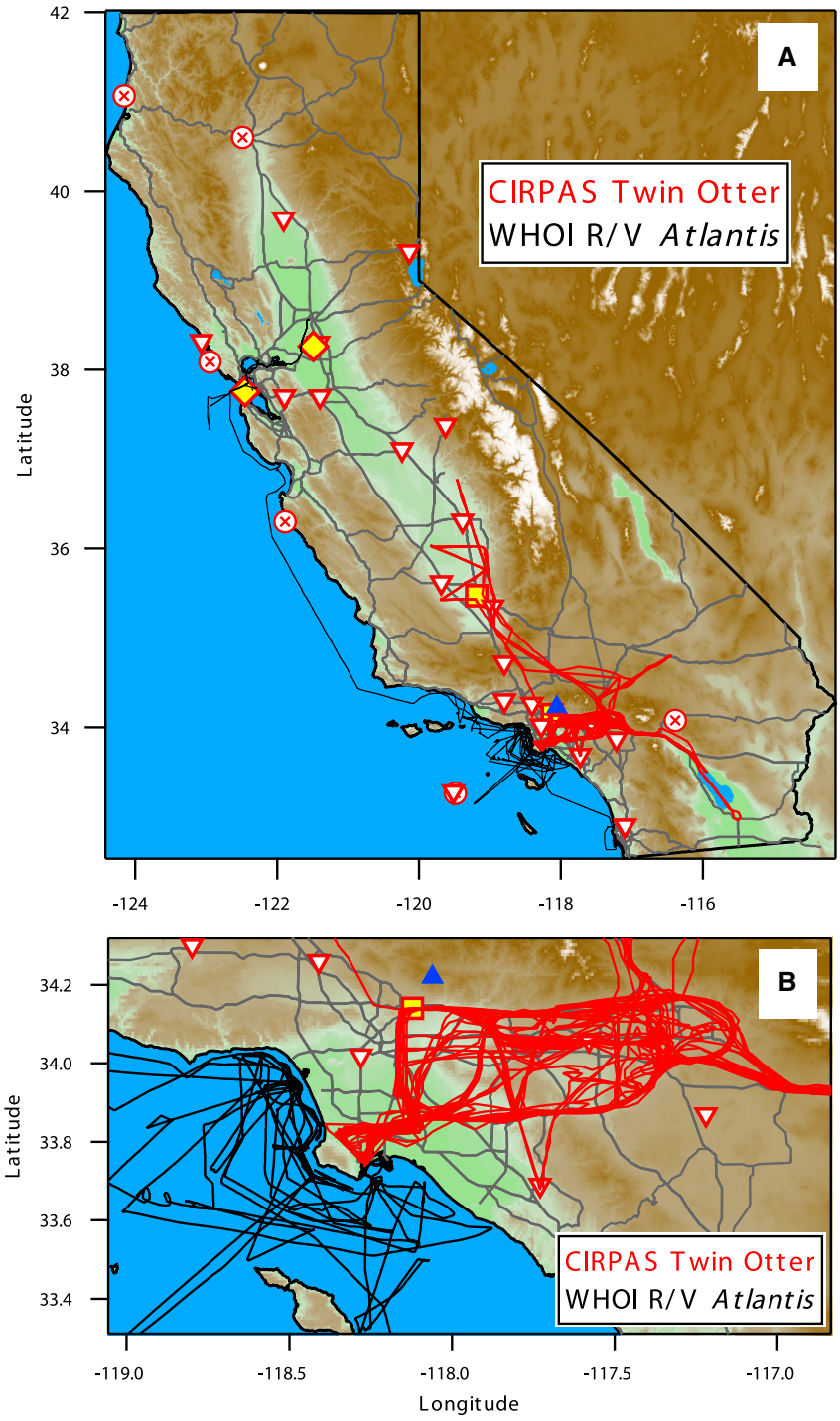

Figure 4. As in Figure 3, for the CIRPAS Twin Otter flight tracks between 4 May and 28 May 2010 (red lines) and the R/V *Atlantis* cruise track between 14 May and 8 June 2010 (black lines).

factor of 3, in CARB inventory CH_4 emissions from rice in the Sacramento Valley.

4.1.4. Nitrous Oxide

[67] N_2O emissions account for 3% of the total GWP in the California annual inventory (Figure 8); the largest anthropogenic emissions in California are thought to be from agriculture and dairy cattle primarily located in the Central Valley. Measurements of N_2O during CalNex were made at the Bakersfield ground site and aboard the NOAA P-3 research aircraft. *Xiang et al*. [2013] used a 3-D mesoscale meteorological model coupled with a Lagrangian particle dispersion model to link N_2O concentrations observed from the P-3 aircraft to source emission areas and concluded that fertilizer application in the Central Valley was the largest source of N_2O during the study period. High-resolution surface emission maps derived from their inversion analysis showed a different spatial pattern of N_2O emissions in the Central Valley than expected

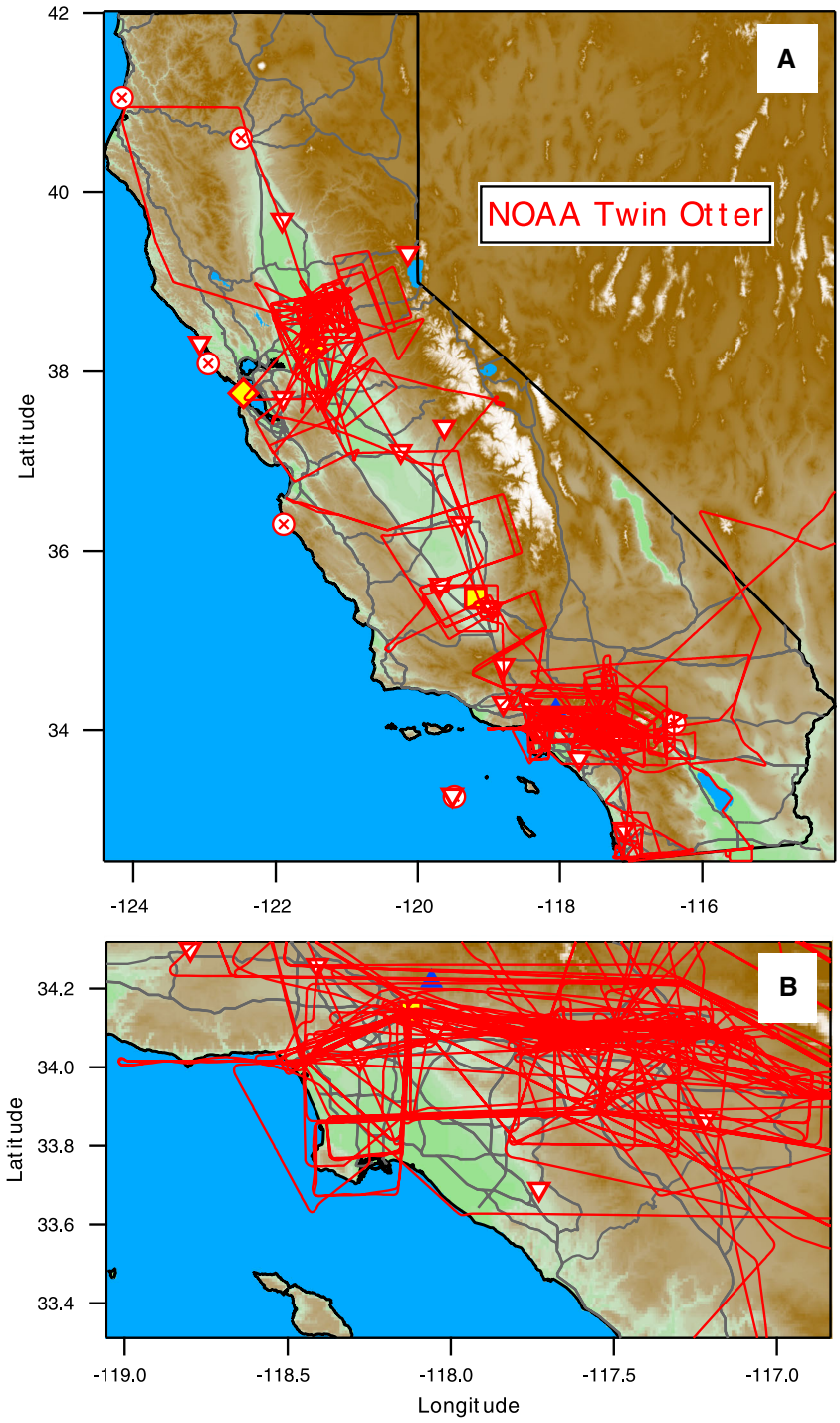

Figure 5. As in Figure 3, for the NOAA Twin Otter flight tracks between 19 May and 19 July 2010 (red lines).

from the EDGAR 4.0 inventory. This conclusion is consistent with a recent inverse modeling study based on long-term tall tower N_2O observations [*Miller et al.*, 2012] of agricultural N_2O emissions derived using top-down methods.

[68] The global total of N_2O emissions is thought to be well known; however, individual source terms in the inventories are uncertain. The potential low bias in agricultural N_2O inventories, coupled with poor spatial [*Xiang et al.*, 2013] and seasonal [*Miller et al.*, 2012] representations, may handicap scientifically sound ozone layer protection and GHG emissions control strategies based on N_2O emissions reductions. These uncertainties further complicate accurate projections of future N_2O emissions under potential climate mitigation or adaptation strategies. The conclusions from CalNex and previous studies suggest that improved quantification of agricultural N_2O sources in California may help the State meet the GHG reduction timelines spelled out in AB32.

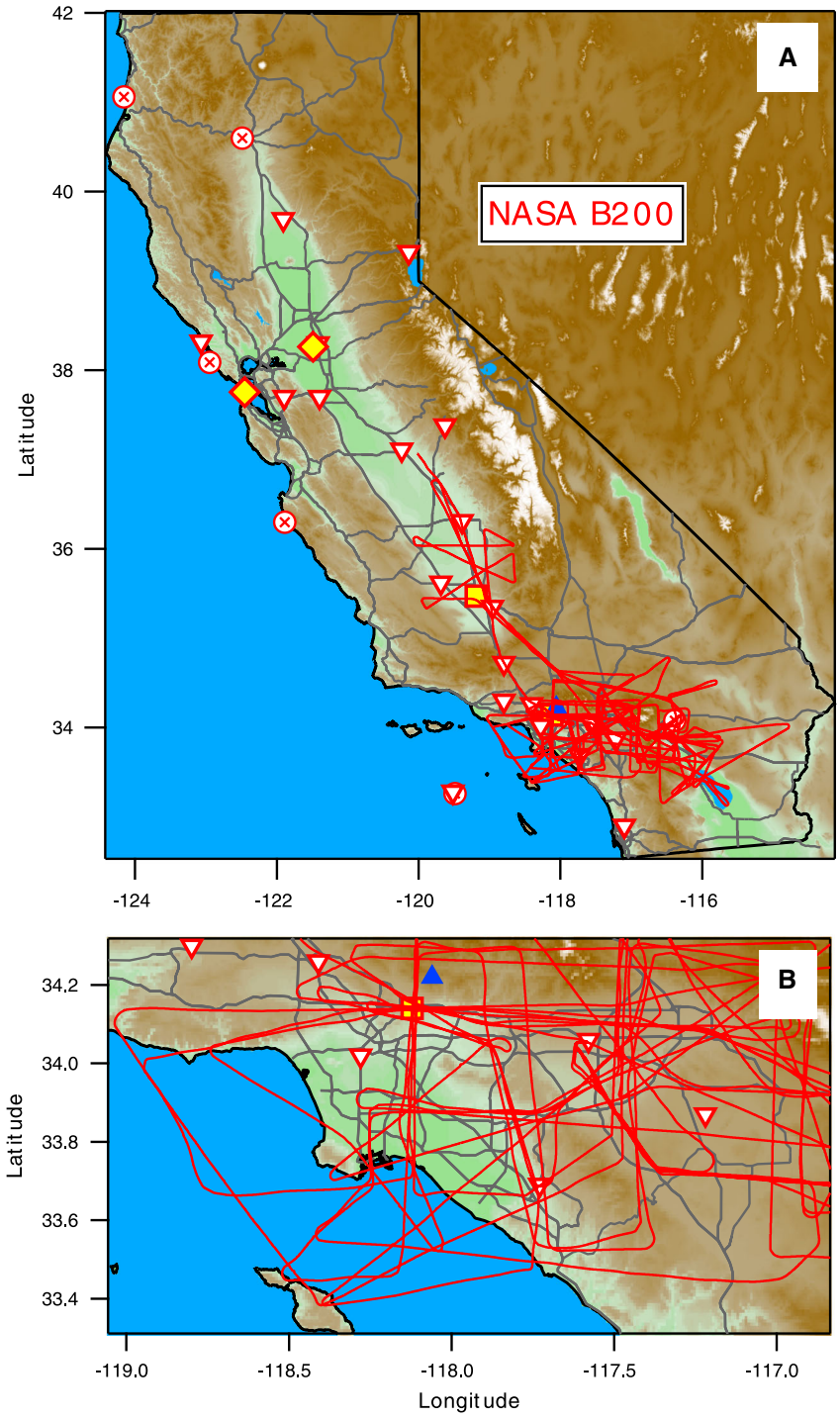

Figure 6. As in Figure 3, for the NASA B200 flight tracks between 12 May and 25 May 2010 (red lines).

4.1.5. Halocarbons

[69] The sum of CFCs, HCFCs, HFCs, and other halogenated gases accounts for 3% of the annual GWP of inventoried California emissions (Figure 8). Halocarbon emissions patterns, trends, and seasonality in California have been previously reported [e.g., *Barletta et al*., 2011; *Gentner et al*., 2010]. These compounds were measured at a variety of sites during CalNex. *Barletta et al*. [2013] used whole-air samples acquired in the Central Valley and Los Angeles basins from the NOAA P-3 during CalNex to show the CARB inventory is generally consistent with their top-down assessment of anthropogenic emissions of halocarbons HFC-134a, HFC-152a, HCFC-22, HCFC-124, HCFC-141b, and HCFC-142b in California.

4.1.6. Ozone Precursors

4.1.7. CO

[70] Urban CO concentrations are dominated by on-road emissions from gasoline-fueled passenger vehicles and have been steadily decreasing over time throughout the U.S. [*Parrish et al*., 2002] in response to control strategies. CO

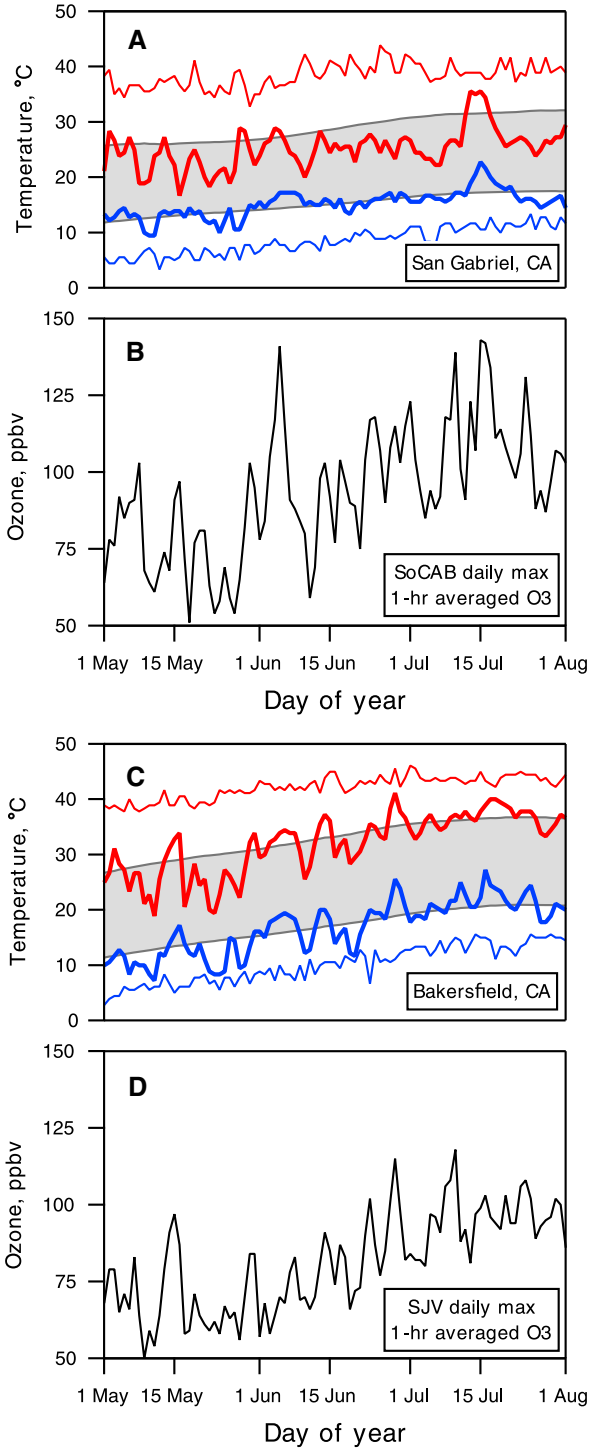

Figure 7. (a) 2010 daily maximum (thick red line) and daily minimum (thick blue line) temperature data from a weather station near the CalNex ground site in Pasadena. Also shown are the record daily maximum (thin red line), record daily minimum (thin blue line) and average daily maximum and minimum (upper and lower bounds of gray shading) temperatures for 1979–2010. (b) Daily 1 h averaged ozone maxima in the air basin containing the Pasadena ground site, obtained from www.arb.ca.gov/aqmis2/aqdselect.php. (c) As in Figure 7a using data from a weather station near the CalNex ground site in Bakersfield. (d) As in Figure 7b using ozone data in the air basin containing the Bakersfield ground site.

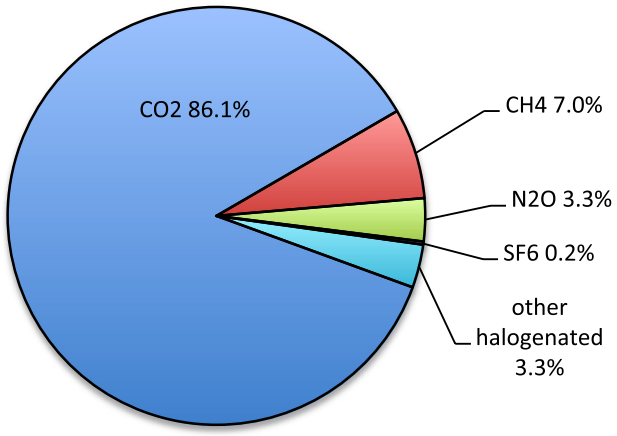

Figure 8. CO_2-equivalent radiative forcing estimated from the 2009 inventory of California greenhouse gas emissions [*CARB*, 2011].

in California shows a similar trend, recently demonstrated by a study using atmospheric CO measurements and the radiocarbon composition of tree rings in the Los Angeles basin as a record of atmospheric CO_2 from fossil fuel [*Djuricin et al*., 2012]. The utility of CO, a conserved tracer for which emissions (www.arb.ca.gov/ei/emissiondata.htm) in California over time are thought to be accurately known, has been exploited in several CalNex studies to calculate mass emissions of other species of interest, either co-emitted with CO [*Barletta et al*., 2013; *Pollack et al*., 2012; *Warneke et al*., 2012] or emitted from different sources but sufficiently mixed following emission such that their atmospheric variability becomes correlated with CO [*Nowak et al*., 2012; *Peischl et al*., 2013; *Peischl et al*., 2012].

4.1.8. VOCs

[71] *Borbon et al*. [2013] used the CalNex Pasadena ground site data to derive top-down emissions estimates of many VOCs relative to CO in vehicular exhaust. *Warneke et al*. [2012] interpreted the decadal trends in observed Los Angeles VOC/CO atmospheric enhancement ratios between 1960 and 2012 to demonstrate declining VOC emissions from gasoline vehicles over the past 50 years, providing measurement-based evidence to quantify the efficacy of mandated vehicular emissions controls. They concluded that deliberate control strategies have successfully reduced VOC (and CO) emissions from gasoline-fueled vehicles in Los Angeles by nearly two orders of magnitude since 1960. *de Gouw et al*. [2012] used the CalNex measurements to show that ethanol (CH_3CH_2OH) has become significantly enriched in U.S. urban atmospheres in the last decade due to its increasing use as a biofuel amendment to gasoline. However, they detected no increase in the ethanol oxidation product acetaldehyde (CH_3CHO), indicating that other sources dominate the atmospheric acetaldehyde budget. This finding provides a key initial constraint on the air quality effects of increasing ethanol emissions in the U.S. [*de Gouw et al*., 2012].

[72] Contrasting similar top-down VOC emissions assessments from the Bakersfield ground site data, from NOAA P-3 VOC data in the Central Valley and Los Angeles basins [*Warneke et al*., 2012], will determine to what extent

emissions differences in the two California air basins can be reconciled with the O_3 record, with implications on the future ability of emissions control strategies to effectively address atmospheric O_3 (Figure 1).

4.1.9. NO_x

[73] Weekday-weekend NO_x emission differences, and their trends over time, are documented from 1990 through the CalNex study in 2010 [*McDonald et al*., 2012; *Pollack et al*., 2012]. *Pollack et al*. [2012] used ambient measurements to show that significant weekend decreases of the NO_x to CO emission ratio, between one third to one half of the characteristic weekday ratio, have been a consistent feature of the South Coast Air Basin since at least the mid-1990s. The resulting effects on ozone production reported in *Pollack et al*. [2012] are discussed in section 5.2. *McDonald et al*. [2012] showed similarly large annually averaged NO_x decreases between 1990 and 2010 for the U.S., California, and its constituent air basins including the South Coast. From the standpoint of California ozone regulatory decision making and its quantitative assessment, it will be particularly interesting to compare the effects of weekly modulation in NO_x, VOC, and the NO_x/VOC ratio purely as a result of weekly driving habits to the effects of changes of similar magnitudes occurring over the span of decades as a result of deliberate control strategies (I.B. Pollack et al., Trends in ozone, its precursors, and related secondary oxidation products in Los Angeles, California: A synthesis of measurements from 1960 to 2010, submitted to Journal of Geophysical Research, 2012) [*Warneke et al*., 2012].

4.1.10. Particulate Matter and Its Precursors

4.1.11. Diesel and Gasoline Emissions

[74] The weekend decrease in NO_x emissions is also seen in emissions of black carbon (BC) [*Metcalf et al*., 2012] and in primary (hydrocarbon-like) organic aerosol (OA) (P.L. Hayes et al., Aerosol composition and sources in Los Angeles during the 2010 CalNex campaign, submitted to Journal of Geophysical Research, 2012) but was not detected in the formation of SOA in Los Angeles. Two separate top-down analyses of CalNex data utilized the lack of a weekend effect in OA mass in the Los Angeles basin, under the assumption that vehicular emissions dominate urban SOA, to conclude that gasoline emissions dominate over diesel emissions in the formation of SOA [*Bahreini et al*., 2012] (Hayes et al., submitted 2012), providing support for SOA control strategies that target gasoline-fueled vehicular emissions. However, a bottom-up approach using detailed fuel chemical composition information, estimates of the SOA formation potential of individual species, and regional fuel sales data [*Gentner et al*., 2012] concluded that diesel is responsible for ~70% the SOA derived from on-road mobile sources in the LA basin. These different conclusions suggest different strategies for effective control of SOA formation, but at present, the reasons for these significant differences in the conclusions of the different studies are not understood.

4.1.12. Ship Emissions

[75] CalNex studies have reported the speed dependence of emissions from a vessel burning low-sulfur fuel (C.D. Cappa et al., The influence of operating speed on gas and particle-phase shipping emissions: Results from the NOAA Ship Miller Freeman, sumbitted to Journal of Geophysical Research, 2012) and from a vessel during a switch from high- to low-sulfur fuel [*Lack et al*., 2011]. These analyses showed that speed reductions led to significant reductions in CO_2 emissions per kilometer traveled, by nearly a factor of 2, and in emissions of other species, demonstrating a substantial climate benefit as a result of an air quality control strategy. Further, *Lack et al*. [2011] used a wide variety of chemical and aerosol measurements from the P-3 aircraft and the R/V *Atlantis* to quantify differences in actual emissions from a single ship observed underway prior to, during, and after switching between high- and low-sulfur fuel. That analysis noted substantial concurrent reductions in emissions of not only SO_2 but also particulate sulfate, particulate organic matter, black carbon, and cloud condensation nuclei as a result of burning low-sulfur fuel. *Lack et al*. [2011] further estimated impacts to both air quality and climate expected as a result of adopting proposed California fuel use regulations. While the emissions reductions clearly led to positive effects on downwind air quality, *Lack et al*. [2011] concluded that warming due to reductions in the indirect effect of primary and secondary sulfate particles dominates the radiative impact of the mandated SO_2 emissions reductions.

4.1.13. Dairy Emissions

[76] *Nowak et al*. [2012] used airborne measurements from the NOAA P-3 to quantify NH_3 emissions from both automobile and dairy facility sources in the LA basin. This analysis compared these two emission sources to state and federal emission inventories and assessed the impact of these NH_3 sources on particulate ammonium nitrate (NH_4NO_3) formation. The estimated NH_3 emissions from automobiles of 62 ± 24 metric tons per day were similar in magnitude to those from the dairy facilities of 33 ± 16 to 176 ± 88 metric tons per day. The inventories examined agreed with the observed automobile NH_3 emissions but substantially underestimated those from dairy facilities. The high emission rates from the spatially concentrated dairy facilities led to a larger impact on NH_4NO_3 particle formation, with the calculated gas-particle equilibrium favoring the particle phase in plumes downwind of the dairy facilities. This paper suggested that NH_3 control strategies addressing dairy rather than automobile emissions would have the larger effect on reducing particulate NH_4NO_3 formation in the LA basin. Similar conclusions were reached by *Ensberg et al*. [2013].

[77] The cause of the day-to-day variability in dairy farm NH_3 emissions seen in the two P-3 flights [*Nowak et al*., 2012] is not fully understood. Understanding variability of the magnitude suggested by the P-3 data may result in an improved ability to address NH_3 emissions, and thus particulate ammonium nitrate formation in the LA basin, via dairy farm management practices. These sources may be a good target for a longer-term, ground-based emissions monitoring effort to better quantify and understand the drivers for such variability.

4.1.14. Black Carbon Aerosol

[78] Analysis of single-particle mass spectra showed substantial differences in the particulate chemical composition of the South Coast, Central Coast, and Central Valley aerosols sampled aboard the R/V *Atlantis* (C.J. Gaston et al., The impact of shipping, agricultural, and urban emissions on single particle chemistry observed aboard the R/V Atlantis during CalNex, submitted to Journal of Geophysical Research, 2012). In the Southern California offshore marine layer, particles mixed with soot made up the largest number

fraction of submicron particles; in the Sacramento area, particles containing organic carbon (OC) comprised the largest number fraction of submicron particles. These observed regional differences in composition and mixing state were suggested to be indicative of different sources of submicron particles, with attendant implications for emissions control strategies in the two regions (C.J. Gaston et al., submitted, 2012).

4.1.15. Ocean-Derived Aerosol

[79] An innovative technique using a subsurface *in situ* particle generator feeding a suite of instruments to measure the physical, chemical, optical, and cloud nucleating properties of the nascent ocean-derived aerosol was deployed on the R/V *Atlantis* during CalNex [*Bates et al*., 2012]. These measurements showed that the nascent aerosol number size distribution peaked between 50 and 150 nm dry diameter and that the particles were an internal mixture of sea salt with a small organic contribution, with essentially all the particles acting as cloud condensation nuclei (CCN) at supersaturations of ≥0.3%. This approach provided key data on initial composition, hygroscopicity, and size distribution of ocean-derived particulate matter against which more extensively processed particles sampled in the overlying marine boundary layer can be compared. This new technique provided data that are critical for accurately simulating ocean-derived aerosol properties and cloud nucleating ability in climate and air quality models.

4.2. Atmospheric Transport and Dispersion

[80] Transport of O_3, particulate matter, and other pollutants into, within, and out of California and its constituent air basins determines the extent to which local control strategies can achieve improvements to local air quality. Analysis of CalNex data [*Cooper et al*., 2011] showed that median values of lower tropospheric baseline O_3 (O_3 flowing into California from the North Pacific Ocean) are equal to more than 80% of the median O_3 measured within the daytime mixed layer above California's Central Valley. Similar comparisons across the polluted regions of southern California show that baseline O_3 is equal to 63–76% of the measured O_3 above Joshua Tree National Park and the LA basin. Given an increasing trend of Pacific free tropospheric background O_3 [*Cooper et al*., 2010], contributions from transport may increase over time and could reduce the efficacy of local emissions reductions strategies on controlling O_3 throughout the state [e.g., *Parrish et al*., 2010].

[81] The effect of longer-range transport of O_3 in central and southern California is difficult to separate from the strong influence of local anthropogenic O_3 formation in these areas. *Neuman et al*. [2012] analyzed O_3 and ancillary data from the NOAA P-3 during CalNex to show that downward mixing of Pacific free tropospheric (FT) air masses, averaging 67 ppbv O_3 at 2–4 km altitudes during the study period, can increase O_3 values at the surface in Los Angeles, in the SJV, and in the high desert. Various sources were found to contribute to enhanced FT O_3, including those from regional emissions and from longer-range transport, as well as O_3 transported from the upper troposphere and stratosphere. O_3 due to long-range transport of anthropogenic emissions from Asia has also been identified in the CalNex data set and quantified in 3-D model simulations [*Lin et al*., 2012b]. Surface O_3 enhancements from stratospheric intrusions during CalNex were episodically predicted and could be traced from the upper troposphere to the surface using transport models, ozonesondes, airborne lidar, and surface monitoring data [*Langford et al*., 2012; *Lin et al*., 2012a; 2012b].

[82] Numerical models of transport provide an additional tool to further interpret atmospheric chemical measurements during CalNex. WRF simulations described and evaluated against CalNex data by [*Angevine et al*., 2012] are integral to several other analyses, including those utilizing inverse modeling techniques to interpret the NOAA P-3 chemical data, [e.g., Santoni et al., submitted 2012; *Xiang et al*., 2013]. Techniques for Lagrangian particle dispersion modeling in California's complex terrain are evaluated by *Brioude et al*. [2012] for further inverse modeling based on the CalNex observations.

4.3. Atmospheric Chemical Processing

4.3.1. Daytime Processing

[83] Several different explanations have been advanced in the literature as to the cause of enhanced O_3 observed on weekends [e.g., *Marr and Harley*, 2002]. CalNex data were analyzed along with data from previous intensive field projects to show that VOCs and NO_x were oxidized more rapidly on weekends than on weekdays [*Pollack et al*., 2012; *Warneke et al*., 2012]. As a result, photochemical oxidation rates, as well as the O_3 formation efficiency per unit NO_x oxidized, were both enhanced on weekends and contributed to the observed increase in weekend O_3 levels in the basin [*Pollack et al*., 2012]. Processes linking gas-phase chemistry to potential SOA species have also been reported. Measurements of C_1–C_4 organic acids at the Pasadena ground site provided evidence for their rapid photochemical production in polluted urban air [*Veres et al*., 2011]. Pasadena ground site data further showed that Henry's law underpredicted the partitioning of formic acid to the aerosol phase [*Liu et al*., 2012a]. *Washenfelder et al*. [2011] analyzed gas-phase glyoxal (CHOCHO) and ancillary data to investigate atmospheric sources and sinks of this compound and concluded that CHOCHO contributed <4% to the SOA mass measured at the Pasadena site, although much larger contributions have been reported for other urban areas [*Volkamer et al*., 2007].

[84] Measurements of atmospheric nanoparticles between 20 and 25 nm diameters by mass spectrometry at the Pasadena ground site showed episodes of rapid number concentration increases on sunny days, indicative of new particle formation even in this particle-rich environment. These episodes were attributed to the processing of motor vehicle emissions during transport from the downtown Los Angeles area to the measurement site [*Pennington et al*., 2012]. Regular and predictable new particle formation events were also observed on most days at the Bakersfield ground site in the southern SJV [*Ahlm et al*., 2012]. Their analysis showed that the new particle mode, initially centered at 20 nm and growing to 40–100 nm by the afternoon peak in mass, was dominated by secondary organic mass due to daytime photochemical processing.

4.3.2. Nighttime Processing

[85] *In situ* measurements of $ClNO_2$, aerosol chloride, and relevant ancillary species were made at the Pasadena ground

site and aboard the NOAA P-3 aircraft to better understand the complex interaction between emissions, chemistry, and transport that determine the balance between sources and sinks of the highly reactive nocturnal nitrogen oxides. Measurements of N_2O_5, $ClNO_2$, molecular chlorine (Cl_2), and aerosol chloride (Cl^-) on the *Atlantis* provided additional key data with which to examine chemistry involving N_2O_5-mediated chlorine release from aerosol particles. *in situ* $ClNO_2$, aerosol chloride, and long-path DOAS measurements of NO_3, NO_2, and O_3 were made from the Pasadena site to simultaneously constrain the chemistry as well as the vertical distribution of the nocturnal nitrogen oxides.

[86] Hayes et al. (submitted 2012) noted that the sea salt aerosol measured at the Pasadena ground site was substantially depleted in chloride due to atmospheric processing, presumably in part due to nocturnal oxidation chemistry involving reactive uptake of N_2O_5; they further noted a parallel increase in supermicron aerosol nitrate. *Young et al*. [2012] used altitude profiles from the NOAA P-3 aircraft to report the first vertically resolved measurements of $ClNO_2$ and noted that different source terms led to very different vertical profiles of $ClNO_2$ and HONO after dark. They used the Pasadena ground site measurements to construct a primary radical budget and showed that contributions from HONO photolysis would be overestimated without proper accounting for significant decreases in the vertical, due to its strong surface source. *Riedel et al*. [2012] used data from the R/V *Atlantis* to show that photolysis of $ClNO_2$ following sunrise dominates the morning-time source of reactive Cl atoms. They used a box model to estimate that Cl atoms contribute ~25% to the daily alkane oxidation relative to the total calculated from reactions with Cl and OH. They further noted that Cl atoms from $ClNO_2$ photolysis dominate the early morning oxidation of alkanes in the polluted coastal marine boundary layer, resulting in increased O_3 production in the LA basin. Full three-dimensional chemical-transport modeling incorporating the CalNex $ClNO_2$ observations has not been published to date. Earlier results using the CMAQ model suggest that chemistry involving $ClNO_2$ could increase monthly mean 8 h O_3 averages in Los Angeles by 1–2 ppbv but could cause larger increases, up to 13 ppbv of O_3, in isolated episodes [*Sarwar et al*., 2012].

[87] L.H. Mielke et al. (Nocturnal NOx reservoir species during Calnex-LA 2010, submitted to Journal of Geophysical Research, 2012) used the Pasadena ground site data to conclude that nocturnal nitrogen oxides constitute a significant reservoir for NO_x at night, with $ClNO_2$ alone contributing 21% on average to the total budget of NO_x oxidation products measured at the site. They further calculated that photolysis of $ClNO_2$ during the study added a median of 0.8 ppbv of Cl radicals and NO_2 to the Pasadena boundary layer following sunrise. Stable isotopic measurements of aerosol nitrate made from the R/V *Atlantis* suggested significant differences in aerosol sources to the inshore marine boundary layers of the South and Central Coasts of California (W.C. Vicars et al., Spatiotemporal variability in nocturnal nitrogen oxide chemistry as reflected in the isotopic composition of atmospheric nitrate: Results from the CalNex 2010 field study, submitted to Journal of Geophysical Research, 2012). This analysis concluded that nocturnal nitrogen oxide chemistry in continental outflow is an important source of aerosol nitrate to the South Coast marine layer, while daytime oxidation of NO_2 by the hydroxyl radical OH was the principal source for aerosol nitrate in the Central Coast marine layer.

[88] Measurements inland at the Bakersfield ground site during CalNex showed that roughly 30% of nighttime increases in organic particle mass were due to particulate total alkyl and multifunctional nitrates (pΣANs) [*Rollins et al*., 2012], demonstrating that their production after dark via NO_3-initiated chemistry was a major source of SOA mass. They further interpret the observed relationship of pΣANs with NO_2 measured at the site and suggest that this major source of particulate mass would be effectively addressed by targeted NO_x emissions reductions in the Central Valley. The SOA from this newly quantified nighttime source is critically dependent on anthropogenic NO_x emissions driving the NO_3 radical chemistry after dark. While the carbon source of the particulate organic nitrates can be biogenic in origin, *Rollins et al*. [2012] show that multiple oxidation steps are necessary, as large amounts of primary biogenic VOC after dark actually suppressed pΣANs formation. Analysis of FTIR and mass spectral data on the aerosol sampled at Bakersfield suggested that the majority of daytime SOA was due to vehicular emissions of longer-chain alkanes and aromatic compounds [*Liu et al*., 2012b]. IR spectra also show the presence of organonitrate functional groups formed by the nighttime oxidation involving NO_3 radical. These analyses of the CalNex Bakersfield ground site data shed new light on poorly understood aspects of the sources, composition, and chemistry of a significant fraction of SOA mass in the Central Valley.

4.3.3. Organic Aerosol

[89] The CIRPAS Twin Otter examined the spatiotemporal distribution of water-soluble organic carbon (WSOC) since this fraction of OA is critical in shaping aerosol hygroscopic and radiative properties [*Duong et al*., 2011]. WSOC was estimated to account for 6–11% of $PM_{2.5}$ in the LA basin and the ratio of WSOC to total nonrefractory organic mass increased along the sea breeze trajectory from the west to east side of the northern LA basin, reaching $53 \pm 34\%$ near Banning Pass. Such an enhancement along the wind path of aging aerosol during transport is most likely attributed to secondary production. The highest WSOC levels in the LA basin were associated with biomass burning plumes, similar to findings from long-term surface measurements a year before during the PACO field campaign in Pasadena [*Wonaschütz et al*., 2011]. Aerosol WSOC content was found to depend on both ambient RH and aerosol hygroscopicity, where reduced levels of aerosol-phase water and higher temperatures promoted re-partitioning of WSOC to the gas phase and, conversely, enhanced aerosol-phase water resulted in particulate WSOC production via some likely combination of favorable partitioning of WSOC precursors to the aerosol phase and subsequent chemistry in the aerosol phase to produce WSOC. WSOC concentrations were typically higher aloft ($\geq$ 500 m) than near the surface, pointing to the importance of considering the vertical structure of this fraction of the regional aerosol.

[90] Analysis of measurements at the Pasadena site indicate that SOA contributes about two thirds of the OA mass on average, with the balance accounted by primary OA emissions (Hayes et al., submitted 2012). About half of the

primary OA was due to cooking sources, consistent with recent results from many other urban areas [e.g., *Mohr et al*., 2012; *Sun et al*., 2011], a finding that is important for understanding modern carbon measurements in urban areas. A substantial fraction of the SOA is of urban origin, but some regional background SOA is also present. The ratios of SOA to odd oxygen ($O_x = O_3 + NO_2$) and to CO in excess of background levels in Pasadena were similar to those measured in Mexico City and the northeastern US, suggesting similar sources and formation processes of SOA at these urban locations. *Zhang et al*. [2012] showed that WSOC in Los Angeles partitioned predominantly to the organic phase and not the aqueous phase, in contrast to results in Atlanta where partitioning to both phases was important.

[91] Analysis of OA measurements in Tijuana during the CalMex project by an aerosol chemical speciation monitor (ACSM) and by Fourier transform infrared (FTIR) absorption spectroscopy, and correlations with black carbon measurements by SP2, suggested that the major sources of OA impacting the Parque Morelos site was fossil fuel combustion (presumably from automobile traffic), industrial and commercial burning activities, and marine aerosol. The degree of oxygenation as indicated by the ACSM combined with mass spectral analysis indicates that as much as 60% may have been transported from the South Coast Air Basin [*Takahama et al*., 2012].

4.4. Aerosol Optical Properties and Radiative Effects

[92] *Cappa et al*. [2012] compared direct measurements of black carbon absorption enhancements (E_{abs}) from two different regions in California to show that the mixing state of aerosol BC enhances its ability to absorb solar radiation by relatively small factors of ~1.06 at 532 nm and ~1.13 at 405 nm. This analysis used the contrast between measurements made offshore from the R/V *Atlantis* during CalNex with those made in Sacramento, CA, during the concurrent CARES project [*Zaveri et al*., 2012] and concluded that many climate models using E_{abs} dependence of up to a factor of 2 may lead to significant overestimates of warming by BC under some conditions. The observed BC in these two data sets was dominated by that from diesel emissions [*Cappa et al*., 2012]. In contrast, a recent study [*Lack et al*., 2012a] measured this effect in biomass burning plumes and found that coatings of organic and inorganic material on BC enhanced absorption by up to a factor of 1.7 at 532 nm and up to a factor of 3 at 405 nm. *Lack et al*. also concluded that while absorption at 532 nm by particulate organic matter (POM) was very weak, significant variability of absorption at 404 nm was important in determining the overall mass absorption efficiency of POM at low wavelengths in the visible range. Taken together, the *Cappa et al*. and *Lack et al*. analyses suggest sufficiently large differences between the radiative effects of BC, and internal mixtures with BC, from anthropogenic and biomass sources to warrant their separate treatment in climate models.

[93] *LeBlanc et al*. [2012] used spectral irradiance measurements taken on board the P-3 above and below an aerosol layer to determine the aerosol direct radiative forcing. The observed spectral aerosol direct radiative forcing was compared, using relative forcing efficiency, to direct radiative forcing from other field missions in different parts of the world. The CalNex relative forcing efficiency spectra agreed with earlier studies that found this parameter to be constrained at each wavelength within 20% per unit of aerosol optical thickness at 500 nm and was found to be independent of aerosol type and location. The diurnally averaged below-layer forcing integrated over the wavelength range of 350–700 nm for CalNex was estimated to be 59 ± 14 W/m^2 of cooling at the surface per unit optical depth.

[94] *Langridge et al*. [2012] used P-3 data to track the evolution of aerosol radiative properties during transport within and downwind of the Los Angeles basin. They documented that changes in aerosol hygroscopicity, secondary organic carbon content, and ammonium nitrate mass occurring during transport over the time scale of hours had significant effects on the aerosol extinction. They noted the implications that these changes in radiative forcing due to semi-volatile aerosol constituents would have for accurate representation in large-scale climate models.

[95] *Zhang et al*. [2011b] analyzed WSOC aerosol data from the Pasadena ground site to show that nitroaromatics contribute significantly to the brown SOA in Los Angeles. They use aerosol radiocarbon (^{14}C) measurements to conclude that anthropogenic carbon dominated the aerosol budget in Los Angeles, in contrast to measurements in Atlanta, GA, showing a minimal anthropogenic component to the water-soluble SOA.

4.5. Cloud Condensation Nuclei and Aerosol Hygroscopicity

[96] Measurements of CCN concentrations throughout the boundary layer in the Los Angeles basin and Central Valley varied by 2 orders of magnitude (~10^2–10^4 cm^{-3} STP), which represents a substantial fraction of the total submicron particle concentration (~10^3–10^5 cm^{-3} STP). Organic species and fully neutralized sulfate were found to constitute more than 75% of the particle volume in all regions, on average, with higher organic fractions observed in the Central Valley than in the Los Angeles basin. Despite this variation, large changes in the regionally averaged CCN-derived aerosol hygroscopicity were not observed, and most CCN were found to activate between 0.2 and 0.4% supersaturation ($\kappa \sim 0.1$–0.4) [*Moore et al*., 2012], where κ is the hygroscopicity parameter [*Petters and Kreidenweis*, 2007]. Hygroscopicities in this range reflect the dominance of oxygenated organic species (particularly in the Central Valley) and are consistent with the emerging global picture of a continental aerosol hygroscopicity of $\kappa \sim 0.3$ [e.g., *Andreae and Rosenfeld*, 2008; *Pringle et al*., 2010].

[97] More significant compositional variation was observed within the Los Angeles basin, resulting in a more complex picture with regard to aerosol hygroscopicity. For example, by analyzing data from a cavity ringdown extinction spectrometer (CRDS), *Langridge et al*. [2012] attributed measured changes in humidified aerosol optical extinction to gas-aerosol partitioning of organic and nitrate species as the urban LA plume moved inland into the warmer, eastern part of the basin. The gas-to-particle partitioning of SOA precursors and the evaporation of semivolatile ammonium nitrate resulted in an overall decrease in hygroscopicity of the aging aerosol. This trend is consistent with *Hersey et al*. [2013], who also observed a decrease (from $\kappa = 0.4$ to $\kappa = 0.2$) in subsaturated aerosol hygroscopicity for 150–250 nm aerosol measured aboard the CIRPAS Twin Otter. Meanwhile,

concurrent CCN measurements aboard the CIRPAS Twin Otter showed the opposite trend, with supersaturated aerosol hygroscopicity increasing with plume photochemical age ($\kappa = 0.2$ to $\kappa = 0.4$) at 0.73% supersaturation. This discrepancy likely reflects size-dependent changes in aerosol composition during plume aging—a conclusion that is supported by particle time-of-flight mass spectrometry compositional data [*Hersey et al.*, 2013]. This sort of size-dependent chemistry was also observed in measurements of a biomass burning (BB) plume sampled by the CIRPAS Twin Otter in the Los Angeles basin, emphasizing the role of BB as a source of CCN even while being effectively nonhygroscopic at relative humidities less than 100%.

5. Summary

[98] The initial CalNex results described above represent currently completed studies stemming from this large collaborative project; additional analyses of observations and model studies are underway that should extend, improve, and in some cases perhaps contradict these early results.

[99] Climate-relevant findings from CalNex include that leakage from natural gas infrastructure accounts for the excess of observed methane over emission estimates in Los Angeles. Methane emissions from rice cultivation appear to be significantly underestimated, and the spatial and seasonal allocation of N_2O emissions in inventories is not fully consistent with inverse models based on the CalNex data. Air-quality relevant findings include the following: mobile fleet VOC significantly declines in 50 years, and NO_x emissions continue to have an impact on ozone in the Los Angeles basin; ammonia emissions from dairy farms appear to be significantly underestimated; the relative contributions of diesel and gasoline emission to secondary organic aerosol are not fully understood; and nighttime NO_3 chemistry contributes significantly to secondary organic aerosol mass in the Central Valley. The contribution of HONO to HO_x radical production depends significantly on the vertical distribution of HONO in the atmosphere. While new particle mass is dominated by SOA from anthropogenic carbon during the day, primary OA contributes about a third of the total OA mass with cooking sources accounting for half of that fraction. Findings simultaneously relevant to climate and air quality include the following: marine vessel emissions changes due to fuel sulfur and speed controls result in a net warming effect but have substantial positive impacts on local air quality, and there are significant differences in the radiative effects of black carbon between anthropogenic and biomass burning sources.

[100] We conclude by emphasizing the continuing scientific and regulatory value of short-term intensive field studies, even in a well-studied region. Many key CalNex analyses [e.g., *McDonald et al.*, 2012; *Warneke et al.*, 2012; Pollack et al., submitted 2012] depended critically on the data provided by previous studies, each of which was designed to be definitive at the time. Subsequent intensive field studies will be necessary to continue to track evolving emissions, verify control strategy efficacy, and improve the understanding of sources of ozone and particulate matter in the California atmosphere.

[101] **Acknowledgments.** We thank L. Dolislager (CARB) for the description of existing long-term criteria pollutant, greenhouse gas, and meteorological measurement sites in California. We also thank G. Sanger and B. Ochs (NWS San Joaquin Valley/Hanford Weather Forecast Office) and L. Dolislager and J. Pederson (CARB) for meteorological forecast summaries. The R/V *Atlantis* cruise and NOAA P-3 flights were supported, in part, by the NOAA Climate Change and, in part, by the NOAA Air Quality programs. NOAA Twin Otter flights were supported by the NOAA Air Quality program and the California Air Resources Board. CIRPAS Twin Otter flights were supported by the NOAA Climate Change program under contract NA090AR4310128. NASA B200 flights were supported by the DOE Atmospheric Systems Research Program and the NASA Radiation Sciences and Tropospheric Chemistry programs. Data collection at the CALGEM tall tower sites was supported by the NOAA Office of Global Programs, the California Energy Commission (CEC) Public Interest Environmental Research Program, and LBNL Laboratory Directed Research through the U.S. Department of Energy under contract DE-AC02-05CH11231. Researchers at the ground sites were supported by the California Air Resources Board, the NOAA Office of Global Programs, the US Department of Energy, and the US National Science Foundation.

References

Adachi, K., and P. R. Buseck (2008), Internally mixed soot, sulfates, and organic matter in aerosol particles from Mexico City, *Atmos. Chem. Phys.*, *8*, doi:10.5194/acp-8-6469-2008.

Ahlm, L., et al. (2012), Formation and growth of ultrafine particles from secondary sources in Bakersfield, *California, J. Geophys. Eng.*, *117* (D00V08), doi:10.1029/2011JD017144.

Allen, G. A., J. Lawrence, and P. Koutrakis (1999), Field validation of a semi-continuous method for aerosol black carbon (aethalometer) and temporal patterns in summertime hourly black carbon measurements in southwestern PA, *Atmos. Environ.*, *33*, 817–823.

Alvarez II, R. J., et al. (2011), Development and application of a compact tunable solid-state airborne ozone lidar system for boundary layer profiling, *J. Atmos. Oceanic Technol.*, *28*, 1258–1272, doi:10.1175/JTECH-D-10-05044.1.

Anderson, T. L., and J. A. Ogren (1998), Determining aerosol radiative properties using the TSI 3563 integrating nephelometer, *Aerosol Sci. Technol.*, *29*(1), 57–69.

Andreae, M. O., and D. Rosenfeld (2008), Aerosol-cloud-precipitation interactions. Part 1. The nature and sources of cloud-active aerosols, *Earth Sci. Rev.*, *89*, 13–41, doi:10.1016/j.earscirev.2008.03.001.

Angevine, W. M., L. Eddington, K. Durkee, C. Fairall, L. Bianco, and J. Brioude (2012), Meteorological model evaluation for CalNex 2010, *Monthly Weather Rev.*, doi:10.1175/MWR-D-12-00042.1

Arnott, W. P., K. Hamasha, H. Moosmüller, P. J. Sheridan, and J. A. Ogren (2005), Towards aerosol light-absorption measurements with a 7-wavelength aethalometer: Evaluation with a photoacoustic instrument and 3-wavelength nephelometer, *Aerosol Sci. Technol.*, *39*(1), 17–29, doi:10.1080/027868290901972.

Arnott, W. P., H. Moosmüller, C. F. Rogers, T. Jin, and R. Bruch (1999), Photoacoustic spectrometer for measuring light absorption by aerosol: Instrument description, *Atmos. Environ.*, *33*, 2845–2852.

Arnott, W. P., J. W. Walker, H. Moosmüller, R. A. Elleman, H. H. Jonsson, G. Buzorius, W. C. Conant, R. C. Flagan, and J. H. Seinfeld (2006), Photoacoustic insight for aerosol light absorption aloft from meteorological aircraft and comparison with particle soot absorption photometer measurements: DOE Southern Great Plains climate research facility and the coastal stratocumulus imposed perturbation experiments, *J. Geophys. Res.*, *111*(D05S02), doi:10.1029/2005JD005964.

Bahreini, R., et al. (2009), Organic aerosol formation in urban and industrial plumes near Houston and Dallas, Texas, *J. Geophys. Res.*, *114*(D00F16), doi:10.1029/2008JD011493.

Bahreini, R., et al. (2012), Gasoline emissions dominate over diesel in formation of secondary organic aerosol mass, *Geophys. Res. Lett.*, *39* (L06805), doi:10.1029/2011GL050718.

Baidar, S., H. Oetjen, S. Coburn, B. Dix, I. Ortega, R. Sinreich, and R. Volkamer (2012), The CU Airborne MAX-DOAS instrument: ground based validation, and vertical profiling of aerosol extinction and trace gases, *Atmos. Meas. Tech. Discuss.*, *5*, 7243–7292, doi:10.5194/amtd-5-7243-2012.

Bao, J. W., S. A. Michelson, P. O. G. Persson, I. V. Djalalova, and J. M. Wilczak (2008), Observed and WRF-simulated low-level winds in a high-ozone episode during the Central California Ozone Study, *J. Appl. Meteorol. Climatol.*, *47*(9), 2372–2394.

Barletta, B., et al. (2013), Emission estimates of HCFCs and HFCs in California from the 2010 CalNex study, *J. Geophys. Res. 118*, doi:10.1002/jgrd.50209.

Barletta, B., P. Nissenson, S. Meinardi, D. Dabdub, F. S. Rowland, R. A. VanCuren, J. Pederson, G. S. Diskin, and D. R. Blake (2011), HFC-152a and HFC-134a emission estimates and characterization of CFCs, CFC replacements, and other halogenated solvents measured during the 2008 ARCTAS campaign (CARB phase) over the South Coast Air Basin of California, *Atmos. Chem. Phys.*, *11*, 2655–2669, doi:10.5194/acp-11-2655-2011.

Bateman, A. P., S. A. Nizkorodov, J. Laskin, and A. Laskin (2010), High-resolution electrospray ionization mass spectrometry analysis of water-soluble organic aerosols collectred with a particle into liquid sampler, *Anal. Chem.*, *82*, 8010–8016, doi:10.1021/ac1014386.

Bates, T. S., P. K. Quinn, D. Coffman, J. E. Johnson, and A. M. Middlebrook (2005), Dominance of organic aerosols in the marine boundary layer over the Gulf of Maine during NEAQS 2002 and their role in aerosol light scattering, *J. Geophys. Res.*, *110*(D18202), doi:10.1029/2005JD005797.

Bates, T. S., P. K. Quinn, D. Coffman, T. L. Miller, D. S. Covert, A. Wiedensohler, S. Leinert, A. Nowak, and C. Neusüss (2001), Regional physical and chemical properties of the marine boundary layer aerosol across the Atlantic during Aerosols99: An overview, *J. Geophys. Res.*, *106*, 20,767–720,782.

Bates, T. S., et al. (2008), Boundary layer aerosol chemistry during TexAQS/GoMACCS 2006: Insights into aerosol sources and transformation processes, *J. Geophys. Res.*, *113*(D00F01), doi:10.1029/2008JD010023.

Bates, T. S., P. K. Quinn, D. S. Covert, D. J. Coffman, J. E. Johnson, and A. Wiedensohler (2000), Aerosol physical properties and processes in the lower marine boundary layer: A comparison of shipboard sub-micron data from ACE-1 and ACE-2, *Tellus*, *52B*, 258–272.

Bates, T. S., et al. (2012), Measurements of ocean derived aerosol off the coast of California, *J. Geophys. Res.*, *117*(D00V15), doi:10.1029/2012JD017588.

Baumgardner, D., H. Jonsson, W. Dawson, D. O'Connor, and R. Newton (2001), The cloud, aerosol, and precipitation spectrometer: A new instrument for cloud investigations, *Atmos. Res.*, *59–60*, 251–264.

Baynard, T., E. R. Lovejoy, A. Pettersson, S. S. Brown, D. Lack, H. Osthoff, P. Massoli, S. Ciciora, W. P. Dubé , and A. R. Ravishankara (2007), Design and application of a pulsed cavity ring-down aerosol extinction spectrometer for field measurements, *Aerosol Sci. Technol.*, *41*(4), 447–462, doi:10.1080/02786820701222801.

Bei, N., et al. (2012), Meteorological overview and plume transport patterns during Cal-Mex 2010, *Atmos. Environ.*, doi:10.1016/j.atmosenv.2012.01.065.

Bertram, T. H., J. R. Kimmel, T. A. Crisp, O. S. Ryder, R. L. N. Yatavelli, J. A. Thornton, M. J. Cubison, M. Gonin, and D. R. Worsnop (2011), A field-deployable, chemical ionization time-of-flight mass spectrometer, *Atmos. Meas. Tech.*, *4*, 1471–1479, doi:10.5194/amt-4-1471-2011.

Bishop, G. A., and D. H. Stedman (2008), A decade of on-road emissions measurements, *Environ. Sci. Technol.*, *42*(5), 1651–1656, doi:10.1021/es702413b.

Blanchard, C. L., and S. J. Tanenbaum (2003), Differences between weekday and weekend air pollutant levels in southern California, *J. Air Waste Manage. Assoc.*, *53*(7), 816–828.

Bon, D. M., et al. (2011), Measurements of volatile organic compounds at a suburban ground site (T1) in Mexico City during the MILAGRO 2006 campaign: Measurement comparison, emission ratios, and source attribution, *Atmos. Chem. Phys.*, *11*, 2399–2421, doi:10.5194/acp-11-2399-2011.

Bond, T. C., T. L. Anderson, and D. Campbell (1999), Calibration and intercomparison of filter-based measurements of visible light absorption by aerosols, *Aerosol Sci. Technol.*, *30*, 582–600, doi:10.1080/027868299304435.

Bond, T. C., D. G. Streets, K. F. Yarber, S. M. Nelson, J.-H. Woo, and Z. Klimont (2004), A technology-based global inventory of black and organic carbon emissions from combustion, *J. Geophys. Res.*, *109*(D14203), doi:10.1029/2003JD003697.

Borbon, A., et al. (2013), Emission ratios of anthropogenic volatile organic compounds in northern mid-latitude megacities: Observations versus emission inventories in Los Angeles and Paris, *J. Geophys. Res. 118*, doi:10.1002/jgrd.50059.

Boucouvala, D., and R. Bornstein (2003), Analysis of transport patterns during an SCOS97-NARSTO episode, *Atmos. Environ.*, *37*(Supplement no. 2), S73–S94, doi:10.1016/S1352-2310(03)00383-2.

Bradley, F., and C. Fairall (2006), A guide to making climate quality meteorological and flux measurements at sea, *Technical Memorandum Rep.*, 108 pp, NOAA.

Brioude, J., W. M. Angevine, S. A. McKeen, and E.-Y. Hsie (2012), Numerical uncertainty at mesoscale in a Lagrangian model in complex terrain, *Geoscientific Model Dev.*, *5*(5), 1127–1136, doi:10.5194/gmd-5-1127-2012.

Brock, C. A., et al. (2011), Characteristics, sources, and transport of aerosols measured in spring 2008 during the aerosol, radiation, and cloud processes affecting Arctic Climate (ARCPAC) Project, *Atmos. Chem. Phys.*, *11*, 2423–2453, D08302, doi:10.5194/acp-11-2423-2011.

Brock, C. A., et al. (2008), Sources of particulate matter in the northeastern United States in summer: 2. Evolution of chemical and microphysical properties, *J. Geophys. Res.*, *113*, doi: 10.1029/2007JD009241.

Bukowiecki, N., A. Richard, M. Furger, E. Weingartner, M. Aguirre, T. Huthwelker, P. Leinemann, R. Gherig, and U. Baltensperger (2009), Deposition uniformity and particle size distribution of ambient aerosol collected with a rotating drum impactor, *Aerosol Sci. Technol.*, *43*(9), 891–901, doi:10.1080/02786820903002431.

Canagaratna, M. R., et al. (2007), Chemical and microphysical characterization of ambient aerosols with the Aerodyne aerosol mass spectrometer, *Mass Spectrom. Rev.*, *26*, 185–222, doi:10.1002/mas.20115.

Cappa, C. D., et al. (2012), Radiative absorption enhancements due to the mixing state of atmospheric black carbon, *Science*, *337*, 1078–1081, doi:10.1126/science.1223447.

CARB (2008), Climate Change Scoping Plan: A Framework for Change, pursuant to AB 32, the California Global Warming Solutions Act of 2006*Rep*.

CARB (2011), California Greenhouse Gas Emissions Inventory: 2000–2009*Rep*.

Carter, D. A., K. S. Gage, W. L. Ecklund, W. M. Angevine, P. E. Johnston, A. C. Riddle, J. Wilson, and C. R. Williams (1995), Developments in UHF lower tropospheric wind profiling at NOAA's Aeronomy Laboratory, *Radio Sci.*, *30*, 977–1001.

Cass, G. R., and F. H. Shair (1984), Sulfate accumulation in a sea breeze/land breeze circulation system, *J. Geophys. Res.*, *89*, 1429–1438.

Chow, J. C., L. W. A. Chen, J. G. Watson, D. H. Lowenthal, K. A. Magliano, K. Turkiewicz, and D. E. Lehrman (2006), $PM_{2.5}$ chemical composition and spatiotemporal variability during the California Regional $PM_{10}/PM_{2.5}$ Air Quality Study (CRPAQS), *J. Geophys. Res.*, *111*(D10S04), doi:10.1029/2005JD006457.

Chu, D. A., Y. J. Kaufman, C. Ichoku, L. A. Remer, D. Tanre, and B. N. Holben (2002), Validation of MODIS aerosol optical depth retrieval over land, *Geophys. Res. Lett.*, *29*(12), 1617.

Coburn, S., B. Dix, R. Sinreich, and R. Volkamer (2011), The CU ground MAX-DOAS instrument: characterization of RMS noise limitations and first measurements near Pensacola, FL of BrO, IO, and CHOCHO, *Atmos. Meas. Tech.*, *4*, 2421–2439.

Colman, J. J., A. L. Swanson, S. Meinardi, B. Sive, D. R. Blake, and F. S. Rowland (2001), Description of the analysis of a wide range of volatile organic compounds in whole air samples collected during PEM-Tropics A and B, *Anal. Chem.*, *73*, 3723–3731, doi:10.1021/ac010027g.

Cooper, O. R., et al. (2011), Measurement of western U.S. baseline ozone from the surface to the tropopause and assessment of downwind impact regions, *J. Geophys. Res.*, *116*(D00V03), doi:10.1029/2011JD016095.

Cooper, O. R., et al. (2010), Increasing springtime ozone mixing ratios in the free troposphere over western North America, *Nature*, *463*(7279), 344–348, doi:10.1038/nature08708.

Davis, K. J., N. Gamage, C. R. Hagelberg, C. Kiemle, D. H. Lenschow, and P. P. Sullican (1999), An objective method for deriving atmospheric structure from airborne lidar observations, *J. Atmos. Oceanic Technol.*, *17*, 1455–1468.

de Gouw, J., and C. Warneke (2006), Measurements of volatile organic compounds in the Earth's atmosphere using proton-transfer-reaction mass spectrometry, *Mass Spectrom. Rev.*, *26*, 223–257, doi:10.1002/mas.20119.

de Gouw, J. A., J. B. Gilman, A. Borbon, C. Warneke, W. C. Kuster, P. D. Goldan, J. S. Holloway, J. Peischl, and T. B. Ryerson (2012), Increasing atmospheric burden of ethanol in the United States, *Geophys. Res. Lett.*, *39*(L15803), doi:10.1029/2012GL052109.

DeCarlo, P. F., et al. (2006), Field-deployable, high-resolution, time-of-flight aerosol mass spectrometer, *Anal. Chem.*, *78*(24), 8281–8289, doi:10.1021/ac061249n.

Dial, K. D., S. Hiemstra, and J. E. Thompson (2010), Simultaneous measurement of optical scattering and extinction on dispersed aerosol samples, *Anal. Chem.*, *82*, 7885–7896, doi:10.1021/ac100617j.

Djuricin, S., D. E. Pataki, and X. Xu (2010), A comparison of tracer methods for quantifying CO_2 sources in an urban region, *J. Geophys. Res.*, *115*(D11303), doi:10.1029/2009JD012236.

Djuricin, S., X. Xu, and D. E. Pataki (2012), The radiocarbon composition of tree rings as a tracer of local fossil fuel emissions in the Los Angeles basin: 1980–2008, *J. Geophys. Res.*, *117*(D12302), doi:10.1029/2011JD017284.

Docherty, K. S., et al. (2011), The 2005 Study of Organic Aerosols at Riverside (SOAR-1): Instrumental intercomparisons and fine particle composition, *Atmos. Chem. Phys.*, *11*, 12387–12420, doi:10.5194/acp-11-12387-2011.

Drummond, J. W., A. Volz, and D. H. Ehhalt (1985), An optimized chemiluminescence detector for tropospheric NO measurements, *J. Atmos. Chem*, *2*(3), 287–306.

Dunlea, E. J., et al. (2006), Technical note: Evaluation of standard ultraviolet absorption ozone monitors in a polluted urban environment, *Atmos. Chem. Phys.*, *6*, 3163–3180.

Dunlea, E. J., et al. (2007), Evaluation of nitrogen dioxide chemiluminescence monitors in a polluted urban environment, *Atmos. Chem. Phys.*, *7*, 2691–2704.

Duong, H. T., A. Sorooshian, J. S. Craven, S. P. Hersey, A. R. Metcalf, X. Zhang, R. J. Weber, H. Jonsson, R. C. Flagan, and J. H. Seinfeld (2011), Water-soluble organic aerosol in the Los Angeles Basin and outflow regions: Airborne and ground measurements during the 2010 CalNex field campaign, *J. Geophys. Res.*, *116*(D00V04), doi:10.1029/2011JD016674.

Dusanter, S., D. Vimal, P. S. Stevens, R. Volkamer, and L. T. Molina (2009), Measurements of OH and HO2 concentrations during the MCMA-2006 field campaign—Part 1: Deployment of the Indiana University laser-induced fluorescence instrument, *Atmos. Chem. Phys.*, *9*, 1665–1685.

Ellis, R. A., J. G. Murphy, E. Pattey, R. van Haarlem, J. M. O'Brien, and S. C. Herndon (2010), Characterizing a quantum cascade tunable infrared laser differential absorption spectrometer (QC-TILDAS) for measurements of atmospheric ammonia, *Atmos. Meas. Tech.*, *3*, 397–406.

Ensberg, J. J., et al. (2013), Inorganic and black carbon aerosols in the Los Angeles Basin during CalNex, *J. Geophys. Res. 118*, doi:10.1029/2012JD018136.

Epa, U. (2007), Inventory of U.S. greenhouse gas emissions and sinks: 1900–2005*Rep. EPA-430-R-07-002*, Washington, D.C.

Fairall, C. W., A. B. White, J. B. Edson, and J. E. Hare (1997), Integrated shipboard measurements of the marine boundary layer, *J. Atmos. Oceanic Technol.*, *14*, 338–359.

Fast, J. D., et al. (2012), Transport and mixing patterns over Central California during the carbonaceous aerosol and radiative effects study (CARES), *Atmos. Chem. Phys.*, *12*, 1759–1783, doi:10.5194/acp-12-1759-2012.

Finlayson-Pitts, B. J. (2003), The tropospheric chemistry of sea salt: A molecular-level view of the chemistry of NaCl and NaBr, *Chem. Rev.*, *103*, 4801–4822.

Fitz, D. R., K. Bumiller, and A. Lashgari (2003), Measurement of NO_y during the SCOS97-NARSTO, *Atmos. Environ.*, *37*(Supplement No. 2), S119–S134, doi:10.1016/S1352-2310(03)00385-6.

Flocke, F. M., A. J. Weinheimer, A. L. Swanson, J. M. Roberts, R. Schmitt, and S. Shertz (2005), On the measurement of PANs by gas chromatography and electron capture detection, *J. Atmos. Chem.*, *52*, 19–43, doi:10.1007/s10874-005-6772-0.

Fortner, E. C., J. Zheng, R. Zhang, W. Berk Knighton, R. M. Volkamer, P. Sheehy, L. Molina, and M. André (2009), Measurements of volatile organic compounds using proton transfer reaction—Mass spectrometry during the MILAGRO 2006 campaign, *Atmos. Chem. Phys.*, *9*, 467–481.

Frisch, A. S., B. E. Martner, and J. S. Gibson (1989), Measurement of the vertical flux of turbulent kinetic energy with a single Doppler radar, *Boundary Layer Meteorol.*, *49*, 331–337, doi:10.1007/BF00123648.

Froidevaux, L., et al. (2008), Validation of Aura Microwave Limb Sounder stratospheric ozone measurements, *J. Geophys. Res.*, *113*(D15S20), doi:10.1029/2007JD008771.

Froyd, K. D., D. M. Murphy, T. J. Sanford, D. S. Thomson, J. C. Wilson, L. Pfister, and L. Lait (2009), Aerosol composition of the tropical upper troposphere, *Atmos. Chem. Phys.*, *9*, 4363–4385.

Fuchs, H., W. P. Dubé, B. M. Lerner, N. L. Wagner, E. J. Williams, and S. S. Brown (2009), A sensitive and versatile detector for atmospheric NO_2 and NO_x based on blue diode laser cavity ring-down spectroscopy, *Environ. Sci. Technol.*, *43*(20), 7831–7836, doi:10.1021/es902067h.

Gard, E., J. E. Mayer, B. D. Morrical, T. Dienes, D. P. Fergenson, and K. A. Prather (1997), Real-time analysis of individual atmospheric aerosol particles: Design and performance of a portable ATOFMS, *Anal. Chem.*, *69*, 4083–4091, doi:10.1021/ac970540n.

Gearn, A. G. (1961), Absorption of ozone in the ultra-violet and visible regions of the spectrum, *Proc. Phys. Soc.*, *78*, 932.

Gentner, D. R., et al. (2012), Elucidating secondary organic aerosol from diesel and gasoline vehicles through detailed characterization of organic carbon emissions, *Proc. Natl. Acad. Sci.*, *109*(45), 18318–18323, doi:10.1073/pnas.1212272109.

Gentner, D. R., A. M. Miller, and A. H. Goldstein (2010), Seasonal variability in anthropogenic halocarbon emissions, *Environ. Sci. Technol.*, *44* (14), 5377–5382, doi:10.1021/es1005362.

Gerbig, C., S. Schmitgen, D. Kley, A. Volz-Thomas, K. Dewey, and D. Haaks (1999), An improved fast-response vacuum-UV resonance fluorescence CO instrument, *J. Geophys. Res.*, *104*, 1699–1704.

Gilardoni, S., et al. (2007), Regional variation of organic functional groups in aerosol particles on four U.S. east coast platforms during the International Consortium for Atmospheric Research on Transport and Transformation 2004 campaign, *J. Geophys. Res.*, *112*(D10S27), doi:10.1029/2006JD007737.

Goldstein, A. H., D. R. Worton, B. J. Williams, S. V. Hering, N. M. Kreisberg, O. Panić, and T. Górecki (2008), Thermal desorption comprehensive two-dimensional gas chromatography for in-situ measurements of organic aerosols, *J. Chromatogr. A*, *1186*, 340–347, doi:10.1016/j.chroma.2007.09.094.

Gorham, K. A., N. J. Blake, R. A. VanCuren, H. E. Fuelberg, S. Meinardi, and D. R. Blake (2010), Seasonal and diurnal measurements of carbon monoxide and nonmethane hydrocarbons at Mt. Wilson, California: Indirect evidence of atomic Cl in the Los Angeles basin, *Atmos. Environ.*, *44*, 2271–2279.

Green, D. C., G. W. Fuller, and T. Baker (2009), Development and validation of the volatile correction model for PM_{10}—An empirical method for adjusting TEOM measurements for their loss of volatile particulate matter, *Atmos. Environ.*, *43*, 2132–2141, doi:10.1016/j.atmosenv.2009.01.024.

Hagler, G. S. W., R. W. Baldauf, E. D. Thoma, T. R. Long, R. F. Snow, J. S. Kinsey, L. Oudejans, and B. K. Gullett (2009), Ultrafine particles near a major roadway in Raleigh, North Carolina: Downwind attenuation and correlation with traffic-related pollutants, *Atmos. Environ.*, *43*, 1229–1234, doi:10.1016/j.atmosenv.2008.11.024.

Hair, J. W., C. A. Hostetler, A. L. Cook, D. B. Harper, R. A. Ferrare, T. L. Mack, W. Welch, L. R. Izquierdo, and F. E. Hovis (2008), Airborne High Spectral Resolution Lidar for profiling aerosol optical properties, *Appl. Opt.*, *47*(36), 6734–6753.

Haman, C. L., B. Lefer, and G. A. Morris (2012), Seasonal variability in the diurnal evolution of the boundary layer in a near-coastal urban environment, *J. Atmos. Oceanic Technol.*, *29*, 697–710, doi:10.1175/JTECH-D-11-00114.1.

Harley, R. A., L. C. Marr, J. K. Lehner, and S. N. Giddings (2005), Changes in motor vehicle emissions on diurnal to decadal time scales and effects on atmospheric composition, *Environ. Sci. Technol.*, *39*(14), 5356–5362, doi:10.1021/es048172+.

Hegg, D. A., D. S. Covert, H. Jonsson, and P. A. Covert (2005), Determination of the transmission efficiency of an aircraft aerosol inlet, *Aerosol Sci. Technol.*, *39*(10), 966–971, doi:10.1080/02786820500377814.

Heidinger, A., A. Evan, M. Foster, and A. Walther (2012), A naïve Bayesian cloud detection scheme derived from CALIPSO and applied within PATMOS-x, *J. Appl. Meteorol. Climatol.*, doi:10.1175/JAMC-D-11-02.1.

Heikes, B. G. (1992), Formaldehyde and hydroperoxides at Mauna Loa Observatory, *J. Geophys. Res.*, *97*, 18,001–018,013.

Hennigan, C. J., M. H. Bergin, J. E. Dibb, and R. J. Weber (2008), Enhanced secondary organic aerosol formation due to water uptake by fine particles, *Geophys. Res. Lett.*, *35*(L18801), doi:10.1029/2008GL035046.

Hering, S. V., and D. L. Blumenthal (1989), Southern California Air Quality Study (SCAQS) description of measurement activities final report, California Air Resources Board.

Herndon, S. C., M. S. Zahniser, D. D. J. Nelson, J. Shorter, J. B. McManus, R. Jiménez, C. Warneke, and J. A. de Gouw (2007), Airborne measurements of HCHO and HCOOH during the New England Air Quality Study 2004 using a pulsed quantum cascade laser spectrometer, *J. Geophys. Res.*, *112*(D10S03), doi:10.1029/2006JD007600.

Hersey, S. P., et al. (2013), Composition and hygroscopicity of the Los Angeles Aerosol: CalNex, *J. Geophys. Res. 118*, doi:10.1002/jgrd.50307.

Hersey, S. P., J. S. Craven, K. A. Schilling, A. R. Metcalf, A. Sorooshian, M. N. Chan, R. C. Flagan, and J. H. Seinfeld (2011), The Pasadena Aerosol Characterization Observatory (PACO): Chemical and physical analysis of the Western Los Angeles Basin aerosol, *Atmos. Chem. Phys.*, *11*, 7417–7443, doi:10.5194/acp-11-7417-2011.

Holben, B. N., et al. (2001), An emerging ground-based aerosol climatology: Aerosol optical depth from AERONET, *J. Geophys. Res.*, *106*, 12,067–012,097.

Holloway, J. S., R. O. Jakoubek, D. D. Parrish, C. Gerbig, A. Volz-Thomas, S. Schmitgen, A. Fried, B. Wert, B. Henry, and J. R. Drummond (2000), Airborne intercomparison of vacuum ultraviolet fluorescence and tunable diode laser absorption measurements of tropospheric carbon monoxide, *J. Geophys. Res.*, *105*, 24,251–224,261.

Holzinger, R., J. Williams, F. Herrmann, J. Lelieveld, N. M. Donahue, and T. Röckmann (2010), Aerosol analysis using a Thermal-Desorption Proton-Transfer-Reaction Mass Spectrometer (TD-PTR-MS): A new approach to study processing of organic aerosols, *Atmos. Chem. Phys.*, *10*, 2257–2267.

Hsu, Y. K., T. VanCuren, S. Park, C. Jakober, J. Herner, M. FitzGibbon, D. R. Blake, and D. D. Parrish (2010), Methane emissions inventory verification in southern California, *Atmos. Environ.*, *44*, 1–7, doi:10.1016/j.atmosenv.2009.10.002.

Huffman, J. A., P. J. Ziemann, J. T. Jayne, D. R. Worsnop, and J. L. Jimenez (2008), Development and characterization of a fast-stepping/scanning thermodenuder for chemically-resolved aerosol volatility measurements, *Aerosol Sci. Technol.*, *42*, 395–407.

Hyslop, N. P., and W. H. White (2008), An evaluation of interagency monitoring of protected visual environments (IMPROVE) collocated precision and uncertainty estimates, *Atmos. Environ.*, *42*, 2691–2705.

Jacob, D. J., et al. (2010), The Arctic Research of the Composition of the Troposphere from Aircraft and Satellites (ARCTAS) mission: Design, execution, and first results, *Atmos. Chem. Phys.*, *10*, 5191–5212, doi:10.5194/acp-10-5191-2010.

Jeong, S., C. Zhao, A. E. Andrews, L. Bianco, J. M. Wilczak, and M. L. Fischer (2012a), Seasonal variation of CH_4 emissions from central California, *J. Geophys. Res.*, *117*(D11306), doi:10.1029/2011JD016896.

Jeong, S., C. Zhao, A. E. Andrews, E. J. Dlugokencky, C. Sweeney, L. Bianco, J. M. Wilczak, and M. L. Fischer (2012b), Seasonal variations

in N_2O emissions from central California, *Geophys. Res. Lett.*, *39* (L16805), doi:10.1029/2012GL052307.

Johansson, M., B. Galle, T. Yu, L. Tang, D. Chen, H. Li, J. X. Li, and Y. Zhang (2008), Quantification of total emission of air pollutants from Beijing using mobile mini-DOAS, *Atmos. Environ.*, *42*, 6296–6933, doi:10.1016/j.atmosenv.2008.05.025.

Kang, E., M. J. Root, D. W. Toohey, and W. H. Brune (2007), Introducing the concept of potential aerosol mass (PAM), *Atmos. Chem. Phys.*, *7*, 5727–5744.

Kercher, J. P., T. P. Riedel, and J. A. Thornton (2009), Chlorine activation by N_2O_5: simultaneous, *in situ* detection of $ClNO_2$ and N_2O_5 by chemical ionization mass spectrometry, *Atmos. Meas. Tech.*, *2*, 193–204.

Khalizov, A. F., H. Xue, L. Wang, J. Zheng, and R. Zhang (2009a), Enhanced light absorption and scattering by carbon soot aerosol internally mixed with sulfuric acid, *J. Phys. Chem. A*, *113*, 1066–1074.

Khalizov, A. F., R. Zhang, D. Zhang, H. Xue, J. Pagels, and P. H. McMurry (2009b), Formation of highly hygroscopic soot aerosols upon internal mixing with sulfuric acid vapor, *J. Geophys. Res.*, *114*(D05208), doi:10.1029/2008JD010595.

King, W. D., D. A. Parkin, and R. J. Handsworth (1978), A hot-wire liquid water device having fully calculable response characteristics, *J. Appl. Meteorol.*, *17*, 1809–1813.

Knipping, E., and D. Dabdub (2003), Impact of chlorine emissions from sea-salt aerosol on coastal urban ozone, *Environ. Sci. Technol.*, *37*(2), 275–284, doi:10.1021/es025793z.

Knobelspiesse, K., et al. (2011), Combined retrievals of boreal forest fire aerosol properties with a polarimeter and lidar, *Atmos. Chem. Phys.*, *11*, 7045–7067, doi:10.5194/acp-11-7045-2011.

Kort, E. A., P. K. Patra, K. Ishijima, B. C. Daube, R. Jiménez, J. Elkins, D. Hurst, F. L. Moore, C. Sweeney, and S. C. Wofsy (2011), Tropospheric distribution and variability of N_2O: Evidence for strong tropical emissions, *Geophys. Res. Lett.*, *38*(L15806), doi:10.1029/2011GL047612.

Kovalev, V. A., A. Petkov, C. Wold, S. Urbanski, and W. M. Hao (2009), Determination of smoke plume and layer heights using scanning lidar data, *Appl. Opt.*, *48*(28), 5287–5294.

Kristensen, K., and M. Glasius (2011), Organosulfates and oxidation products from biogenic hydrocarbons in fine aerosols from a forest in North West Europe during spring, *Atmos. Environ.*, *45*(27), 4546–4556, doi:10.1016/j.atmosenv.2011.05.063

Król, S., B. Zabiegała, and J. Namieśnik (2010), Monitoring VOCs in atmospheric air. I. On-line gas analyzers, *Trends Anal. Chem.*, *29*(9), 1092–1100, doi:10.1016/j.trac.2010.05.007.

Kuster, W. C., B. T. Jobson, T. Karl, D. Riemer, E. Apel, P. D. Goldan, and F. C. Fehsenfeld (2004), Intercomparison of volatile organic carbon measurement techniques and data at La Porte during the TexAQS2000 air quality study, *Environ. Sci. Technol.*, *38*(1), 221–228, doi:10.1021/es034710r.

Lack, D. A., et al. (2011), Impact of fuel quality regulation and speed reductions on shipping emissions: Implications for climate and air quality, *Environ. Sci. Technol.*, *45*, 9052–9060, doi:10.1021/es2013424.

Lack, D. A., J. M. Langridge, R. Bahreini, C. D. Cappa, A. M. Middlebrook, and J. P. Schwarz (2012a), Brown carbon and internal mixing in biomass burning particles, *Proc. Natl. Acad. Sci.*, *109*(37), 14802–14807, doi:10.1073/pnas.1206575109.

Lack, D. A., M. S. Richardson, D. Law, J. M. Langridge, C. D. Cappa, R. J. McLaughlin, and D. M. Murphy (2012b), Aircraft instrument for comprehensive characterization of aerosol optical properties. Part 2: Black and brown carbon absorption enhancement measured with photo acoustic spectroscopy, *Aerosol Sci. Technol.*, *46*(5), 555–568, doi:10.1080/02786826.2011.645955.

Lance, S., C. A. Brock, D. Rogers, and J. A. Gordon (2010), Water droplet calibration of the Cloud Droplet Probe (CDP) and in-flight performance in liquid, ice, and mixed-phase clouds during ARCPAC, *Atmos. Meas. Tech.*, *3*, 1683–1706, doi:10.5194/amt-3-1683-2010.

Landis, M. S., R. K. Stevens, F. Schaedlich, and E. M. Prestbo (2002), Development and characterization of an annular denuder methodology for the measurement of divalent inorganic reactive gaseous mercury in ambient air, *Environ. Sci. Technol.*, *36*(13), 3000–3009, doi:10.1021/es015887t.

Langford, A. O., J. Brioude, O. R. Cooper, C. J. Senff, R. J. Alvarez II, R. M. Hardesty, B. J. Johnson, and S. J. Oltmans (2012), Stratospheric influence on surface ozone in the Los Angeles area during late spring and early summer of 2010, *J. Geophys. Res.*, *117*(D00V06), doi:10.1029/2011JD016766.

Langford, A. O., C. J. Senff, R. J. I. Alvarez, R. M. Banta, and R. M. Hardesty (2010), Long-range transport of ozone from the Los Angeles Basin: A case study, *Geophys. Res. Lett.*, *37*(L06807), doi:10.1029/2010GL042507.

Langford, A. O., C. J. Senff, R. J. I. Alvarez, R. M. Banta, R. M. Hardesty, D. D. Parrish, and T. B. Ryerson (2011), Comparison between the TOPAZ airborne ozone lidar and in situ measurements during TexAQS 2006, *IEEE J. Oceanic Atmos. Technol.*, *28*, 1243–1257, doi:10.1175/JTECH-D-10-05043.1.

Langridge, J. M., et al. (2012), Evolution of aerosol properties impacting visibility and direct climate forcing in an ammonia-rich urban environment, *J. Geophys. Res.*, *117*(D00V11), doi:10.1029/2011JD017116.

Langridge, J. M., M. S. Richardson, D. Lack, D. Law, and D. M. Murphy (2011), Aircraft instrument for comprehensive characterization of aerosol optical properties. Part I: Wavelength-dependent optical extinction and its relative humidity dependence measured using cavity ringdown spectroscopy, *Aerosol Sci. Technol.*, *45*(11), 1305–1318, doi:10.1080/02786826.2011.592745.

Laskin, A., J. P. Cowin, and M. J. Iedema (2006), Analysis of individual environmental particles using modern methods of electron microscopy and X-ray microanalysis, *J. Electron. Spectrosc. Relat. Phenom.*, *150*, 260–274, doi:10.1016/j.elspec.2005.06.008.

Law, D. C., S. A. McLaughlin, M. J. Post, B. L. Weber, D. C. Welsh, D. E. Wolfe, and D. A. Merritt (2002), An electronically stabilized phased array system for shipborne atmospheric wind profiling, *J. Atmos. Oceanic Technol.*, *19*(6), 924–933, doi:10.1175/1520-0426.

LeBlanc, S. E., K. S. Schmidt, P. Pilewskie, J. Redemann, C. Hostetler, R. Ferrare, J. Hair, J. M. Langridge, and D. A. Lack (2012), Spectral aerosol direct radiative forcing from airborne radiative measurements during CalNex and ARCTAS, *J. Geophys. Res.*, *117*(D00V20), doi:10.1029/2012JD018106.

Lee, M., B. C. Noone, D. O'Sullivan, and B. G. Heikes (1995), Method for the collection and HPLC analysis of hydrogen peroxide and C_1 and C_2 hydroperoxides in the atmosphere, *J. Atmos. Oceanic Technol.*, *12*, 1060–1070.

Lerner, B. M., P. C. Murphy, and E. J. Williams (2009), Field measurements of small marine craft gaseous emission factors during NEAQS 2004 and TexAQS 2006, *Environ. Sci. Technol.*, *43*(21), 8213–8219, doi:10.1021/es901191p.

Lhermitte, R. (1987), A 94-GHz Doppler radar for cloud observations, *J. Atmos. Oceanic Technol.*, *4*, 36–48.

Liang, J., B. Jackson, and A. Kaduwela (2006), Evaluation of the ability of indicator species ratios to determine the sensitivity of ozone to reductions in emissions of volatile organic compounds and oxides of nitrogen in northern California, *Atmos. Environ.*, *40*, 5156–5166, doi:10.1016/j.atmosenv.2006.03.060.

Lin, M., A. M. Fiore, O. R. Cooper, L. W. Horowitz, A. O. Langford, H. Levy II, B. J. Johnson, B. Naik, S. J. Oltmans, and C. J. Senff (2012a), Springtime high surface ozone events over the western United States: Quantifying the role of stratospheric intrusions, *J. Geophys. Res.*, *117* (D00V22), doi:10.1029/2012JD018151.

Lin, M., et al. (2012b), Transport of Asian ozone pollution into surface air over the western United States in spring, *J. Geophys. Res.*, *117* (D00V07), doi:10.1029/2011JD016961.

Liu, J., et al. (2012a), On the gas-particle partitioning of soluble organic aerosol in two urban atmospheres with contrasting emissions: 2. Gas and particle phase formic acid, *J. Geophys. Res.*, *117*(D00V21), doi:10.1029/2012JD017912,.

Liu, S., et al. (2012b), Secondary organic aerosol formation from fossil fuel sources contribute majority of summertime organic mass at Bakersfield, *J. Geophys. Res.*, *117*(D00V26), doi:10.1029/2012JD018170.

Liu, S., S. Takahama, L. M. Russell, S. Gilardoni, and D. Baumgardner (2009), Oxygenated organic functional groups and their sources in single and submicron organic particles in MILAGRO 2006 campaign, *Atmos. Chem. Phys.*, *9*, 6849–6863.

Livesey, N. J., et al. (2008), Validation of Aura Microwave Limb Sounder O_3 and CO observations in the upper troposphere and lower stratosphere, *J. Geophys. Res.*, *113*(D15S02), doi:10.1029/2007JD008805.

Lu, R., and R. P. Turco (1996), Ozone distributions over the Los Angeles Basin: Three-dimensional simulations with the SMOG model, *Atmos. Environ.*, *30*, 4155–4176.

Marr, L. C., K. Dzepina, J. L. Jimenez, F. Reisen, H. L. Bethel, J. Arey, J. S. Gaffney, N. A. Marley, L. T. Molina, and M. J. Molina (2006), Sources and transformations of particle-bound polycyclic aromatic hydrocarbons in Mexico City, *Atmos. Chem. Phys.*, *6*, 1733–1745.

Marr, L. C., and R. A. Harley (2002), Modeling the effect of weekday-weekend differences in motor vehicle emissions on photochemical air pollution in central California, *Environ. Sci. Technol.*, *36*(19), 4099–4106, doi:10.1021/es020629x.

Massoli, P., P. L. Kebabian, T. B. Onasch, F. B. Hills, and A. Freedman (2010), Aerosol light extinction measurements by cavity attenuated phase shift (CAPS) spectroscopy: Laboratory validation and field deployment of a compact aerosol particle extinction monitor, *Aerosol Sci. Technol.*, *44* (6), 428–435, doi:10.1080/02786821003716599.

May, P. T., R. G. Strauch, K. P. Moran, and W. L. Ecklund (1990), Temperature sounding by RASS with wind profiler radars: A preliminary study, *IEEE Trans. Geosci.Remote Sens.*, *28*, 19–28.

McAdam, K., P. Steer, and K. Perrotta (2011), Using continuous sampling to examine the distribution of traffic related air pollution in proximity to

a major road, *Atmos. Environ.*, *45*, 2080–2086, doi:10.1016/j.atmosenv.2011.01.050.

McBride, P. J., K. S. Schmidt, P. Pilewskie, A. Walther, A. K. Heidinger, D. E. Wolfe, C. W. Fairall, and S. Lance (2012), CalNex cloud properties retrieved from a ship-based spectrometer and comparisons with satellite and aircraft retrieved cloud properties, *J. Geophys. Res.*, *117*(D00V23), doi:10.1029/2012JD017624.

McDonald, B. C., T. R. Dallmann, E. W. Martin, and R. A. Harley (2012), Long-term trends in nitrogen oxide emissions from motor vehicles at National, State, and air basin scales, *J. Geophys. Res.*, *117*(D00V18), doi:10.1029/2012JD018304.

McMillan, A. M. S., M. L. Goulden, and S. C. Tyler (2007), Stoichiometry of CH_4 and CO_2 flux in a California rice paddy, *J. Geophys. Res.*, *112* (G01008), doi:10.1029/2006JG000198.

Metcalf, A. R., J. S. Craven, J. J. Ensberg, J. Brioude, W. Angevine, A. Sorooshian, H. T. Duong, H. H. Jonsson, R. C. Flagan, and J. H. Seinfeld (2012), Black carbon aerosol over the Los Angeles Basin during CalNex, *J. Geophys. Res.*, *117*(D00V13), doi:10.1029/2011JD017255.

Mielke, L. H., A. Furgeson, and H. D. Osthoff (2011), Observation of ClNO2 in a mid-continental urban environment, *Environ. Sci. Technol.*, *45*, 8889–8896, doi:10.1021/es210955u.

Miller, S. M., et al. (2012), Regional sources of nitrous oxide over the United States: Seasonal variation and spatial distribution, *J. Geophys. Res.*, *117*(D06310), doi:10.1029/2011JD016951.

Mirme, A., E. Tamm, G. Mordas, M. Vana, J. Uin, S. Mirme, T. Bernotas, L. Laakso, A. Hirsikko, and M. Kulmala (2007), A wide-range multichannel air ion spectrometer, *Boreal Environ. Res.*, *12*(3), 247–264.

Moffett, R. C., T. Henn, A. Laskin, and M. K. Gilles (2010a), Automated chemical analysis of internally mixed aerosol particles using X-ray spectromicroscopy at the carbon K-edge, *Anal. Chem.*, *82*, 7906–7914, doi:10.1021/ac1012909.

Moffett, R. C., A. Tivanski, and M. K. Gilles (2010b), Scanning transmission X-ray microscopy: Applications in atmospheric aerosol research, in *Fundamentals and Applications in Aerosol Spectroscopy*, edited by R. Signorelli and J. Reid, pp. 420–462, CRC Press.

Mohr, C., et al. (2012), Identification and quantification of organic aerosol from cooking and other sources in Barcelona using aerosol mass spectrometer data, *Atmos. Chem. Phys.*, *12*, 1649–1665, doi:10.5194/acp-12-1649-2012.

Moore, R. H., K. Cerully, R. Bahreini, C. A. Brock, A. M. Middlebrook, and A. Nenes (2012), Hygroscopicity and composition of California CCN during summer 2010, *J. Geophys. Res.*, *117*(D00V12), doi:10.1029/2011JD017352.

Moore, R. H., and A. Nenes (2009), Scanning flow CCN analysis—A method for fast measurements of CCN spectra, *Aerosol Sci. Technol.*, *43*(12), 1192–1207, doi:10.1080/02786820903289780.

Moore, T. O., D. C. Doughty, and L. C. Marr (2009), Demonstration of a mobile flux laboratory for the atmospheric measurement of emissions (FLAME) to assess emissions inventories, *J. Environ. Monit.*, *11*(2), 259–268, doi:10.1039/b810798j.

Murphy, D. M., D. J. Cziczo, K. D. Froyd, P. K. Hudson, B. M. Matthew, A. M. Middlebrook, T. E. Peltier, A. SUllivan, D. S. Thomson, and R. J. Weber (2006), Single-particle mass spectrometry of tropospheric aerosol particles, *J. Geophys. Res.*, *111*(D23S32), doi:10.1029/2006JD007340.

Neuman, J. A., et al. (2002), Fast-response airborne in situ measurements of HNO_3 during the Texas 2000 Air Quality Study, *J. Geophys. Res.*, *107* (4436), doi:10.1029/2001JD001437.

Neuman, J. A., et al. (2012), Observations of ozone transport from the free troposphere to the Los Angeles basin, *J. Geophys. Res.*, *117*(D00V09), doi:10.1029/2011JD016919.

Newman, S., et al. (2012), Diurnal tracking of anthropogenic CO_2 emissions in the Los Angeles basin megacity during spring, 2010, *Atmos. Chem. Phys. Discuss.*, *12*, 5771–5801, doi:10.5194/acpd-12-5771-2012.

Newman, S., X. Xu, J. P. Affek, E. Stolper, and S. Epstein (2008), Changes in mixing ratio and isotopic composition of CO_2 in urban air from the Los Angeles basin, California, between 1972 and 2003, *J. Geophys. Res.*, *113* (D23304), doi:10.1029/2008JD009999.

Ng, N. L., et al. (2011), An aerosol chemical speciation monitor (ACSM) for routine monitoring of the composition and mass concentrations of ambient aerosol, *Aerosol Sci. Technol.*, *45*, 780–794, doi:10.1080/02786826.2011.560211.

Nizkorodov, S. A., J. A. Laskin, and A. Laskin (2011), Molecular chemistry of organic aerosols through the application of high resolution mass spectrometry, *Phys. Chem. Chem. Phys.*, *13*, 3612–3629, doi:10.1039/c0cp02032j.

Nowak, J. B., J. A. Neuman, R. Bahreini, A. M. Middlebrook, J. S. Holloway, S. A. McKeen, D. D. Parrish, T. B. Ryerson, and M. Trainer (2012), Ammonia sources in the California South Coast Air Basin and their impact on ammonium nitrate formation, *Geophys. Res. Lett.*, *39* (L07804), doi:10.1029/2012GL051197.

Nowak, J. B., J. A. Neuman, K. Kozai, L. G. Huey, D. J. Tanner, J. S. Holloway, T. B. Ryerson, G. J. Frost, S. A. McKeen, and F. C. Fehsenfeld (2007), A chemical ionization mass spectrometry technique for airborne measurements of ammonia, *J. Geophys. Res.*, *112*, D10S02 doi:10.1029/2006JD007589.

Obrist, D., A. G. Hallar, I. McCubbin, B. B. Stephens, and T. Rahn (2008), Atmospheric mercury concentrations at Storm Peak Laboratory in the Rocky Mountains: Evidence for long-range transport from Asia, boundary layer contributions, and plant mercury uptake, *Atmos. Environ.*, *42*, 7579–7589, doi:10.1016/j.atmosenv.2008.06.051.

Onasch, T. B., A. Trimborn, E. C. Fortner, J. T. Jayne, G. L. Kok, L. R. Williams, P. Davidovits, and D. R. Worsnop (2012), Soot particle aerosol mass spectrometer: development, validation, and initial application, *Aerosol Sci. Technol.*, *46*(7), 804–817, doi:10.1080/02786826.2012.663948.

Osthoff, H. D., et al. (2008), High levels of nitryl chloride in the polluted subtropical marine boundary layer, *Nat. Geosci.*, *1*, 324–328, doi:10.1038/ngeo177.

Parrish, D. D., K. C. Aikin, S. J. Oltmans, B. J. Johnson, M. Ives, and C. Sweeney (2010), Impact of transported background ozone inflow on summertime air quality in a California ozone exceedance area, *Atmos. Chem. Phys.*, *10*, 10093–10109, doi:10.5194/acp-10-10093-2010.

Parrish, D. D., et al. (2009), Overview of the Second Texas Air Quality Study (TexAQS II) and the Gulf of Mexico Atmospheric Composition and Climate Study (GoMACCS), *J. Geophys. Res.*, *114*(D00F13), doi:10.1029/2009JD011842.

Parrish, D. D., Y. Kondo, O. R. Cooper, C. A. Brock, D. A. Jaffe, M. Trainer, T. Ogawa, G. Hübler, and F. C. Fehsenfeld (2004), Intercontinental Transport and Chemical Transformation 2002 (ITCT 2K2) and Pacific Exploration of Asian Continental Emission (PEACE) experiments: An overview of the 2002 winter and spring intensives, *J. Geophys. Res.*, *109*(D23S01), doi:10.1029/2004JD004980.

Parrish, D. D., M. Trainer, D. Hereid, E. J. Williams, K. J. Olszyna, R. A. Harley, J. F. Meagher, and F. C. Fehsenfeld (2002), Decadal change in carbon monoxide to nitrogen oxide ratio in U.S. vehicular emissions, *J. Geophys. Res.*, *107*(D124140), doi:10.1029/2001JD000720.

Pearson, G., F. Davies, and C. Collier (2009), An analysis of the performance of the UFAM pulsed doppler lidar for observing the boundary layer, *J. Atmos. Oceanic Technol.*, *26*, 240–250.

Peischl, J., et al. (2013), Quantifying Sources of Methane and Light Alkanes in the Los Angeles Basin, California, *J. Geophys. Res.*, doi:10.1029/2012JD019232.

Peischl, J., et al. (2010), A top-down analysis of emissions from selected Texas power plants during TexAQS 2000 and 2006, *J. Geophys. Res.*, *115*(D16303), doi:10.1029/2009JD013527.

Peischl, J., et al. (2012), Airborne observations of methane emissions from rice cultivation in the Sacramento Valley of California, *J. Geophys. Res.*, *117*(D00V25), doi:10.1029/2012JD017994.

Pennington, M. R., J. P. Klems, B. R. Bzdek, and M. V. Johnston (2012), Nanoparticle chemical composition and diurnal dependence at the CalNex Los Angeles ground site, *J. Geophys. Res.*, *117*(D00V10), doi:10.1029/2011JD017061.

Petters, M. D., and S. M. Kreidenweis (2007), A single parameter representation of hygroscopic growth and cloud condensation nucleus activity, *Atmos. Chem. Phys.*, *7*, 1961–1971, doi:10.5194/acp-8-6273-2008.

Pettersson, A., E. R. Lovejoy, C. A. Brock, S. S. Brown, and A. R. Ravishankara (2004), Measurement of aerosol optical extinction at 532 nm with pulsed cavity ring down spectroscopy, *J. Aerosol Sci.*, *35*, 995–1011, doi:10.1016/j.jaerosci.2004.02.008.

Pierce, R. B., et al. (2010), Impacts of background ozone production on Houston and Dallas, Texas, air quality during the Second Texas Air Quality Study field mission, *J. Geophys. Res.*, *114*(D00F09), doi:10.1029/2008JD011337.

Pierce, R. B., et al. (2007), Chemical data assimilation estimates of continental U.S. ozone and nitrogen budgets during the Intercontinental Chemical Transport Experiment-North America, *J. Geophys. Res.*, *112* (D12S21), doi:10.1029/2006JD007722.

Pikelnaya, O., S. C. Hurlock, S. Trick, and J. Stutz (2007), Intercomparison of multiaxis and long-path differential optical absorption spectroscopy measurements in the marine boundary layer, *J. Geophys. Res.*, *112* (D10S01), doi:10.1029/2006JD007727.

Pilewskie, P., J. Pommier, R. Bergstrom, W. Gore, S. Howard, M. Rabbette, B. Schmid, P. V. Hobbs, and S. C. Tsay (2003), Solar spectral radiative forcing during the Southern African Regional Science Initiative, *J. Geophys. Res.*, *108*(D138486), doi:10.1029/2002JD002411.

Pollack, I. B., B. M. Lerner, and T. B. Ryerson (2010), Evaluation of ultraviolet light-emitting diodes for detection of atmospheric NO_2 by photolysis-chemiluminescence, *J. Atmos. Chem.*, *65*(2–3), 111–125, doi:10.1007/s10874-011-9184-3.

Pollack, I. B., et al. (2012), Airborne and ground-based observations of a weekend effect in ozone, precursors, and oxidation products in the California South Coast Air Basin, *J. Geophys. Res.*, *117*(D00V05), doi:10.1029/2011JD016772.

Pratt, K. A., et al. (2009), Development and characterization of an aircraft aerosol time-of-flight mass spectrometer, *Anal. Chem.*, *81*, 1792–1800, doi:10.1021/ac801942r.

Pringle, K. J., H. Tost, A. Pozzer, U. Pöschl, and J. Lelieveld (2010), Global distribution of the effective aerosol hygroscopicity parameter for CCN activation, *Atmos. Chem. Phys.*, *10*, 5241–5255, doi:10.5194/acp-10-5241-2010.

Pusede, S. E., and R. C. Cohen (2012), On the observed response of ozone to NO_x and VOC reactivity reductions in San Joaquin Valley California 1995–present, *Atmos. Chem. Phys. Discuss.*, *12*, 9771–9811, doi:10.5194/acpd-12-9771-2012.

Qin, X., and K. A. Prather (2006), Impact of biomass emissions on particle chemistry during the California Regional Particulate Air Quality Study, *Int. J. Mass spectrom.*, *258*, 142–150, doi:10.1016/j.ijms.2006.09.004.

Querol, X., et al. (2008), PM speciation and sources in Mexico during the MILAGRO-2006 campaign, *Atmos. Chem. Phys.*, *8*, 111–128.

Quinn, P. K., and T. S. Bates (2005), Regional aerosol properties: Comparisons of boundary layer measurements from ACE 1, ACE 2, Aerosols99, INDOEX, ACE Asia, TARFOX, and NEAQS, *J. Geophys. Res.*, *110* (D14202), doi:10.1029/2004JD004755.

Quinn, P. K., T. S. Bates, D. Coffman, and D. S. Covert (2008), Influence of particle size and chemistry on the cloud nucleating properties of aerosols, *Atmos. Chem. Phys.*, *8*, 1029–1042.

Remer, L. A., et al. (2005), The MODIS aerosol algorithm, products, and validation, *J. Atmos. Sci.*, *62*(4), 947–973.

Ren, X., et al. (2010), Measurement of atmospheric nitrous acid at Blodgett Forest during BEARPEX2007, *Atmos. Chem. Phys.*, *10*, 6283–6294, doi:10.5194/acp-10-6283-2010.

Riedel, T. P., et al. (2012), Nitryl chloride and molecular chlorine in the coastal marine boundary layer, *Environ. Sci. Technol.*, *46*, 10463–10470, doi:10.1021/es204632r.

Rinehart, L. R., E. M. Fujita, J. C. Chow, K. Magliano, and B. Zeilinska (2006), Spatial distribution of $PM_{2.5}$ associated organic compounds in central California, *Atmos. Environ.*, *40*, 290–303, doi:10.1016/j.atmosenv.2005.09.035.

Roach, P. J., J. Laskin, and A. Laskin (2010), Molecular characterization of organic aerosols using nanospray desorption electrospray ionization mass spectrometry, *Anal. Chem.*, *82*, 7979–7986, doi:10.1021/ac101449p.

Roberts, G. C., and A. Nenes (2005), A continuous-flow streamwise thermal-gradient CCN chamber for atmospheric measurements, *Aerosol Sci. Technol.*, *39*(3), 206–221, doi:10.1080/027868290913988.

Rogers, R. R., et al. (2009), NASA LaRC airborne high spectral resolution lidar aerosol measurements during MILAGRO: observations and validation, *Atmos. Chem. Phys.*, *9*, 4811–4826, doi:10.5194/acp-9-4811-2009.

Rollins, A. W., et al. (2012), Evidence for NO_x control over nighttime SOA formation, *Science*, *337*(6099), 1210–1212, doi:10.1126/science.1221520.

Rosenthal, J. S., R. A. Helvey, T. E. Battalino, C. Fisk, and P. W. Greiman (2003), Ozone transport by mesoscale and diurnal wind circulations across southern California, *Atmos. Environ.*, *37*(Supplement no. 2), S51–S71.

Russell, L. M. (2003), Aerosol organic-mass-to-organic-carbon ratio measurements, *Environ. Sci. Technol.*, *37*(13), 2982–2987, doi:10.1021/es026123w.

Russell, L. M., S. Takahama, S. Liu, L. N. Hawkins, D. S. Covert, P. K. Quinn, and T. S. Bates (2009), Oxygenated fraction and mass of organic aerosol from direct emission and atmospheric processing measured on the R/V *Ronald Brown* during TEXAQS/GoMACCS 2006, *J. Geophys. Res.*, *114*(D00F05), doi:10.1029/2008JD011275.

Russell, L. M., S. H. Zhang, R. C. Flagan, J. H. Seinfeld, M. R. Stoltzenburg, and R. Caldow (1996), Radially classified aerosol detector for aircraft-based submicron aerosol measurements, *J. Atmos. Oceanic Technol.*, *13*, 598–609.

Ryerson, T. B., et al. (1998), Emissions lifetimes and ozone formation in power plant plumes, *J. Geophys. Res.*, *103*, 22,569–522,583.

Ryerson, T. B., L. G. Huey, K. Knapp, J. A. Neuman, D. D. Parrish, D. T. Sueper, and F. C. Fehsenfeld (1999), Design and initial characterization of an inlet for gas-phase NO_y measurements from aircraft, *J. Geophys. Res.*, *104*, 5483–5492.

Sanford, T. J., D. M. Murphy, D. S. Thomson, and R. W. Fox (2008), Albedo measurements and optical sizing of single aerosol particles, *Aerosol Sci. Technol.*, *42*(11), 958–969, doi:10.1080/02786820802363827.

Sarwar, G., H. Simon, P. Bhave, and G. Yarwood (2012), Examining the impact of heterogeneous nitryl chloride production on air quality across the United States, *Atmos. Chem. Phys.*, *12*, 6455–6473, doi:10.5194/acp-12-6455-2012.

Schauer, J. J., et al. (2003), ACE-Asia intercomparison of a thermal-optical method for the determination of particle-phase organic and elemental carbon, *Environ. Sci. Technol.*, *37*(5), 993–1001, doi:10.1021/es020622f.

Schauer, J. J., W. G. Rogge, L. M. Hildemann, M. A. Mazurek, and G. R. Cass (1996), Source apportionment of airborne particulate matter using organic compounds as tracers, *Atmos. Environ.*, *30*, 3837–3855.

Schauffler, S., E. L. Atlas, S. G. Donnelly, A. Andrews, S. A. Montzka, J. W. Elkins, D. F. Hurst, P. A. Romashkin, G. S. Dutton, and V. Stroud (2003), Chlorine budget and partitioning during the Stratospheric Aerosol and Gas Experiment (SAGE) III Ozone Loss and Validation Experiment (SOLVE), *J. Geophys. Res.*, *108*(D5), 4173, doi:10.1029/2001JD002040.

Schwarz, J. P., et al. (2008), Measurement of the mixing state, mass, and optical size of individual black carbon particles in urban and biomass burning emissions, *Geophys. Res. Lett.*, *35*, (L13810) doi: 10.1029/2008GL033968.

Shair, F. H., et al. (1982), Transport and dispersion of airborne pollutants associated with the land breeze-sea breeze system, *Atmos. Environ.*, *16*, 2043–2053.

Sheesley, R. J., J. J. Schauer, E. Bean, and D. Kenski (2004), Trends in secondary organic aerosol at a remote site in Michigan's upper peninsula, *Environ. Sci. Technol.*, *38*(24), 6491–6500, doi:10.1021/es049104q.

Shetter, R. E., and M. Müller (1999), Photolysis frequency measurements using actinic flux spectroradiometry during the PEM-Tropics mission: Instrumentation description and some results, *J. Geophys. Res.*, *104*, 5647–5661.

Skamarock, W. C., R. Rotunno, and J. B. Klemp (2002), Catalina eddies and coastally trapped disturbances, *J. Atmos. Sci.*, *59*, 2270–2278.

Sorooshian, A., S. Hersey, F. J. Brechtel, A. Corless, R. C. Flagan, and J. H. Seinfeld (2008), Rapid, size-resolved aerosol hygroscopic growth measurements: Differential aerosol sizing and hygroscopicity spectrometer probe (DASH-SP), *Aerosol Sci. Technol.*, *42*(6), 445–464, doi:10.1080/02786820802178506.

Stark, H., B. M. Lerner, R. Schmitt, R. Jakoubek, E. J. Williams, T. B. Ryerson, D. D. Parrish, and F. C. Fehsenfeld (2007), Atmospheric in situ measurement of nitrate radical (NO_3) and other photolysis rates using spectroradiometry and filter radiometry, *J. Geophys. Res.*, *112*, (D10S04) doi:10.1029/2006JD007578.

Stöhr, J. (1992), *NEXAFS Spectroscopy*, 407 pp., Springer Verlag, Berlin.

Subramanian, R., et al. (2010), Black carbon over Mexico: The effect of atmospheric transport on mixing state, mass absorption cross-section, and BC/CO ratios, *Atmos. Chem. Phys.*, *10*, 219–237, doi:10.5194/acp-10-219-2010.

Sullivan, A. P., R. E. Peltier, C. A. Brock, J. A. de Gouw, J. S. Holloway, C. Warneke, A. G. Wollny, and R. J. Weber (2006), Airborne measurements of carbonaceous aerosol soluble in water over northeastern United States: Method development and an investigation into water-soluble organic carbon sources, *J. Geophys. Res.*, *111*(D23S46), doi:10.1029/2006JD007072.

Sun, Y. L., et al. (2011), Characterization of the sources and processes of organic and inorganic aerosols in New York city with a high-resolution time-of-flight aerosol mass spectrometer, *Atmos. Chem. Phys.*, *11*, 1581–1602, doi:10.5194/acp-11-1581-2011.

Surratt, J. D., et al. (2008), Organosulfate formation in biogenic secondary organic aerosol, *J. Phys. Chem. A*, *112*, 8345–8378, doi:10.1021/jp802310p.

Szidat, S., T. M. Jenk, H. A. Synal, M. Kalberer, L. Wacker, I. Hajdas, A. Kasper-Giebl, and U. Baltensperger (2006), Contributions of fossil fuel, biomass-burning, and biogenic emissions to carbonaceous aerosols in Zurich as traced by ^{14}C, *J. Geophys. Res.*, *111*(D07206), doi:10.1029/2005JD006590.

Tajima, N., N. Fukushima, K. Ehara, and H. Sakurai (2011), Mass range and optimized operation of the aerosol particle mass analyzer, *Aerosol Sci. Technol.*, *45*(2), 196–214, doi:10.1080/02786826.2010.530625.

Takahama, S., A. Johnson, J. G. Morales, L. M. Russell, R. Duran, G. Rodriguez, J. Zheng, R. Zhang, D. Toom-Sauntry, and W. R. Leaitch (2012), Submicron organic aerosol in Tijuana, Mexico, from local and Southern California sources during the CalMex campaign, *Atmos. Environ.*, doi:10.1016/j.atmosenv.2012.07.057.

Takahama, S., S. Liu, and L. M. Russell (2010), Coatings and clusters of carboxylic acids in carbon-containing atmospheric particles from spectromicroscopy and their implications for cloud-nucleating and optical properties, *J. Geophys. Res.*, *115*(D01202), doi:10.1029/2009JD012622.

Thalman, R., and R. Volkamer (2010), Inherent calibration of a blue LED-CE-DOAS instrument to measure iodine oxide, glyoxal, methyl glyoxal, nitrogen dioxide, water vapour and aerosol extinction in open cavity mode, *Atmos. Meas. Tech.*, *3*, 1797–1814, doi:10.5194/amt-3-1797-2010.

Thompson, J. E., P. L. Hayes, J. L. Jimenez, K. Adachi, X. Zhang, J. Liu, R. J. Weber, and P. R. Buseck (2012), Aerosol optical properties at Pasadena, CA during CalNex 2010, *Atmos. Environ.*, *55*, 190–200, doi:10.1016/j.atmosenv.2012.03.011.

Tonse, S. R., N. J. Brown, R. A. Harley, and L. Jin (2008), A process-analysis based study of the ozone weekend effect, *Atmos. Environ.*, *42*, 7728–7736, doi:10.1016/j.atmosenv.2008.05.061.

Townsend-Small, A., S. C. Tyler, D. E. Pataki, X. Xu, and L. E. Christensen (2012), Isotopic measurements of atmospheric methane in Los Angeles, California, USA: Influence of "fugitive" fossil fuel emissions, *J. Geophys. Res.*, *117*(D07308), doi:10.1029/2011JD016826.

Turner, D., S. Clough, J. Liljegren, E. Clothiaux, K. Cady-Periera, and K. Gaustad (2007), Retrieving liquid water path and precipitable water vapor from the Atmospheric Radiation Measurement (ARM) microwave radiometers, *Trans. Geosci. Remote Sens.*, *45*(11), 3680–3690.

Turpin, B. J., and J. J. Huntzicker (1995), Identification of secondary organic aerosol episodes and quantitation of primary and secondary organic aerosol concentrations during SCAQS, *Atmos. Environ.*, *29*(23), 3527–3544.

Veres, P., J. M. Roberts, C. Warneke, D. Welsh-Bon, M. Zahniser, S. Herndon, R. Fall, and J. de Gouw (2008), Development of negative-ion proton-transfer chemical-ionization mass spectrometry (NI-PT-CIMS) for the measurement of gas-phase organic acids in the atmosphere, *Int. J. Mass spectrom.*, *274*, 48–55, doi:10.1016/j.ijms.2008.04.032.

Veres, P. R., et al. (2011), Evidence of rapid production of organic acids in an urban air mass, *Geophys. Res. Lett.*, *38*(L17807), doi:10.1029/2011GL048420.

Villani, P., D. Picard, V. Michaud, P. Laj, and A. Wiedensohler (2008), Design and validation of a volatility hygroscopic tandem differential mobility analyzer (VH-TDMA) to characterize the relationships between the thermal and hygroscopic properties of atmospheric aerosol particles, *Aerosol Sci. Technol.*, *42*(9), 729–741, doi:10.1080/02786820802255668.

Volkamer, R., S. Coburn, B. Dix, and R. Sinreich (2009), MAX-DOAS observations from ground, ship, and research aircraft: Maximizing signal-to-noise to measure "weak" absorbers, *Proc. SPIE*, 7462, doi:10.1117/12.826792.

Volkamer, R., F. San Martini, L. T. Molina, D. Salcedo, J. L. Jimenez, and M. J. Molina (2007), A missing sink for gas-phase glyoxal in Mexico City: Formation of secondary organic aerosol, *Geophys. Res. Lett.*, *34* (L19807), doi:10.1029/2007GL030752.

Wagner, N. L., W. P. Dubé, R. A. Washenfelder, C. J. Young, I. B. Pollack, T. B. Ryerson, and S. S. Brown (2011), Diode laser-based cavity ring-down instrument for NO_3, N_2O_5, NO, NO_2, and O_3 from aircraft, *Atmos. Meas. Tech.*, *4*, 1227–1240, doi:10.5194/amt-4-1227-2011.

Wakimoto, R. M., and J. L. McElroy (1986), Lidar observation of elevated pollution layers in Los Angeles, *J. Clim. Appl. Meteorol.*, *25*, 1583–1599.

Wang, S., R. Ackermann, and J. Stutz (2006), Vertical profiles of O3 and NOx chemistry in the polluted nocturnal boundary layer in Phoenix, AZ: I. Field observations by long-path DOAS, *Atmos. Chem. Phys.*, *6*, 2671–2693.

Wang, S. C., and R. C. Flagan (1990), Scanning electrical mobility spectrometer, *Aerosol Sci. Technol.*, *13*, 230–240, doi:10.1080/02786829008959441.

Warneke, C., J. A. de Gouw, J. S. Holloway, J. Peischl, T. B. Ryerson, E. Atlas, D. Blake, M. Trainer, and D. D. Parrish (2012), Multi-year trends in volatile organic compounds in Los Angeles, California: Five decades of improving air quality, *J. Geophys. Res.*, *117*(D00V17), doi:10.1029/2012JD017899.

Warneke, C., J. A. de Gouw, E. R. Lovejoy, P. C. Murphy, W. C. Kuster, and R. Fall (2005), Development of proton-transfer ion trap-mass spectrometry: On-line detection and identification of volatile organic compounds in air, *J. Am. Soc. Mass Spectrom.*, *16*, 1316–1324.

Washenfelder, R. A., A. O. Langford, H. Fuchs, and S. S. Brown (2008), Measurement of glyoxal using an incoherent broadband cavity enhanced absorption spectrometer, *Atmos. Chem. Phys.*, *8*, 7779–7793.

Washenfelder, R. A., et al. (2011), The glyoxal budget and its contribution to organic aerosol for Los Angeles, California, during CalNex 2010, *J. Geophys. Res.*, *116*(D00V02), doi:10.1029/2011JD016314.

Weber, B. L., D. B. Wuertz, D. C. Welsh, and R. McPeek (1993), Quality controls for profiler measurements of winds and RASS temperatures, *J. Atmos. Oceanic Technol.*, *10*.

Weber, R. J., D. Orsini, Y. Daun, Y.-N. Lee, P. J. Klotz, and F. Brechtel (2001), A particle-into-liquid collector for rapid measurements of aerosol bulk chemical composition, *Aerosol Sci. Technol.*, *35*, 718–727, doi:10.1080/02786820152546761.

Wennberg, P. O., et al. (2012), On the sources of methane to the Los Angeles atmosphere, *Environ. Sci. Technol.*, *46*, 9282–9289, doi:10.1021/es301138y.

White, A. B., C. J. Senff, and R. M. Banta (1999), A comparison of mixing depths observed by ground-based wind profilers and an airborne lidar, *J. Atmos. Oceanic Technol.*, *16*, 584–590.

White, A. B., C. J. Senff, A. N. Keane, L. S. Darby, I. V. Djalalova, D. C. Ruffieux, D. E. White, B. J. Williams, and A. H. Goldstein (2006), A wind profiler trajectory tool for air quality transport applications, *J. Geophys. Res.*, *111*(D23S23), doi:10.1029/2006JD007475.

Whittlestone, S., and W. Zahorowski (1998), Baseline radon detectors for shipboard use: Development and deployment in the First Aerosol Characterization Experiment (ACE 1), *J. Geophys. Res.*, *103*, 16,743–716,751.

Williams, B. J., A. H. Goldstein, N. M. Kreisberg, and S. V. Hering (2006a), An in-situ instrument for speciated organic composition of atmospheric aerosols: Thermal desorption aerosol GC/MS-FID (TAG), *Aerosol Sci. Technol.*, *40*(8), 627–638, doi:10.1080/02786820600754631.

Williams, E. J., F. C. Fehsenfeld, B. T. Jobson, W. C. Kuster, P. D. Goldan, J. Stutz, and W. A. McClenny (2006b), Comparison of ultraviolet absorbance, chemiluminescence, and DOAS instruments for ambient ozone monitoring, *Environ. Sci. Technol.*, *40*(18), 5755–5762, doi:10.1021/es0523542.

Williams, E. J., B. M. Lerner, P. C. Murphy, S. C. Herndon, and M. S. Zahniser (2009), Emissions of NO_x, SO_2, CO, and HCHO from commercial marine shipping during Texas Air Quality Study (TexAQS) 2006, *J. Geophys. Res.*, *114*(D21306), doi:10.1029/2009JD012094.

Williams, E. J., D. D. Parrish, M. P. Buhr, F. C. Fehsenfeld, and R. Fall (1988), Measurement of soil NO_x emissions in Central Pennsylvania, *J. Geophys. Res.*, *93*, 9539–9546.

Wilson, J. C., B. G. LaFleur, H. Hilbert, W. R. Seebaugh, J. Fox, D. W. Gesler, C. A. Brock, B. J. Huebert, and J. Mullen (2004), Function and performance of a low turbulence inlet for sampling supermicron particles from aircraft platforms, *Aerosol Sci. Technol.*, *38*(8), 790–802, doi:10.1080/027868290500841.

Wolfe, D. E., et al. (2007), Shipboard multisensor merged wind profiles from the New England Air Quality Study 2004, *J. Geophys. Res.*, *112* (D10S15), doi:10.1029/2006JD007344.

Wonaschütz, A., S. P. Hersey, A. Sorooshian, J. S. Craven, A. R. Metcalf, R. C. Flagan, and J. H. Seinfeld (2011), Impact of a large wildfire on water-soluble organic aerosol in a major urban area: the 2009 Station Fire in Los Angeles County, *Atmos. Chem. Phys.*, *11*, 8257–8270, doi:10.5194/acp-11-8257-2011.

Worton, D. R., N. M. Kreisberg, G. Isaacman, A. P. Teng, C. McNeish, T. Gorecki, S. V. Hering, and A. H. Goldstein (2012), Thermal desorption comprehensive two-dimensional gas chromatography: An improved instrument for in-situ speciated measurements of organic aerosols, *Aerosol Sci. Technol.*, *46*(4), 380–393, doi:10.1080/02786826.2011.634452

Wu, Z., M. Hu, S. Liu, B. Wehner, S. Bauer, A. Maßling, A. Wiedensohler, T. Petäjä, M. Dal Maso, and M. Kulmala (2007), New particle formation in Beijing, China: Statistical analysis of a 1-year data set, *J. Geophys. Res.*, *112*(D09209), doi:10.1029/2006JD007406.

Wunch, D., P. O. Wennberg, G. C. Toon, G. Keppel-Aleks, and Y. G. Yavin (2009), Emissions of greenhouse gases from a North American megacity, *Geophys. Res. Lett.*, *36*(L15810), doi:10.1029/2009GL039825.

Xiang, B., et al. (2013), Nitrous oxide (N_2O) emissions from California based on 2010 CalNex airborne measurements *J. Geophys. Res. 118*, doi:10.1002/jgrd.50189.

Young, C. J., et al. (2012), Vertically resolved measurements of nighttime radical reservoirs in Los Angeles and their contribution to the urban radical budget, *Environ. Sci. Technol.*, *46*, 10965–10973, doi:10.1021/es302206a.

Zaveri, R. A., et al. (2012), Overview of the 2010 Carbonaceous Aerosols and Radiative Effects Study (CARES), *Atmos. Chem. Phys.*, *12*, 7647–7687, doi:10.5194/acp-12-7647-2012.

Zhang, H., J. D. Surratt, Y. H. Lin, J. Bapat, and R. M. Kamens (2011a), Effect of relative humidity on SOA formation from isoprene/NO photooxidation: Enhancement of 2-methylglyceric acid and its corresponding oligoesters under dry conditions, *Atmos. Chem. Phys*, *11*, 6411–6424, doi:10.5194/acp-11-6411-2011.

Zhang, X., Y.-H. Lin, J. D. Surratt, P. Zotter, A. S. H. Prévôt, and R. J. Weber (2011b), Light-absorbing soluble organic aerosol in Los Angeles and Atlanta: A contrast in secondary organic aerosol, *Geophys. Res. Lett.*, *38*(L21810), doi:10.1029/2011GL049385.

Zhang, X., J. Liu, E. T. Parker, P. L. Hayes, J. L. Jimenez, J. A. de Gouw, J. H. Flynn, N. Grossberg, B. L. Lefer, and R. J. Weber (2012), On the gas-particle partitioning of soluble organic aerosol in two urban atmospheres with contrasting emissions: 1. Bulk water-soluble organic carbon, *J. Geophys. Res.*, *117*(D00V16), doi:10.1029/2012JD017908.

Zheng, J., et al. (2011a), Measurements of gaseous H_2SO_4 by AP-ID-CIMS during CAREBeijing 2008 Campaign, *Atmos. Chem. Phys.*, *11*, 7755–7765, doi:10.5194/acp-11-7755-2011.

Zheng, J., A. Khalizov, L. Wang, and R. Zhang (2010), Atmospheric pressure-ion drift chemical ionization mass spectrometry for detection of trace gas species, *Anal. Chem.*, *82*(17), 7302–7308, doi:10.1021/ac101253n.

Zheng, W., F. M. Flocke, G. S. Tyndall, A. Swanson, J. J. Orlando, J. M. Roberts, L. G. Huey, and D. J. Tanner (2011b), Characterization of a thermal decomposition chemical ionization mass spectrometer for the measurement of peroxy acyl nitrates (PANs) in the atmosphere, *Atmos. Chem. Phys.*, *11*, 6529–6547, doi:10.5194/acp-11-6529-2011.

Zhou, L., Y. Zeng, P. D. Hazlett, and V. Matherne (2007), Ambient air monitoring with auto-gas chromatography running in trigger mode, *Anal. Chim. Acta*, *596*(1), 156–163.

Zielinski, M., H. Riimmelt, and G. Fruhmann (1997), Ambient air soot concentrations in Munich public transportation systems, *Sci. Total Environ.*, *196*, 107–110.

Zordan, C. A., S. Wang, and M. V. Johnston (2008), Time-resolved chemical composition of individual nanoparticles in urban air, *Environ. Sci. Technol.*, *42*(17), 6631–6636, doi:10.1021/es800880z.